Global scale observations of atmospheric molecular hydrogen and its stable isotopic composition

Anneke M. Batenburg MSc

ISBN 978-94-6191-391-3

A digital version of this thesis will be made available on
www.projects.science.uu.nl/atmosphereclimate/anneke.php.

Institute for Marine and Atmospheric research Utrecht (IMAU)
Faculty of Science, Department of Physics and Astronomy
Utrecht University, The Netherlands

Cover: Picture of GC-IRMS setup courtesy Sylvia Walter

Global scale observations of atmospheric molecular hydrogen and its stable isotopic composition

Wereldwijde metingen van atmosferische moleculaire waterstof en zijn stabiele-isotoopsamenstelling

(met een samenvatting in het Nederlands)

Proefschrift

ter verkrijging van de graad van doctor aan de Universiteit Utrecht
op gezag van de rector magnificus, prof. dr. G.J. van der Zwaan,
ingevolge het besluit van het college voor promoties
in het openbaar te verdedigen op

maandag 10 september 2012 des middags te 4.15 uur

door

Anneke Martien Batenburg

geboren op 31 januari 1983 te Haren (Gr.)

Promotor: Prof. dr. T. Röckmann

This research was supported by the Netherlands Organisation for Scientific Research (NWO) under the ACTS project "Sustainable Hydrogen" number 053.61.026. It was also supported by the EUROHYDROS project, which was funded via the Sixth Framework Programme of the European Union (SUSTDEV-2005-3.I.2.1 Atmospheric composition change: Methane, Nitrous Oxide and Hydrogen).


Proper tools

are a girl's best friend.

Abstract

With average mixing ratios (χ) around 550 ppb (nmole/mole), molecular hydrogen (H_2) is the most abundant reduced gas in our atmosphere after methane (CH_4), but considerably less studied. H_2 is also a promising energy carrier that might replace fossil fuels in vehicles. As H_2 burns cleanly to water, this could have great advantages for the environment, but it may also have side effects. Large scale leakage of H_2 into the atmosphere might affect the atmosphere's oxidative capacity and stratospheric ozone chemistry. To assess these risks, a better understanding of the atmospheric H_2 cycle is needed.

Stable isotopic composition measurements can be used to constrain the source and sink terms in the budgets of atmospheric trace gases, as the different processes affect the stable isotopic composition of the gases in different ways. For H_2, the effects are particularly large, due to the large relative mass difference between the isotopes (H and D). The largest source, hydrocarbon oxidation, yields D-enriched H_2, whereas the smaller combustion-related sources and the minor microbial sources yield D-depleted and extremely D-depleted H_2, respectively. Both sink processes, uptake in soils and reaction with hydroxyl radicals (OH), have a D-enriching effect, but the effect is much stronger for OH. Despite its usefulness, few environmental observations of H_2 isotopic composition (δD(H_2), or for brevity, δD) are available. We present three new χ(H_2) and δD datasets to fill this gap.

First, we present one- to five-year long time series from six globally distributed, predominantly background stations. As expected from previous observations, average χ(H_2) and δD values were larger in the southern hemisphere (SH) than in the northern hemisphere (NH). But unexpectedly, the minimum in δD was found at the NH midlatitude stations, which is likely a result of fossil fuel combustion. χ(H_2) and δD showed more variation with season in the NH than in the SH. At the three NH coastal and island stations, seasonal δD-cycles were observed, which were five to six months out-of-phase with the χ(H_2)-cycles. No seasonal cycles in δD were observed at the other sites. For the three coastal/island NH stations, a tentative analysis was made of the relative contribution of the two sink processes. This indicated that the relative contribution of soil uptake increases with latitude.

In the next chapter, δD data are presented from samples collected by the

CARIBIC passenger aircraft. This commercial aircraft flies in the upper troposphere (UT) but also regularly crosses the tropopause into the lowermost stratosphere (LMS). In the LMS, tight correlations are found between δD and $\chi(CH_4)$. This correlation has applications in global models of δD. UT samples collected over India during the summer monsoon show a decrease in δD that is correlated with a previously found CH_4 increase, possibly indicating a hitherto unknown microbial H_2-source.

Lastly, we present a three-year long time series from the Cabauw tall tower in the Netherlands (200 m), which shows excursions to high $\chi(H_2)$ and low δD values, especially in winter. These excursions indicate that the local H_2-cycle is under heavy anthropogenic influence, which is confirmed by an analysis of the apparent isotopic source signature. In addition, several $\chi(H_2)$ and δD height profiles (20, 60, 120 and 200 m) were measured. These show that the local soil uptake of H_2 is weak.

Contents

1 Introduction **1**

1.1 H_2 in the atmosphere 1
1.1.1 History 2
1.1.2 Sources and sinks of H_2 2
1.1.3 Temporal and spatial variation in H_2 6
1.1.4 Possible consequences of large scale H_2 production . . . 8

1.2 The isotopic composition of H_2 10
1.2.1 Isotope effects in the sources and sinks of H_2 12
1.2.2 Environmental observations of $\delta D(H_2)$ 16
1.2.3 $\delta D(H_2)$ in models 17

1.3 This thesis 20

2 Temporal and spatial variability of $\delta D(H_2)$: observations at six EUROHYDROS stations **25**

2.1 Introduction 26

2.2 Experimental 29

2.3 Results and discussion 32
2.3.1 Time series 32
2.3.2 Latitudinal gradients 41
2.3.3 Latitude dependence of the apparent fractionation factor 42

2.4 Conclusions 47

3 $\delta D(H_2)$ in the tropopause region probed by the CARIBIC aircraft **49**

3.1 Introduction 50
3.1.1 Atmospheric Molecular Hydrogen (H_2) 50
3.1.2 Stable isotope studies of H_2 51
3.1.3 δD in the stratosphere 53

3.2 Experimental 54
3.2.1 Sampling and in-situ measurements 54
3.2.2 GHG analysis 55
3.2.3 Analysis of $\chi(H_2)$ and $\delta D(H_2)$ 55
3.2.4 Selection of stratospheric and polluted samples 56
3.3 Results and discussion 57
3.3.1 Pollution signatures 57
3.3.2 The stratosphere 60
3.3.3 Indian summer monsoon 64
3.4 Conclusions 68

4 $\chi(H_2)$ and $\delta D(H_2)$ observations at the Cabauw tall tower 69
4.1 Introduction 70
4.2 Methods 72
4.2.1 Tower location and continuous on-site measurements . . 72
4.2.2 Collection of Cabauw flask samples 72
4.2.3 Collection of Royal Holloway flask samples 73
4.2.4 Analysis of the flask samples 73
4.3 Results and Discussion 74
4.3.1 Time series 74
4.3.2 Source signature studies 75
4.3.3 Diurnal cycles at the Royal Holloway site 79
4.3.4 Height profiles 79
4.4 Conclusions and outlook 82

5 Conclusions and outlook 85
5.1 $\delta D(H_2)$ variations with latitude and season 85
5.2 $\delta D(H_2)$ effect of STE 86
5.3 Fossil fuel combustion in NW Europe 88
5.4 Soil deposition at Cabauw 88
5.5 These observations in model studies 89
5.6 Remaining questions 89

Bibliography 93

Samenvatting 103

Dankwoord 109

Curriculum Vitae 111

Publications 113

Chapter 1

Introduction

1.1 H_2 in the atmosphere

The chemical composition of the Earth's atmosphere influences our climate and the health of people, animals and plants. For these reasons, atmospheric chemists study the chemical composition of the atmosphere and the factors that control it. Remarkably, the largest part of this research effort is directed to a very small part of the atmosphere: the trace gases, which comprise all atmospheric gases that are not nitrogen (N_2), oxygen (O_2), argon (Ar) or water (H_2O). Because the main atmospheric constituents are relatively inert and do not absorb much infrared radiation, the trace gases are responsible for most of the chemistry and climate effects. Figure 1.1 lists the most abundant gases in the atmosphere with their mixing ratios (the number of moles of a substance per mole of air). The subject of this thesis is atmospheric molecular hydrogen (H_2). The mixing ratio of H_2 may seem small in Figure 1.1, but H_2 is in fact the most abundant reduced (or "oxidizable") atmospheric gas after methane (CH_4). H_2 is not toxic and not a greenhouse gas by itself, but it is connected by its chemistry to gases that are.

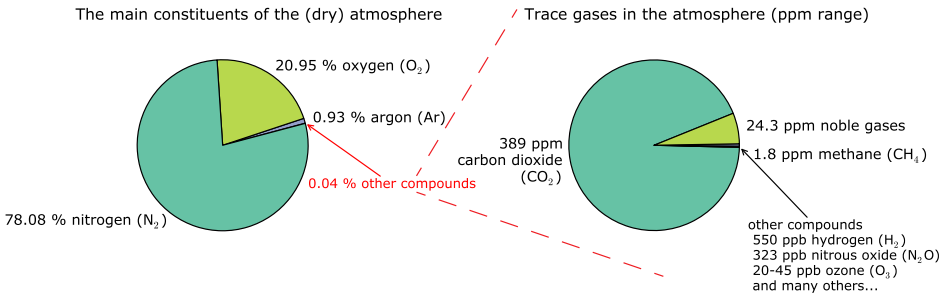

Figure 1.1: A pie-chart representation of the mixing ratios of all gases in dry air, based on values by *Ahrens* (2007), *Jacob* (1999), *WMO* (2011) and *Vingarzan* (2004).

1.1.1 History

That H_2 is present in the atmosphere has been known since at least the start of the 20^{th} century. Accurately measuring its concentration proved more difficult, though, due to H_2 contamination by equipment. The initial numbers that were reported were a factor of two to more than one hundred too large. The first to publish a number that is, as we now know, correct was *Paneth* (1937), who reported a mixing ratio ($\chi(H_2)$) of $5 \cdot 10^{-5}$ %, or 0.5 ppm (1 ppm = 1 μmole/mole) from measurements at a Bavarian air liquefaction plant. In the 1970s, more accurate and convenient methods to measure $\chi(H_2)$ became available, based on the reduction of mercuric oxide (HgO) by the H_2 in purified sample air and optical detection of the resulting mercury (Hg) vapor (*Schmidt and Seiler*, 1970), or based on gas chromatographic separation of the H_2 and detection of the H_2 by a radio frequency discharge glow detector (*Heidt and Ehhalt*, 1972). This enabled researchers to collect enough measurements to get some idea of the spatial and temporal distribution of H_2, and to make a first estimate of the tropospheric H_2 budget (*Schmidt*, 1974; *Ehhalt et al.*, 1977). An influential paper was published by *Novelli et al.* (1999), who presented time series of $\chi(H_2)$ from 50 globally distributed stations and a budget estimate that is still in agreement with more recent estimates (see (*Ehhalt and Rohrer*, 2009) for a literature review, and see Table 1.1 for examples of recent budget estimates). Since the start of this century, there has been a marked increase of studies related to atmospheric H_2. This is partly because the H_2 cycle is linked to other atmospheric trace gases of interest, like methane (CH_4) and carbon monoxide (CO), but it is also because H_2 is expected to play a role in future energy supply chains, which may lead to leakage of H_2 into the atmosphere.

1.1.2 Sources and sinks of H_2

Table 1.1 lists a number of estimates of the production terms (sources) and destruction terms (sinks) in the global budget of H_2 (see also the upper pane of Figure 1.8). It shows that the the H_2 budget is dominated by its largest sink, uptake by soils, which removes about three quarters of the H_2; photochemical oxidation removes the remaining quarter. The largest sources are photochemical oxidation of CH_4 and other hydrocarbons, and combustion of fossil fuels or biomass. Microbial processes constitute minor sources. The result of these processes is an atmospheric H_2 burden of 155 Tg, with an H_2 lifetime of $\approx$ 2 years (*Ehhalt and Rohrer*, 2009).

Oxidation sources

Oxidation is a key process in the atmosphere and the most important sink for many pollutants and greenhouse gases, including CH_4. The oxidation chain of CH_4 (and most other species) starts with a reaction with the hydroxyl radical (OH or ·OH), in which the OH abstracts an H atom from the CH_4 to leave a methyl radical (CH_3). The CH_3 radical subsequently enters into a chain of reactions (listed by *Novelli et al.* (1999)), and schematically shown in the left part of Figure 1.2) that eventually leads to the formation of formaldehyde (HCHO). The roughly 95 % of the HCHO that is not lost by wet or dry deposition, then,

Table 1.1: Recent H_2 budget estimates from different authors. Magnitudes are in Tg yr^{-1}. *Rhee et al.* (2006b) estimated the budget with a top-down isotopic approach, whereas *Price et al.* (2007), *Pieterse et al.* (2011), *Yashiro et al.* (2011) and *Yver et al.* (2011a) used global chemistry models. The models of *Price et al.* (2007) and *Pieterse et al.* (2011) included isotope chemistry. Estimates by *Hauglustaine and Ehhalt* (2002), *Sanderson et al.* (2003), *Xiao et al.* (2007) and *Bousquet et al.* (2011) are not included in this table because of space limitations.

	Novelli et al. (1999)	*Rhee et al.* (2006b)	*Price et al.* (2007)	*Ehhalt and Rohrer* (2009)	*Pieterse et al.* (2011)	*Yashiro et al.* (2011)	*Yver et al.* (2011a)
Sources							
CH_4 oxidation	26 ± 9	64 ± 12	24.5	23 ± 8	37.3	38–39	46.5 ± 0.2
NMHC oxidation	14 ± 7	incl. above	9.8	18 ± 7	incl. above	incl. above	incl. above
Fossil fuels	15 ± 10	15 ± 6	18.3	11 ± 4	17.0^{+3}_{-6}	15.1–15.4	18.5
Biomass burning	16 ± 5	16 ± 3	10.1	15 ± 6	15.0 ± 5	8–15	7.8
Biofuels	incl. above	incl. above	4.4	incl. above	incl. above	incl. above	incl. above
N_2 fixation land	3 ± 1	6 ± 5	0	3 ± 2	3.0 ± 3	3	9.4
Oceans	3 ± 2	6 ± 5	6.0 ± 3	6 ± 3	5.0^{+1}_{-2}	6	incl. above
Sinks							
Soil deposition	56 ± 41	88 ± 11	55 ± 8	60^{+30}_{-20}	55.8	$57–60 \pm 12$	58.8 ± 9
Oxidation by OH	19 ± 5	19 ± 3	18	19 ± 5	22.1	17–18	18.2 ± 0.4

is decomposed by the following three reactions:

$$\begin{aligned} HCHO + OH &\rightarrow HCO + H_2O && (1.1)\\ HCHO + h\nu &\rightarrow HCO + H && (1.2)\\ &\quad ``radical\ channel" \\ HCHO + h\nu &\rightarrow CO + H_2 && (1.3)\\ &\quad ``molecular\ channel" \end{aligned}$$

From these three reactions we can see that the amount of H_2 formed from the HCHO depends on the fraction of the HCHO that undergoes photolysis instead of reacting with OH, and on the quantum yield of the molecular channel (eqn. 1.3). *Novelli et al.* (1999) estimated, with a calculation along the lines of *Warneck* (1988) that involved assumptions about the global burden of CH_4, average χ(OH), the photolyzed fraction of HCHO and the mean quantum yield of eqn 1.3, that this process produces 26 ± 9 Tg H_2 per year in the troposphere. *Ehhalt and Rohrer* (2009) updated this value to 23 ± 8 Tg yr^{-1}.

The oxidation of Non-Methane HydroCarbons (NMHCs) also starts by an initial reaction with a radical, followed by a chain of reactions that eventually forms the intermediate HCHO, which is then decomposed according to reactions 1.1-1.3. The production of H_2 by NMHC oxidation is harder to quantify as emission estimates for NMHCs are more uncertain than for CH_4 and their chemistry is more complex. *Ehhalt and Rohrer* (2009) estimated a gobal production of 18 ± 7 Tg H_2 yr^{-1}, adding up to a total of 41 ± 11 Tg H_2 yr^{-1} for all photochemical sources. This is in reasonable agreement with recent model studies by *Yashiro et al.* (2011) and *Yver et al.* (2011a), and also with a model study by *Pieterse et al.* (2011) (see Table 1.1), whose reaction scheme was based on an extensive evaluation of the CH_4 and NMHC oxidation pathways (*Pieterse et al.*, 2009, see also section 1.2.1).

Combustion sources

In combustion processes, H_2 is co-emitted with CO. Since the CO-cycle has been studied more, estimates of H_2 emissions by fossil fuel combustion are usually based on CO emissions, multiplied with H_2:CO emission ratios. The H_2:CO emission ratio for vehicles seems better known than the ratio for other fossil fuel combustion processes (industrial processes and domestic heating). *Ehhalt and Rohrer* (2009) assigned H_2:CO ratios of 0.5 ± 0.1 to vehicle emissions and 0.2 ± 0.15 to others, and arrived at a total source estimate of 11 ± 4 Tg H_2 yr^{-1}, which is lower than the other estimates of this source (see Table 1.1). Presently, these quantities are likely changing. CO emissions from vehicles are subject to more and more stringent emission regulations, and recent studies show that in the developed world, the H_2:CO ratio may be increasing due to changes in the vehicle fleet and/or driving conditions (*Hammer et al.*, 2009; *Bond et al.*, 2010; *Grant et al.*, 2010b; *Popa et al.*, 2011). On the other hand, *Vollmer et al.* (2012) investigated H_2 and CO emissions from combustion sources other than gasoline cars, and found lower H_2:CO emission ratios.

H_2 emissions from biomass burning are sometimes also estimated by scaling to CO, but most estimates have been made by multiplying an estimate of the total amount of burned material by an emission factor. Both the amount of burned material and the emission factors have large uncertainties; *Ehhalt and Rohrer* (2009) arrive at an uncertainty of $\pm$ 6 Tg H_2 yr^{-1} for their 15 Tg H_2 yr^{-1} estimate. Their estimate is quite similar to the other estimates in Table 1.1, with the exception of the estimate by *Yver et al.* (2011a).

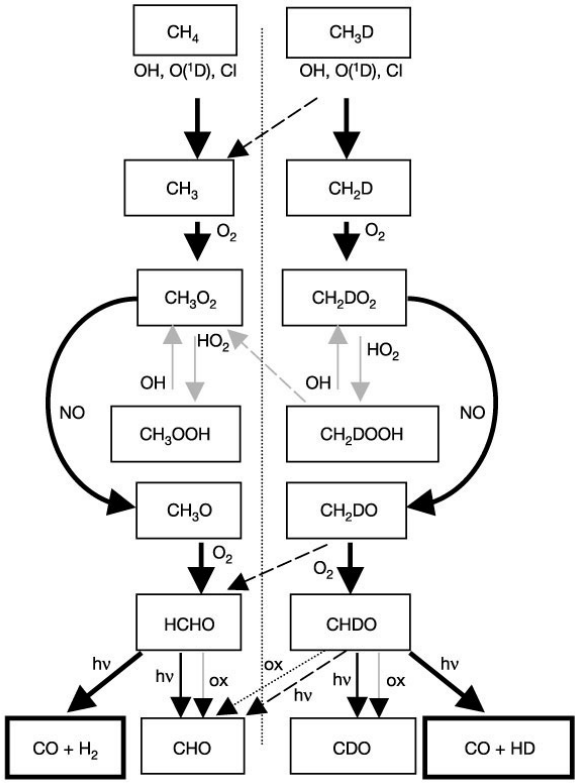

Figure 1.2: A schematic representation of the reaction chain from CH_4 (left) and deuterated methane (CH_3D) (right) to H_2, taken from *Rahn et al.* (2003).

Microbial sources

H_2 is a by-product of several bacterial processes, of which the most important are fermentation and the fixation of N_2 by bacteria in the root nodules of leguminous plants. The bacteria generally recycle a large part of this H_2, but *Conrad and Seiler* (1979) showed that significant amounts are released to the atmosphere from soils. They proceeded to measure the H_2 production rates at two field stations in Germany, and scaled them up to an estimate of 2.4–4.9 Tg H_2 yr^{-1} for the global production of H_2 by N_2 fixers on land (*Conrad and Seiler*, 1980). This estimate is the basis of most estimates of this source. *Rhee et al.* (2006b) found a larger value in their isotope budget analysis, and *Yver et al.* (2011a) reported the largest value so far (9.4 Tg H_2 yr^{-1}) in a variational inversion study, so the original estimate could be too low. Very few field measurements have been performed to refine the estimate.

In the 1970s, it was observed that ocean surface waters were supersaturated with H_2. This H_2 is likely produced by nitrogen-fixating bacteria in the ocean, but this was not tested. *Schmidt* (1974) estimated a global source strength of 4 Tg H_2 yr^{-1}, but more

recent estimates are higher, and still associated with large uncertainties (*Price et al.*, 2007; *Ehhalt and Rohrer*, 2009).

Sinks

A unique feature of the tropospheric H_2 budget compared to the budget of other long-lived trace gases is that the H_2 budget is so dominated by the soil uptake term. It is also the most uncertain term in the literature, as making a global estimate requires scaling up from many different ecosystems and soil types. Work by *Conrad and Seiler* (1981) suggested that in the soil, most of the H_2 is probably decomposed by abiontic enzymes of uncertain origin, and not by living microbial organisms. However, *Constant et al.* (2010) found indications that bacteria might play a bigger role, so the exact details of the process remain unresolved. The uptake rate depends on soil temperature and soil moisture; moisture seems the most important factor of the two in field experiments (*Smith-Downey et al.*, 2006; *Schmitt et al.*, 2009; *Ehhalt and Rohrer*, 2009, 2011, and references therein). The rates also depend on soil characteristics and snow cover. A number of field studies of the uptake rate have been performed, but the coverage is not global (*Smith-Downey et al.*, 2008; *Lallo et al.*, 2008; *Ehhalt and Rohrer*, 2009; *Hammer and Levin*, 2009; *Schmitt et al.*, 2009).

Most model studies use rather crude parameterizations for the soil uptake rates, though some take soil moisture and temperature (*Yashiro et al.*, 2011) or ecosystem type and soil moisture into account (*Sanderson et al.*, 2003; *Pieterse et al.*, 2011). The estimated magnitudes of the soil uptake term vary between 55 (*Price et al.*, 2007) and 85 Tg H_2 yr^{-1} (*Xiao et al.*, 2007) in the model studies, and these values have large uncertainties. *Rhee et al.* (2006b) arrived at 88 ± 11 Tg H_2 yr^{-1} by interpreting isotope measurements, but the most recent model studies suggest that the lower values are more likely (*Pieterse et al.*, 2011, 2012; *Yashiro et al.*, 2011; *Yver et al.*, 2011a).

The smaller sink term, oxidation by OH, is better constrained. It is a second-order reaction:

$$OH + H_2 \rightarrow H_2O + H \tag{1.4}$$

of which the rate constant is well-established (*Sander et al.*, 2006). The uncertainty, therefore, depends mostly on the uncertainties in the used OH field.

1.1.3 Temporal and spatial variation in H_2

The most comprehensive dataset of $\chi(H_2)$ observations was published by *Novelli et al.* (1999), who collected these data from the NOAA/GMD flask sampling network. This dataset provides much information about the global distribution of H_2 and regional differences in the H_2 cycle. The globally averaged $\chi(H_2)$ was 548 ± 6 ppb (nmole/mole, calculated to the latest $\chi(H_2)$ scale developed by *Jordan and Steinberg* (2011)). The largest annual averages of $\chi(H_2)$ were found in the southern tropics. The annual averages decreased slightly towards the Antarctic, and much more steeply towards the Arctic (Figure 1.3). This gradient is mostly a result of the seasonal minima; while the seasonal maxima are similar across the globe, the seasonal minima are deeper in the Northern Hemisphere (NH) than in the Southern Hemisphere (SH), as can be observed in Figure 1.4. This is a result of the larger total land area on the NH, where H_2 is deposited to the soil. The soil uptake also explains the timing of the seasonal cycle on the NH, with a maximum in spring (before the season with maximum soil uptake starts) and a minimum in early autumn (at the end of the season with maximum soil uptake). In the SH, the maximum is shifted towards

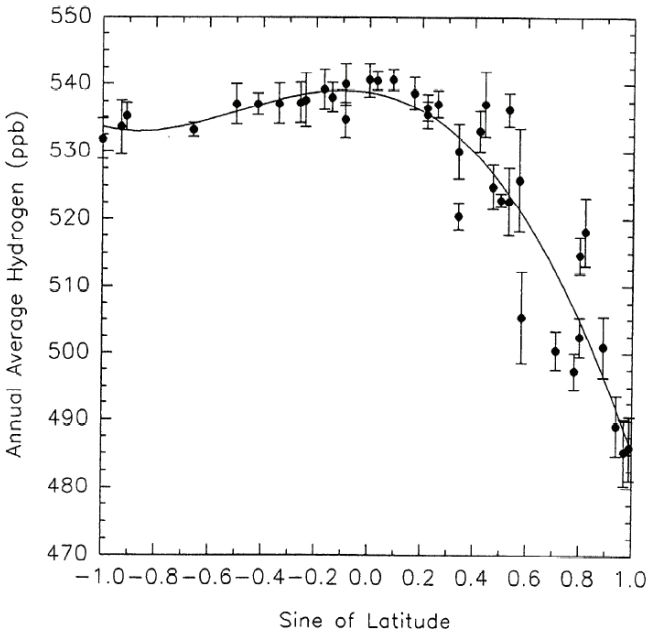

Figure 1.3: Annually averaged gradient during 1992-1995 based on samples from 50 globally distributed locations presented by *Novelli et al.* (1999). Error bars represent standard deviation of the annual means.

(austral) summer, and the minimum is in late winter. In all, this difference in the largest sink term leads to an $\approx$ 3 % larger H_2 burden in the SH than in the NH.

Since H_2 is produced from the oxidation of CH_4, of which the levels have been rising since the Industrial Revolution (although with varying rates), and since it is also produced from fossil fuel combustion, which is steadily increasing as well, one may expect to see an increase in $\chi(H_2)$. *Khalil and Rasmussen* (1990) reported an increasing trend of 3.2 ± 0.5 ppb yr^{-1} in $\chi(H_2)$ time series that they had collected from six latitudinally distributed sites. Later studies (*Novelli et al.*, 1999; *Simmonds et al.*, 2000) found either a negative or a smaller trend, however, and there is currently no clear and universally accepted evidence that there is a long-term $\chi(H_2)$ trend (*Ehhalt and Rohrer*, 2009).

The vertical gradient of $\chi(H_2)$ in the troposphere was measured in several studies, of which the most extensive are the ones by *Ehhalt et al.* (1977), *Schmidt* (1978) and NOAA/GMD (*Price et al.*, 2007). These data indicate that on average, the vertical gradients of $\chi(H_2)$ are weak. Some stronger (positive or negative) gradients can occur in the boundary layer, as a result of local sources and sinks. Especially at NH continental sites, vertical gradients of tens of ppb's are found with the lower $\chi(H_2)$ values at the ground as a result of soil uptake. These gradients are also found in model studies by *Hauglustaine and Ehhalt* (2002) and *Pieterse et al.* (2011) (see left pane of Figure 1.5). The vertical profile of H_2 in the stratosphere seems relatively uniform.

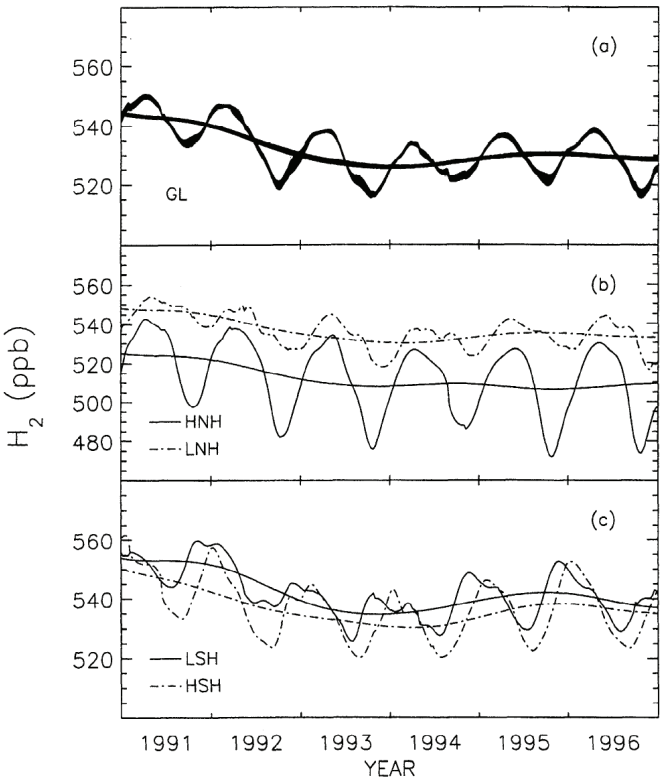

Figure 1.4: Zonally averaged time series and fitted trend presented by *Novelli et al.* (1999). (a) Global average with shading to indicate the uncertainty, (b) Averages for the high Northern Hemisphere (HNH, 45-90° N) and the low Northern Hemisphere (LNH, 0-45° N), (c) Averages for the low Southern Hemisphere (LNH, 0-45° S) and the high Southern Hemisphere (HSH, 45-90° S).

1.1.4 Possible consequences of large scale H_2 production associated with a ``hydrogen economy''

H_2 can be burnt cleanly to H_2O, and is therefore an attractive energy carrier, especially to power vehicles. Use of H_2 as an energy carrier may improve air quality, at least locally, and if it is made with energy generated in carbon-free processes, it will help reducing the emissions of carbon dioxide (CO_2). H_2 is, however, extremely volatile and some leakage of H_2 during production, transport, storage and use is inevitable. This may become a significant source of H_2 to the atmosphere. What the magnitude of this source will be depends on the technology that will be used and on the extent to which H_2 will replace fossil fuels. Both are at present difficult to predict. Different authors arrive at different estimates, from best-case estimates of 7–50 Tg yr^{-1} (*Schultz et al.*, 2003) to worst-case

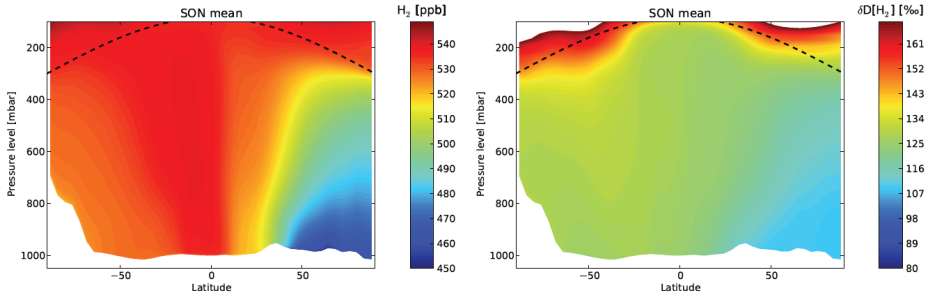

Figure 1.5: September-November (SON) zonal means of $\chi(H_2)$ (left) and δD (right) calculated by *Pieterse et al.* (2011). In this season, the modeled vertical $\chi(H_2)$ gradient in the NH extratropics is strongest as a result of the strong deposition to soil during summer. The δD gradient is small in this season.

estimates of 120 Tg yr^{-1} (*Tromp et al.*, 2003) or even more than 300 Tg yr^{-1} (*Warwick et al.*, 2004). When this is compared to the terms of the natural sources in the H_2 budget (Table 1.1), a significant increase of atmospheric H_2 levels seems possible. This has raised concerns that revolve around two subjects: the effect additional H_2 may have on stratospheric ozone chemistry and the effect of increased H_2 levels on the oxidative capacity of the atmosphere (see Figure 1.6).

The additional H_2 produced in a hydrogen economy may partly end up in the stratosphere. Here, it is oxidized to H_2O and could make the stratosphere more moist. This moistening of the stratosphere would contribute to the formation of Polar Stratospheric Clouds (PSCs), by cooling the stratosphere and by providing more substrate for PSC formation. Ozone is destroyed on PSCs. Modeling results from *Tromp et al.* (2003) indicate that this could affect the (recovery of the) ozone layer substantially (Figure 1.7), but this work was much criticized, especially for using very high H_2 leakage estimates (*Kammen et al.*, 2003). *Warwick et al.* (2004) found a much smaller increase of stratospheric H_2O than *Tromp et al.* (2003) with similar emissions, and concluded that the effect of a hydrogen economy on stratospheric ozone would likely be small. *Feck et al.* (2008) did not find a large effect either, and subsequently *Vogel et al.* (2012) concluded in a review article that the potential risks for stratospheric ozone are probably negligible.

The oxidative capacity of the atmosphere, i.e. the ability to remove greenhouse gases and other pollutants by oxidation, is largely determined by the mixing ratio of OH, the "detergent" of the atmosphere. As detailed in subsection 1.1.2, H_2 reacts with OH. Therefore, in a future with high $\chi(H_2)$ values, the reaction of H_2 with OH might reduce OH levels. This would increase the lifetimes of pollutants and greenhouse gases, indirectly causing worse air quality and an additional greenhouse effect. Of course, it is important to balance these potential negative effects against the benefits of reduced fossil fuel use for climate and air quality. Also the method chosen to produce H_2 is very important (*Jacobsen et al.*, 2005; *van Ruijven et al.*, 2007, 2008). A model study by *Schultz et al.* (2003) indicates that *if* half of the fossil fuel that is used today is replaced by H_2 generated in processes that do not produce greenhouse gases or other pollutants, this may lead to reduced climate forcing and better air quality. However, *Warwick et al.* (2004) simulated

different scenarios with different magnitudes for the H_2 emissions and the reductions of other species, and found significant variation in the outcomes for the different scenarios. It seems, therefore, that the climate and air quality effects of the introduction of an H_2 economy depend heavily on *how* it is introduced. *Jacobsen* (2008) concluded that if all H_2 is to be generated by wind power, air quality and climate will not be adversely affected.

Considering that there are still such uncertainties about the effects of leaking H_2 on both the troposphere and the stratosphere, more research is clearly needed. Likely scenarios should be identified, and assessed. This also requires a more accurate knowledge of the present-day H_2 cycle.

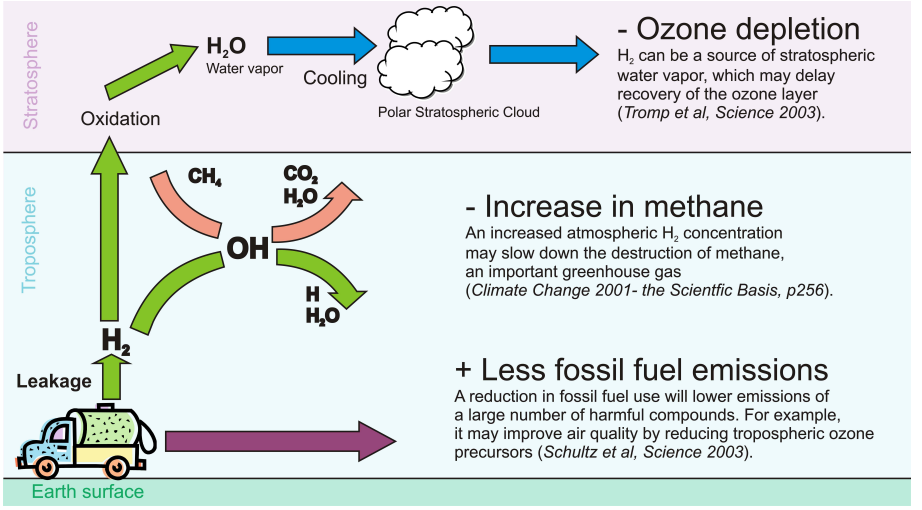

Figure 1.6: Cartoon representation of the different effects a hydrogen-powered vehicle fleet could have on the atmosphere.

1.2 The isotopic composition of H_2

In addition to mixing ratio measurements, isotope measurements provide a way to learn about the cycles of atmospheric constituents (and many other subjects that are outside the scope of this thesis). By definition, each chemical element comprises all atoms that have the same atomic number, which is the number of protons in the nucleus. Isotopes are subclasses of elements; for each element, different isotopes can exist that each comprise all atoms of that element that have the same mass number, which is the number of protons and neutrons in the nucleus. Some isotopes are unstable and decay over time while emitting ionizing radiation, and some are stable. We will only discuss stable isotopes from now on. Different isotopes of the same element display similar chemical behavior, which means that they generally undergo the same reactions and form the same chemical compounds. The molecules that are formed from atoms that differ only in isotopic compo-

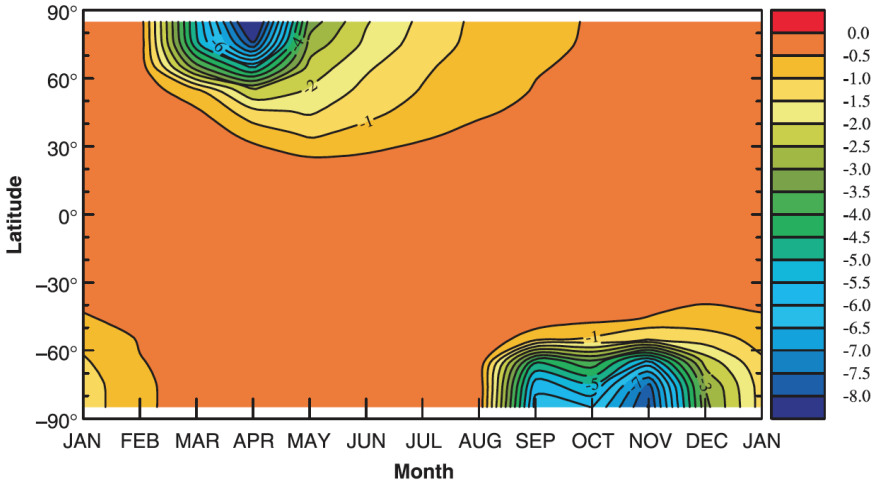

Figure 1.7: The % ozone depletion calculated by *Tromp et al.* (2003) for a scenario where $\chi(H_2)$ at the ground is increased fourfold, plotted against season and altitude.

sition, are termed isotopologues. The mass differences between the isotopes and isotopologues (and sometimes some more complicated quantum mechanical effects), however, cause differences in the speeds or the equilibrium states of the reactions for the different isotopologues that are generally specific for the type of reaction. Organisms often have a preference for certain isotopologues. Different processes can therefore alter the isotopic composition of the various reservoirs of an element in specific ways. It is these effects that make stable isotopes useful in atmospheric research. For example, the isotopologues of H_2O contain much information about the hydrological cycle, and the isotopologues of CO_2 contain information about carbon processing by the biosphere and CO_2 uptake by different reservoirs (*Brand and Coplen*, 2012).

The element hydrogen (H) has two stable isotopes, the "light" isotope protium or "ordinary" hydrogen (H or ^{1}H), and the "heavy" isotope deuterium (D or ^{2}H) (we do not discuss the unstable isotope tritium here). The nucleus of the light hydrogen consists of one proton only, whereas deuterium has an extra neutron that approximately doubles the atomic mass. Molecular hydrogen (H_2) can therefore exist as the "light" HH, the "deuterated" HD or the doubly deuterated DD. Since DD is very rare, it is neglected in the rest of this thesis.

The isotopic composition of a substance is usually expressed as the ratio of the heavy isotope over the light isotope. Because this is often a very small number, and because the isotopic measurement techniques that have been used most so far are able to measure differences in ratios with respect to another material more accurately than absolute ratios, this ratio is commonly expressed in isotopic "δ"-notation. For molecular hydrogen, the isotopic composition, or deuterium content, is then expressed as:

$$\delta\mathrm{D}(\mathrm{H_2}) = \left(\frac{R_{Sample}}{R_{VSMOW}} - 1\right) \cdot 1000‰ = \left(\frac{\left(\frac{\mathrm{D}}{\mathrm{H}}\right)_{Sample}}{\left(\frac{\mathrm{D}}{\mathrm{H}}\right)_{VSMOW}} - 1\right) \cdot 1000‰ \qquad (1.5)$$

where $R_{Sample} = (D/H)_{Sample}$ is the ratio of the number of D atoms to the number of H atoms in the H_2 of the sample, and $R_{VSMOW} = (D/H)_{VSMOW}$, is this ratio in Vienna Standard Mean Ocean Water (VSMOW), the standard material for D/H ratios. The D/H ratio in VSMOW is (155.76 ± 0.08) ppm (*de Wit et al.*, 1980; *Gonfiantini et al.*, 1993). Positive $\delta D(H_2)$ values mean that there is relatively more D in the H_2 of a sample than in VSMOW, negative $\delta D(H_2)$ values mean that there is relatively less D in the H_2 of a sample than in VSMOW. For brevity, δD will be used instead of $\delta D(H_2)$ in most of this thesis. δ-values are dimensionless, but because they are small, they are usually written in ‰. The term "1000‰" (=1) is explicitly included in equation 1.5 to stress the difference with a previously used definition of δ-values that included a factor 1000 ($\neq$1).

1.2.1 Isotope effects in the sources and sinks of H_2

Because HH and HD have a large relative mass difference ($\approx$ 50 %), the isotope effects in the H_2 cycle are particularly large. Table 1.2 and Figure 1.8 list the δD values of H_2 produced by different sources and the fractionation effects of the different sinks, which are discussed below.

Oxidation sources

It was postulated from tropospheric budget considerations that H_2 produced from CH_4 oxidation would be enriched in D (*Gerst and Quay*, 2001), but this was first observed in the stratosphere during a research aircraft campaign by *Rahn et al.* (2003) and during a balloon campaign by *Röckmann et al.* (2003). In the stratosphere, H_2 is only produced or destroyed by oxidation processes, which can thus be studied without interference from surface processes. Both *Rahn et al.* (2003) and *Röckmann et al.* (2003) observed δD values from normal tropospheric levels ($\approx$ +130 ‰) to extremely high values of +400 ‰. After analysis with box models, they concluded that during CH_4 oxidation, deuterium is concentrated in the product H_2. *Röckmann et al.* (2003) calculated a source signature of (+180 ± 50) ‰ for H_2 that is photochemically produced near the tropopause, in agreement with the calculations of *Rahn et al.* (2003), and argued that this range should also be representative of the troposphere. This signature changes higher up in the stratosphere, as the relative reaction rates change with changing temperature and pressure, and the isotopic composition of the source CH_4 changes as well. *Rhee et al.* (2006a) estimated from these and additional balloon measurements that H_2 produced by CH_4 oxidation has a source signature of (+310 ± 60) ‰ in the stratosphere and (+190 ± 50) ‰ in the troposphere, but *Mar et al.* (2007) indicated with a 2D model that these values could vary considerably with latitude and altitude and that the uncertainties could be larger than the estimates by *Rhee et al.* (2006a). *Price et al.* (2007) estimated a source signature of (+162 ± 57) ‰ by budget closure with a global chemistry transport model, which agrees well with the previous estimates.

Several reaction chamber experiments have been performed to study the fractionation effects in the different steps of the oxidation chain (Figure 1.2). Photolysis of the intermediate formaldehyde was shown to proceed faster for the light than for the deuterated species (*Feilberg et al.*, 2007; *Rhee et al.*, 2008; *Röckmann et al.*, 2010b). This is also the case for the initial abstraction of a hydrogen atom from CH_4 (*Sander et al.*, 2006). This must be compensated by D-enriching effects in other steps in the chain, as was shown to be the case for the reaction of the methoxy radical (CH_3O) with oxygen (O_2) to formaldehyde

Table 1.2: Estimates of the terms in the global H_2 budget and their isotopic signature by different authors.

	Rhee et al. (2006b)		*Price et al.* (2007)		*Pieterse et al.* (2011)	
Sources	Magnitude [Tg yr^{-1}]	Source signature [‰]	Magnitude [Tg yr^{-1}]	Source signature [‰]	Magnitude [Tg yr^{-1}]	Source signature [‰]
CH_4 oxidation	64 ± 12	+190	24.5	$+162 \pm 57$	37.3	+116
NMHC oxidation	incl. above	incl. above	9.8	$+162 \pm 57$	incl. above	incl. above
Fossil fuels	15 ± 6	-270	18.3	-196	17.0^{+3}_{-6}	-196^{+10}_{-74}
Biomass burning	16 ± 3	-90	10.1	-290	15.0 ± 5	-260 ± 60
Biofuels	incl. above	incl. above	4.4	-290	incl. above	incl. above
N_2 fixation land	6 ± 5	-700	0		3.0 ± 3	-628^{+0}_{-72}
Oceans	6 ± 5	-700	6.0 ± 3	-628	5.0^{+1}_{-2}	-628^{+0}_{-72}
Sinks	Magnitude [Tg yr^{-1}]	Fractionation factor (k_{HD}/k_{HH})	Magnitude [Tg yr^{-1}]	Fractionation factor (k_{HD}/k_{HH})	Magnitude [Tg yr^{-1}]	Fractionation factor (k_{HD}/k_{HH})
Soil deposition	88 ± 11	0.943 ± 0.007	55 ± 8	0.943	55.8	0.925
Oxidation by OH	19 ± 3	0.58 ± 0.07	18	0.568	22.1	0.542

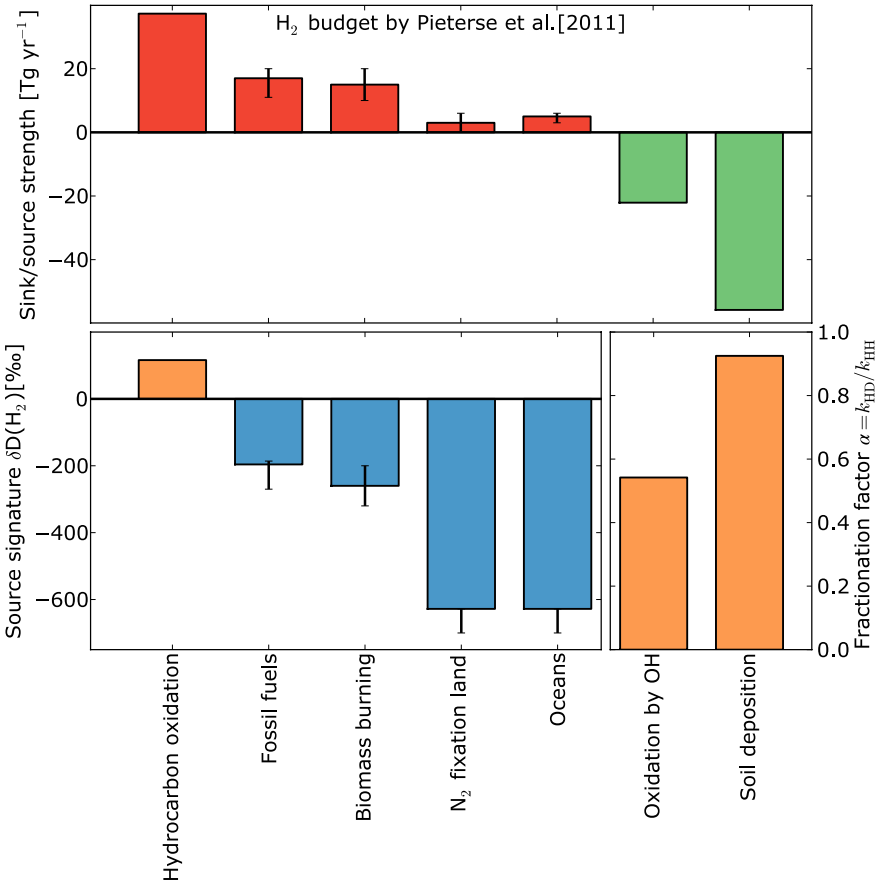

Figure 1.8: Estimate of the terms in the global H_2 budget and isotopic signatures from *Pieterse et al.* (2011). In the upper pane, red indicates sources and green indicates sinks. In the lower pane, blue indicates terms with a D-depleting effect on the ambient H_2 reservoir, and orange indicates terms with a D-enriching effect.

(*Nilsson et al.*, 2007). Reaction chamber measurements also showed a that some isotope effects in the chain are dependent on pressure (*Nilsson et al.*, 2010).

Pieterse et al. (2009) developed the most extensive hydrogen isotope chemistry scheme for the oxidation of hydrocarbons in models and incorporated this in global model TM5. The first results of this model indicated a relatively low tropospheric source signature of +116 ‰ (*Pieterse et al.*, 2011), which is still in the range of the results of *Price et al.* (2007). *Pieterse et al.* (2011) also claimed that although oxidation processes are the largest H_2 source, they do not affect ambient δD much, because their source signature is close to ambient δD values.

Combustion sources

It has been known since the 1960s that the H_2 produced from fossil fuel combustions is depleted by hundreds of ‰ (*Begemann and Friedman*, 1959; *Gonsoir and Friedman*, 1962; *Gonsoir et al.*, 1963, 1966; *Ehhalt et al.*, 1963, 1966). *Gerst and Quay* (2001) measured samples from the Seattle region that experienced different degrees of urban pollution, and found a source signature of (-196 ± 10) ‰ for fossil fuel combustion. *Rahn et al.* (2002b) sampled at different locations in California and directly from car exhaust, and found a source signature of -270 ‰. Wit a test bench setup with a modern vehicle engine, *Vollmer et al.* (2010) found relatively high δD values in the exhaust gas before passage through a three-way catalytic converter (-140 to -195 ‰) and very low δD values after (-270 to -370 ‰). They also found a dependence on driving conditions, and claimed that temporal, geographical and seasonal variations in δD of H_2 from fossil fuel burning are well possible. *Vollmer et al.* (2012) published δD measurements from the exhausts of different domestic heaters and waste incinerators. δD values as low as -206 ‰ and -357 ‰ were observed in the exhaust H_2 of heaters and waste incinerators, respectively.

Gerst and Quay (2001) also measured the δD of H_2 emitted during the combustion of pine branches and needles, and on that basis, estimated that the global source signature of biomass burning should be -290 ± 60 ‰. *Rhee et al.* (2006b) arrived at a much higher estimate (-90 ‰) by an isotopic "top-down" approach applied on samples from the free troposphere. Recent results indicate that the lower estimate is the more likely (*Röckmann et al.*, 2010a; *Haumann et al.*, 2012). *Röckmann et al.* (2010a) also showed that the source signature varies with combustion efficiency, and with the deuterium content of the local precipitation.

Microbial sources

H_2 from microbial sources is the most D-depleted, as it is close to the value for the thermodynamic isotopic equilibrium between H_2 and H_2O. *Bottinga* (1969) calculated that this equilibrium value ranges from -752 to -693 ‰ for temperatures between 0 and 40° C. *Rahn et al.* (2002b) observed a δD value of -778 ‰ in the headspace of a jar with termites, and a δD value of -690 ‰ in the headspace of a jar with water from a eutrophic pond. *Price et al.* (2007) and *Pieterse et al.* (2011) used a measured value of -628 ‰. *Walter et al.* (2011) investigated H_2 produced by different cultures of organisms during the fermentation of different substrates, and found an overall signature of (-741 ±13) ‰. This extreme source signature means that, although microbial H_2 production is only a small term in the H_2 budget (Table 1.1 and 1.2), it can have a large influence on the isotope budget, especially on local scales.

Sinks

Both sinks of H_2, deposition to soils and destruction by OH, preferentially remove light hydrogen, so that under the influence of the sinks, the remaining H_2 reservoir becomes more enriched. The strength of this isotope effect differs strongly between the two processes, and is usually expressed as a fractionation factor α, the ratio of the removal rate of the isotopically heavy species to the removal rate of the isotopically light species ($\alpha = k_{HD}/k_{HH}$).

For the deposition to soils, *Gerst and Quay* (2001) found an α_{soil} of 0.943 ± 0.024, *Rahn et al.* (2002a) found 0.94 ±0.01, and *Rice et al.* (2011) found 0.943 ± 0.005 with considerable variability. While these values are close together, it should be noted that

they are only based on measurements around Seattle and in Alaska. Measurements at other locations would be desirable to verify if the average of these values can be used for the global soil sink.

The fractionating effect of removal by OH is much stronger. According to results of *Talukdar et al.* (1996), α_{OH} is 0.57 at 20° C, in reasonable agreement with the 0.61 ± 0.02 found by *Ehhalt et al.* (1989). An analysis by *Pieterse et al.* (2011) shows that because of this, removal by OH has in general a larger effect on the isotope reservoir than soil deposition, despite removing less H_2.

1.2.2 Environmental observations of $\delta D(H_2)$

Troposphere

A number of studies of δD were made in the 1960s and 70s (*Friedman and Scholz*, 1974; *Kaye*, 1987, and references therein), often together with studies of the tritium content of H_2. These measurements often had to be corrected for incomplete collection efficiency, which caused a limited precision. Nevertheless, it could be concluded that background H_2 was enriched in D with respect to water. With an improved technique, *Gerst and Quay* (2000) measured samples from two North-American stations and a Pacific research cruise. From these measurements, they calculated a global average δD of $(+130 \pm 4)$ ‰. The average in the NH $(+123 \pm 3)$ ‰ was slightly lower than the SH average $(+138 \pm 8)$ ‰ (Figure 1.9). A similar gradient was found by *Rice et al.* (2010) in data from six Pacific Ocean transects.

Rhee et al. (2006b) presented data from three commercial aircraft flights in the free troposphere. From this, they extrapolated seasonal cycles for the NH and SH. In the NH, the seasonal cycles of $\chi(H_2)$ and δD were out-of-phase, in line with a situation where H_2 from depleted sources accumulates over winter, and H_2 is taken up strongly during summer (which enriches the remaining reservoir, as explained in section 1.2.1). In the SH, the seasonal cycles of $\chi(H_2)$ and δD were smaller and in phase, which indicates a relatively smaller role for the sinks and important roles for photochemical production and exchange with the NH. The hemispheric averages of the upper tropospheric observations of *Rhee et al.* (2006b) do not show a large difference with the ground hemispheric averages of *Gerst and Quay* (2000). *Rice et al.* (2010) observed the smallest hemispheric gradient during their September–October and November cruises, and the largest during the April cruise, which is in agreement with the seasonal cycles of *Rhee et al.* (2006b).

Together, the data collected by *Gerst and Quay* (2000), *Rhee et al.* (2006b) and *Rice et al.* (2010) provide important information on the distribution of δD, but these data are too sparse to fully characterize the spatial and temporal variation in tropospheric δD.

Stratosphere

A stratospheric research aircraft campaign (*Rahn et al.*, 2003) and stratospheric balloon campaigns (*Röckmann et al.*, 2003; *Rhee et al.*, 2006a) have shown extreme D-enrichments of H_2 in the stratosphere. In the observed altitude range (up till $\approx$ 33 km), this enrichment increases with altitude above the tropopause and reaches values up to +460 ‰. This is a result of the isotope effects in the two processes that affect H_2 in the stratosphere; production by CH_4 oxidation and removal by oxidation by OH. Both these processes have an enriching effect on the H_2 reservoir (see section 1.2.1). Because these processes have almost the same magnitude, $\chi(H_2)$ does not change much in the strato-

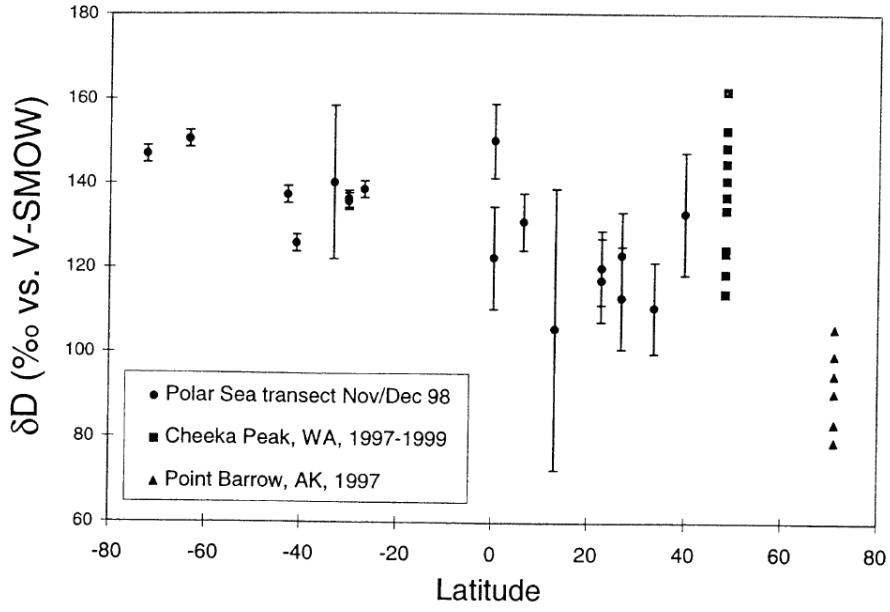

Figure 1.9: The latitudinal gradient of δD presented by *Gerst and Quay* (2000), based on samples from a Pacific Ocean transect and from the Cheeka Peak (48° N) and Point Barrow (71° N) observatories.

sphere (Figure 1.10). The strong enrichment of stratospheric H_2 means that stratosphere-troposphere exchange (STE) of H_2 has an enriching effect on the tropospheric H_2 reservoir, even while this does not affect tropospheric $\chi(H_2)$ much (*Pieterse et al.*, 2011, see section 1.2.3).

Plumb (2007) found that very compact correlations exist between species with long lifetimes with respect to stratospheric transport times. For lack of variation in $\chi(H_2)$ such a relation cannot be observed between $\chi(H_2)$ and other species, but such correlations do occur for δD. Both *Rahn et al.* (2003) and *Röckmann et al.* (2003) found a compact correlation between δD and CH_4 (Figure 1.10). *McCarthy et al.* (2004) used *Rahn et al.* (2003)'s correlation in a calculation of the deuterium content of water vapor in the stratosphere, and this correlation also has applications in chemical models.

1.2.3 δD(H_2) in models

Isotope measurements can provide extra constraints for models that are used to study the global budget of a compound. In this way, the uncertainties on the different terms in the budget can be reduced. So far, two global chemistry transport models have been adapted to model δD, in order to constrain the budget of H_2. The first of these models is the GEOS-Chem model used by *Price et al.* (2007). The δD results of this model were compared to data from two North-American stations, and several Pacific Ocean transects

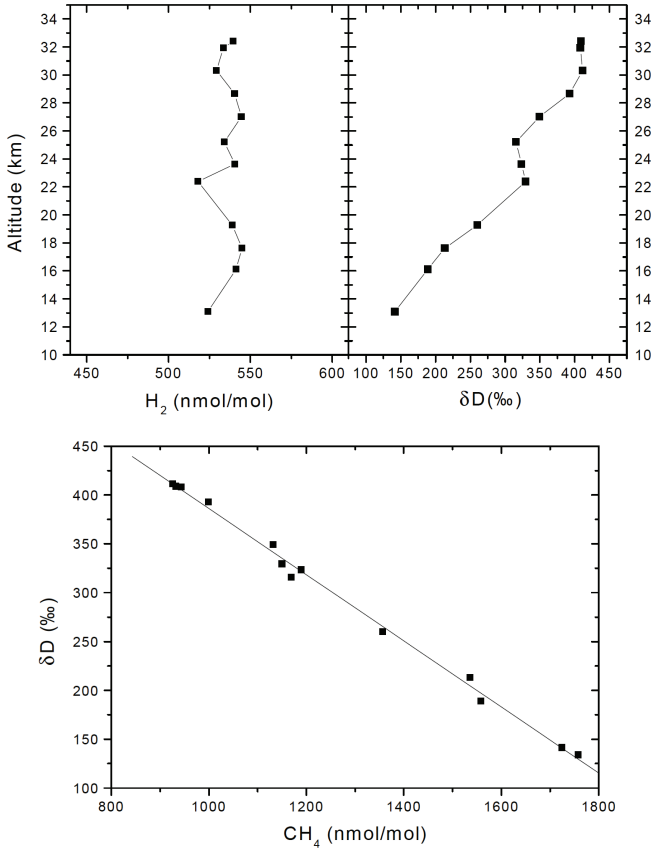

Figure 1.10: Figures from *Röckmann et al.* (2003) that illustrate the general features of $\chi(H_2)$ and $\delta D(H_2)$ in the stratosphere. Upper panes: altitude profiles of $\chi(H_2)$ and δD. Lower pane: δD plotted against methane mixing ratio ($\chi(CH_4)$).

(*Gerst and Quay*, 2000; *Rice et al.*, 2010, and other data). A reasonable agreement with these data was obtained, but the study was limited by the small number of δD observations. Sensitivity runs showed that STE contributed on average +37 ‰ to tropospheric δD values, and yielded an estimate for δD of H_2 from photochemical sources of $(+162 \pm 57)$ ‰, as well as constraints on the soil sink and the microbial ocean source.

The second of these models is TM5, which is the first to contain an explicit isotope reaction scheme for photochemical H_2 production (*Pieterse et al.*, 2009, 2011). For stratospheric δD, a parametrization relative to CH_4 was used, based on (*McCarthy et al.*, 2004). The modelled δD was compared with δD measurements from ship cruises (*Rice et al.*, 2010) and from six latitudinally distributed stations (*Batenburg et al.*, 2011, also included in this thesis, see chapter 2). The model captured $\chi(H_2)$ patterns well, but produced δD values that were biased low with respect to the observations. This bias could be resolved

by adjusting the parameters within their uncertainty range, but with the flip side that the isotope budget could not be uniquely constrained (Figure 1.11). The calculated source signature for photochemical production was +116 ‰, which is lower than other estimates, but still in agreement with the results of *Price et al.* (2007). Sensitivity runs showed that because of this signature is so close to the reservoir δD, photochemical production has only a small effect on ambient δD despite being a large source. The STE contribution to tropospheric δD was modeled to be +29 ‰, and was shown to be highly sensitive to the δD assumed for the stratosphere (an increase of 20 ‰ in the stratospheric parameterization caused an average 12 ‰ increase in the troposphere) (Figure 1.11). *Pieterse et al.* (2012) adapted TM5 for the new $\chi(H_2)$ scale developed by *Jordan and Steinberg* (2011), and also updated the stratospheric δD parametrization with δD results from samples collected in the lowermost stratosphere (LMS) by a commercial aircraft (*Batenburg et al.*, 2012, also included in this theses, see chapter 3). The source and sink terms in this model had to be adjusted to fit with the new $\chi(H_2)$ data that are $\approx$ 3 % higher due to the scale change. A reduction in soil deposition yielded the most realistic results for both $\chi(H_2)$ and δD, and was therefore adopted to update the global budget. TM5 also offers the possibility to study H_2 on a regional scale.

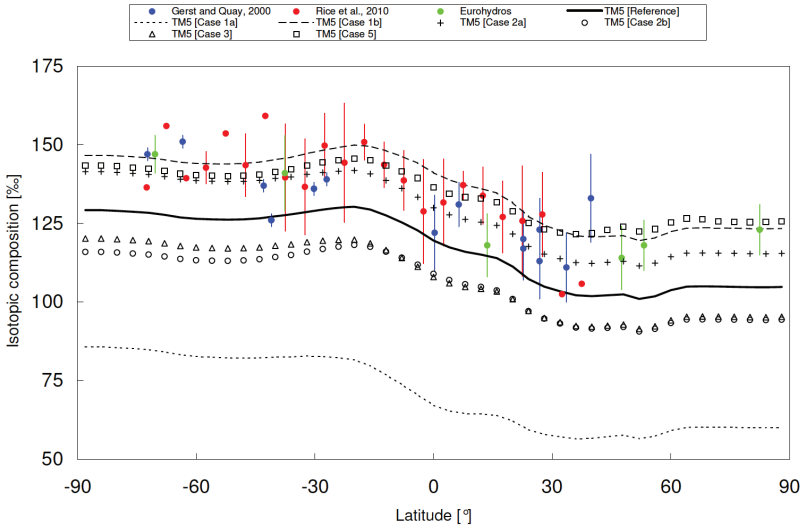

Figure 1.11: Latitudinal gradient of δD, modeled by *Pieterse et al.* (2011), with measurements from different authors. The black solid line indicates the output of the model with default parameters, other lines indicate sensitivity runs for which different parameters were varied. Case 2a (crosses) is a scenario where the stratospheric isotopic composition in increased by 20 ‰.

1.3 This thesis

In this introduction, an overview of the current state of knowledge of the atmospheric H_2 cycle was presented. Clearly, there are still large uncertainties in our understanding of the H_2 cycle, and isotope information can provide us with more information. But to be able to use the isotopes optimally, we need accurate knowledge of the isotope effects associated with different processes, and we need information on the spatial and temporal variation of δD. In this thesis, we investigate several questions related to this. We focus on:

- How does δD vary with latitude and season, and which processes drive these variations?
- What is the optimal way to describe the δD value of H_2 that is imported into the troposphere by STE?
- What is the source signature of the fossil fuel combustion source of H_2 in Northwest Europe, and how does this source affect the local to regional H_2 cycle?
- Can we find and characterize the signal of H_2 deposition to soil by measuring vertical gradients of $\chi(H_2)$ and δD in the Netherlands?

To obtain the data to answer these questions, we used a Gas Chromatography - Isotope Ratio Mass Spectrometry (GC-IRMS) system, as described by *Rhee et al.* (2004) and *Röckmann et al.* (2010a), which can analyze samples for $\chi(H_2)$ and δD routinely. Figure 1.12 shows a diagram of the system. Three new sets of $\chi(H_2)$ and δD data are presented that greatly expand the number of available δD data. These data in themselves provide information about the processes that act on H_2 on local, regional and global scales. They can also be used (and were already used) for the validation of models that model $\chi(H_2)$ and δD, and to constrain the terms in such models, thereby reducing the uncertainties in the global H_2 budget. Potentially, they could also be used in studies of the compounds that are chemically linked to H_2 (such as CH_4, H_2O, HCHO, …).

Chapter 2: Global scale spatial and temporal variability of $\chi(H_2)$ and δD

In Chapter 2, the question how $\chi(H_2)$ and δD vary with latitude and season is investigated. To this end, data were collected from six stations that are part of the EUROpean network for atmospheric HYDRogen Observations and Studies (EUROHYDROS) (*Engel*, 2009). Due to their locations on islands or at coasts, the stations Alert (Arctic Canada), Mace Head (Ireland), Cape Verde (Atlantic archipelago, $\approx$ 600 km west of Senegal and Mauritania), Amsterdam Island (Indian Ocean) and Neumayer (Antarctic coast) can all be considered as "background" stations. The continental mountain station Schauinsland (southern Germany) is a relatively "background" station, because it is usually above the planetary boundary layer and therefore experiences free tropospheric air, but it is also under local and regional influence. This particular subset of the EUROHYDROS network was chosen because it covers a large latitudinal range, with emphasis on Europe. Thus, these data provide the opportunity to study the background cycle of atmospheric H_2 and latitudinal differences therein.

We discuss the observed seasonal cycles at each station and the latitudinal gradient in $\chi(H_2)$ and δD, and we make a tentative assessment of the relative contribution of the two different sink processes (soil deposition and oxidation by OH) to the total uptake for the three coastal stations in the NH.

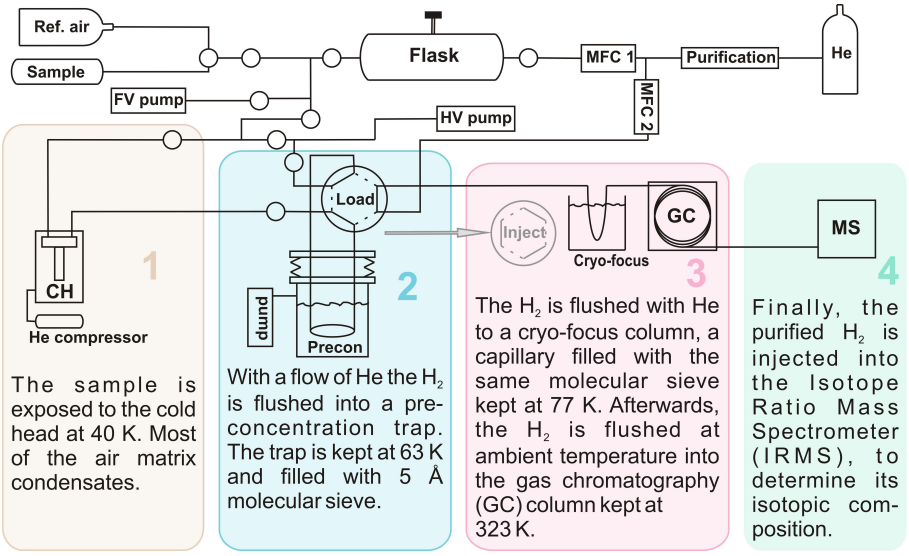

Figure 1.12: Schematic representation of the GC-IRMS system, described by *Rhee et al.* (2004) and *Röckmann et al.* (2010a), that was used to measure the $\delta D(H_2)$ values and some of the $\chi(H_2)$ values presented in this thesis. The highlighted areas represent the different steps in which the H_2 is isolated from the air sample, purified and analyzed.

Chapter 3: $\chi(H_2)$ and δD in the Upper Troposphere - Lower Stratosphere

In the next chapter, we investigate how the isotopic composition of H_2 that is imported from the stratosphere into the troposphere can best be quantified. As detailed in section 1.2.3, this is an important question for the modeling of the H_2 isotope cycle. To obtain data from the area of interest, the Upper Troposphere - Lower Stratosphere region (UTLS), samples were analyzed that were collected by the CARIBIC (Civil Aircraft for the Regular Investigation of the atmosphere Based on an Instrument Container) aircraft. The CARIBIC project uses a measurement container on board of a passenger aircraft (Figure 1.13) to make in-situ measurements and sample air and aerosol at aircraft cruise altitude (*Brenninkmeijer et al.*, 2007). The cruise altitude is generally between 9 and 12 km, which means that the aircraft regularly crosses the tropopause (TP) when flying in the extratropics. This offers a good opportunity to study the interesting region around the TP where the interaction between tropospheric and stratospheric air takes place. With the data from the samples that were collected in the LMS, we update the correlation functions between δD and $\chi(CH_4)$ and between δD en nitrous oxide mixing ratios ($\chi(N_2O)$) that can be used to parameterize δD of the H_2 that is imported to the troposphere by STE.

Studying samples from the CARIBIC aircraft has additional benefits.The CARIBIC observations are complementary to the ground station observations in that they allow us to study $\chi(H_2)$ and δD in the free troposphere, in the absence of surface sources. Another advantage of the CARIBIC project is that it offers near-global coverage. We present, for example, the first δD data that were measured in or over the Indian subcontinent.

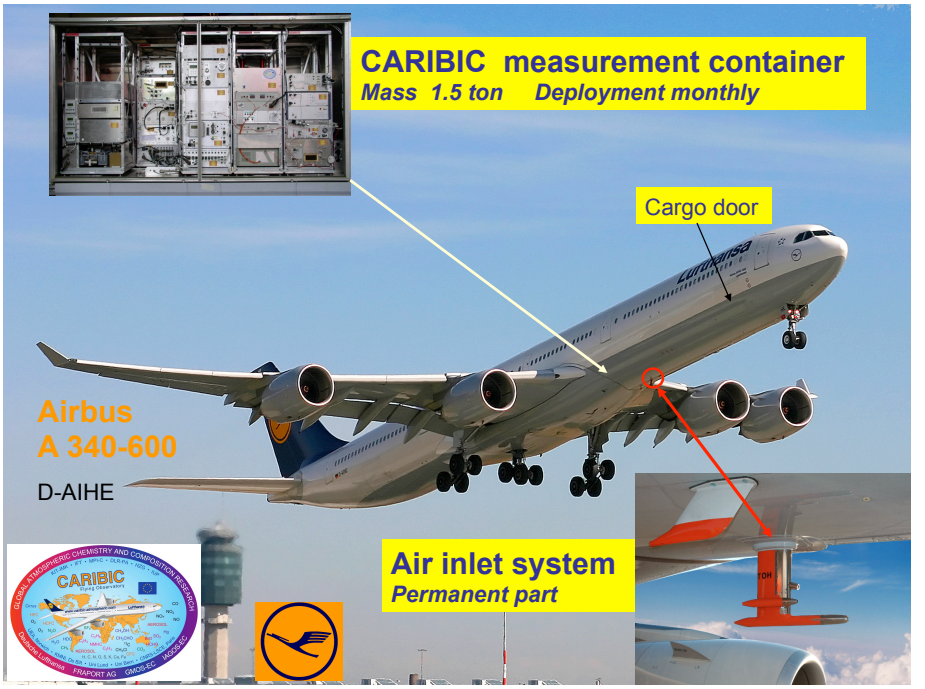

Figure 1.13: Slide by C. A. M. Brenninkmeijer that depicts the CARIBIC measurement platform. The Lufthansa-owned aircraft is equipped with a fixed air inlet system. The measurement container is installed in the cargo area for one flight per month. More materials can be found on `www.caribic-atmospheric.com`.

We discuss the general features of these data obtained in the UTLS, their geographic variation, their features and correlations with other compounds in the stratosphere and their variation in the Indian summer monsoon.

Chapter 4: The influence of anthropogenic sources and soil uptake on the H_2 cycle in the Netherlands

In Chapter 4 we investigate the anthropogenic (fossil fuel burning) sources, and how these make the H_2 cycle in a polluted region different from the H_2 cycle at background locations. We also try to find and characterize soil uptake signals. The Cabauw tall tower in the Netherlands (Figure 1.14) was chosen as the sampling location to answer these questions. This station is located in an agricultural area in the so-called "Green Heart" of the Netherlands, which is surrounded by the Randstad conurbation. Measurements of GHGs, carbon monoxide mixing ratios (χ(CO)) and $\chi(H_2)$ at four sampling heights (20, 60, 120 and 200 m) are performed (semi-)continuously at this site (*Vermeulen et al.*, 2011; *Popa et al.*, 2011). Measuring $\chi(H_2)$ and δD at this site allows us to compare data from a region that is under heavy anthropogenic influence with $\chi(H_2)$ and δD data from the

more remote locations that were studied (Chapter 2). By sampling at the different heights, different "footprints" or influence areas are probed, and a soil sink signal may be detected. Such studies can can help in assessing how future H_2 emissions might affect climate and air quality in heavily populated regions. Also, by sampling at the different heights, we have the opportunity to compare different Northwest-European influence regions.

We discuss the observed seasonal variation in the Cabauw data, contrast them with data from a background location (Mace Head), determine the δD source signature of the source mix and investigate the differences between the different sampling heights.

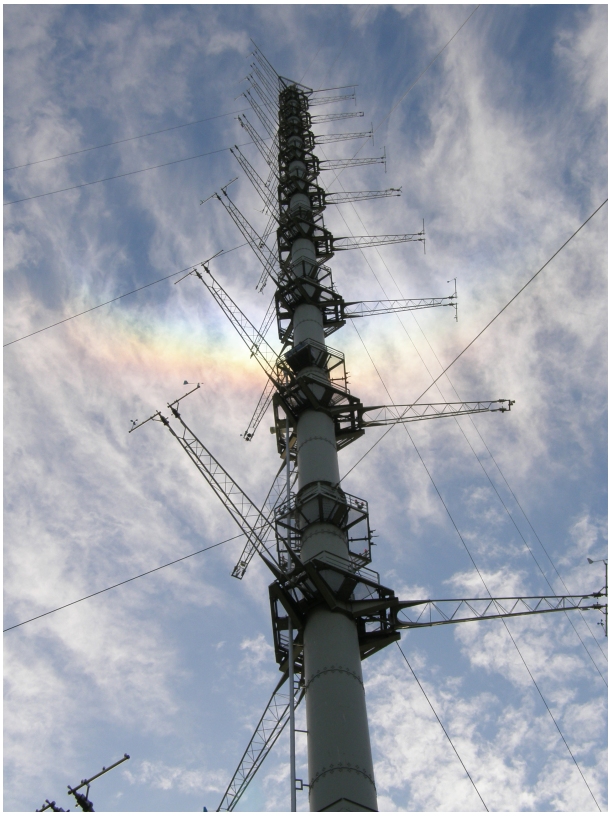

Figure 1.14: Picture by M. E. Popa of the Cabauw tall tower station

In the final chapter, we provide an overview of what has been learned from these data. We also identify what are, in our opinion, the most important remaining gaps in our understanding of the cycle of atmospheric H_2 and the isotope effects in the cycle.

Chapter 2

Temporal and spatial variability of δD(H_2): observations at six EUROHYDROS stations

This chapter is based on:

Batenburg, A. M., Walter, S., Pieterse, G., Levin, I., Schmidt, M., Jordan, A., Hammer, S., Yver, C., and Röckmann, T.: *Temporal and spatial variability of the stable isotopic composition of atmospheric molecular hydrogen: observations at six EUROHYDROS stations*, Atmos. Chem. Phys., **11**, 6985–6999, doi: 10.5194/acp-11-6985-2011, 2011. URL: `www.atmos-chem-phys.net/11/6985/2011/acp-11-6985-2011.html`

Abstract

Despite the potential of isotope measurements to improve our understanding of the global atmospheric molecular hydrogen (H_2) cycle, few H_2 isotope data have been published so far. Now, within the EUROpean network for atmospheric HYDRogen Observations and Studies project (EUROHYDROS), weekly to monthly air samples from six locations in a global sampling network have been analysed for H_2 mixing ratio ($\chi(H_2)$) and the stable isotopic composition of the H_2 (δD(H_2), hereafter referred to as δD). The time series thus obtained now cover one to five years for all stations. This is the largest set of ground station observations of δD so far.

Annual average δD values are higher at the Southern Hemisphere (SH) than at the Northern Hemisphere (NH) stations; the maximum is observed at Neumayer (Antarctica), and the minimum at the non-arctic NH stations. The maximum seasonal differences in δD range from $\approx 18\,‰$ at Neumayer to $\approx 45\,‰$ at

Schauinsland (Southern Germany); in general, seasonal variability is largest at the NH stations. The timing of minima and maxima differs per station as well. In Alert (Arctic Canada), the variations in δD and $\chi(H_2)$ can be approximated as simple harmonic functions with a $\approx$ 5-month relative phase shift. This out-of-phase seasonal behaviour of δD and $\chi(H_2)$ can also be detected, but delayed and with a $\approx$ 6-month relative phase shift, at Mace Head and Cape Verde. However, no seasonal δD cycle could be observed at Schauinsland, which likely reflects the larger influence of local sources and sinks at this continental station. At the two SH stations, no seasonal cycle could be detected in the δD data. If it is assumed that the sink processes are the main drivers of the observed seasonality in $\chi(H_2)$ and δD on the NH, the relative seasonal variations can be used to estimate the relative sink strength of the two major sinks, deposition to soils and atmospheric oxidation by the hydroxyl (OH) radical. For the NH coastal and marine stations this analysis suggests that the relative contribution of soil uptake to the total annual H_2 removal increases with latitude.

2.1 Introduction

Molecular hydrogen (H_2) is present in the atmosphere with a typical mixing ratio ($\chi(H_2)$) of more than 500 ppb (nmole mole^{-1}) (*Glueckauf and Kitt*, 1957; *Schmidt and Seiler*, 1970; *Schmidt*, 1974; *Ehhalt et al.*, 1977). Over the last decades, several studies examined the magnitude of the source and sink terms in the global H_2 budget (*Novelli et al.*, 1999; *Hauglustaine and Ehhalt*, 2002; *Sanderson et al.*, 2003; *Rhee et al.*, 2006b; *Price et al.*, 2007; *Xiao et al.*, 2007; *Ehhalt and Rohrer*, 2009; *Pieterse et al.*, 2011; *Yashiro et al.*, 2011, see Table 2.1 for the budgets that included isotopes). These show that the largest H_2 sources are the atmospheric oxidation of methane and other hydrocarbons, and combustion processes. Production by nitrogen-fixing bacteria, on land or in the oceans, constitutes a smaller source. About three quarters of the H_2 thus produced is taken up by soil; the other quarter is oxidized by the hydroxyl radical (OH). However, large quantitative uncertainties still exist in the global H_2 budget. For example, the estimates for the sink strength of soil uptake – the largest term in the budget – vary widely between these studies.

Research into the atmospheric H_2 budget has increased in recent years, because H_2 may become an important energy carrier in the future. In this case, emissions of H_2 to the atmosphere are likely to rise as a result of the inevitable leakage during production, storage and distribution of H_2 (*Schultz et al.*, 2003). The associated rise of atmospheric H_2 levels is expected to affect the oxidative capacity of the atmosphere, with implications for the atmospheric lifetime of many species, including the strong greenhouse gas methane. Higher concentrations of H_2 will also affect stratospheric ozone levels, although estimates of the impact vary significantly among authors (*Tromp et al.*, 2003; *Warwick et al.*, 2004; *Feck et al.*, 2008).

Due to the large relative mass difference between deuterated hydrogen (HD) and non-deuterated hydrogen (HH), particularly large isotope effects occur in the chemical processes that produce or remove H_2. These result, for example, in very different isotopic signatures for H_2 produced by combustion processes, by oxidation sources or by biological processes (see Table 2.1). For this reason, determination of the isotopic composition is a promising addition to $\chi(H_2)$ observations to distinguish between different H_2 source

and sink processes and to constrain the terms in the global budget. In this paper, the following definition of δD is used to indicate the isotopic composition of the hydrogen:

$$\delta\mathrm{D} = \delta\mathrm{D}(\mathrm{H_2}) = \left(\frac{R_{\mathrm{Sample}}}{R_{\mathrm{VSMOW}}} - 1 \right) \cdot 1000\ ‰ \tag{2.1}$$

where R_{Sample} is the ratio of the number density of "heavy" deuterium atoms (D) to the number density of "light" hydrogen atoms (H) in the H_2 of the sample, and R_{VSMOW} is the ratio of the number density of deuterium atoms to the number density of H atoms in Vienna Standard Mean Ocean Water, which is (155.75 ± 0.08) ppm (*de Wit et al.*, 1980; *Gonfiantini et al.*, 1993). Note that the ‰-sign is explicitly included in this formula.

Following up the initial work by (*Ehhalt et al.*, 1966; *Gerst and Quay*, 2000, 2001), new analytical techniques that have become available recently have significantly simplified H_2 isotope analysis so that many more data have become available in the past few years (*Rahn et al.*, 2002b; *Rhee et al.*, 2004). This has led to new constraints on the isotopic signatures of the most important sources and sinks. The isotopic composition of H_2 from CH_4 oxidation was first examined by measurements in the stratosphere (*Rahn et al.*, 2003; *Röckmann et al.*, 2003; *Rhee et al.*, 2006a), but also individual steps in the oxidation sequence have been investigated, especially photolysis of formaldehyde (HCHO) (*Feilberg et al.*, 2007; *Mar et al.*, 2007; *Nilsson et al.*, 2007; *Rhee et al.*, 2008; *Röckmann et al.*, 2010b). Furthermore, more information on the main surface sources, biomass burning and fossil fuel combustion (*Röckmann et al.*, 2010a; *Vollmer et al.*, 2010) and the largest sink, uptake in soil (*Rahn et al.*, 2002a; *Gerst and Quay*, 2001; *Rice et al.*, 2011), has become available.

At the same time, $\chi(H_2)$ and δD have been incorporated into chemical transport models (*Price et al.*, 2007; *Pieterse et al.*, 2009, 2011). Until now, δD observations to validate these model results have been scarce. Data have been published from Pacific Ocean transects, the Cheeka Peak observatory (Washington, US), the Point Barrow observatory (Alaska, US) and the CARIBIC aircraft sampling program (*Gerst and Quay*, 2000; *Rhee et al.*, 2006b; *Rice et al.*, 2010). These datasets have limited spatial coverage and temporal resolution, most notably in the higher latitudes of the NH. Here we present observations from six ground stations covering high latitudes of both the NH and SH and all seasons, that contribute to the closing of this observational gap. The interpretation of the isotope record we present here is semi-quantitative. A more rigorous quantification of the terms in the global budget will require the use of the aforementioned global chemistry models. Our data have already been used with the global chemistry transport model TM5 (*Pieterse et al.*, 2011).

Table 2.1: The global budget of atmospheric H_2, with source and sink strengths and isotopic signatures used by different authors.

	Rhee et al. (2006b)		*Price et al.* (2007)		*Pieterse et al.* (2011)	
Sources	Source strength (Tg H_2 a^{-1})	Source signature (‰)	Source strength (Tg H_2 a^{-1})	Source signature (‰)	Source strength (Tg H_2 a^{-1})	Source signature (‰)
Fossil fuel burning	15 ± 6	-270	18.3	-196	17.0^{+3}_{-6}	-196
Biomass burning	16 ± 3	-90	10.1	-290	15.0^{+5}_{-5}	-260
Biofuel			4.4	-290		
Ocean	6 ± 5	-700	6	-628	5.0^{+1}_{-2}	-628
Land N_2 fixation	6 ± 5	-700	0		3.0^{+3}_{-3}	-628
Methane oxidation	64 ± 12	+190	24.5	+162	37.3	+116
VOC oxidation	(incl. VOC)		9.8	+162		
Sinks	Sink strength (Tg H_2 a^{-1})	Sink fractionation factor (α=k_{HD}/k_{H_2})	Sink strength (Tg H_2 a^{-1})	Sink fractionation factor (α=k_{HD}/k_{H_2})	Sink strength (Tg H_2 a^{-1})	Sink fractionation factor (α=k_{HD}/k_{H_2})
Uptake by soils	88 ± 11	0.943 ± 0.007	55	0.943	55.8	0.925
Oxidation by OH	19 ± 3	0.58 ± 0.07	18	0.568	22.1	0.542

2.2 Experimental

Air samples were collected by the Institut für Umweltphysik of the University of Heidelberg (UHEI-IUP), the Max Planck Institute for Biogeochemistry in Jena (MPI-BGC) and the Laboratoire des Sciences du Climat et de l'Environnement in Gif sur Yvette (LSCE) at the six stations listed in Table 2.2 and depicted in Figure 2.1. These six stations are part of the EUROpean network for atmospheric HYDRogen Observations and Studies (EUROHYDROS) (*Engel*, 2009). 1 l or 2 l borosilicate 3.3 glass flasks with Kel-F (PCTFE) O-ring-sealed stopcocks (Normag) were used for most of the samples. This type of flask is known to be stable for a number of trace gases (Rothe et al., 2004). Storage tests performed at the MPI-BGC indicated that – except for a few individual outliers – $\chi(H_2)$ is also stable in these flasks. Only for Amsterdam Island, an older type of flask with Teflon PFA O-rings was sometimes used until May 2007. Most flasks were covered with a black shrink hose, and all flasks were stored in closed metal boxes when not in use, minimizing photochemical H_2 production after sampling.

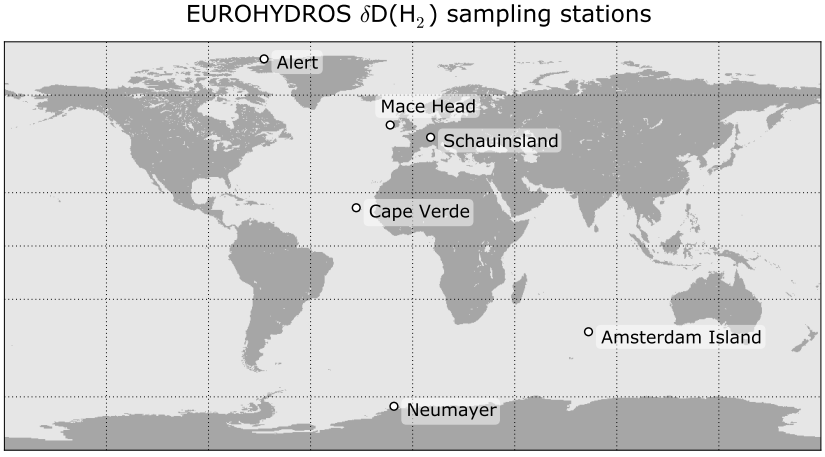

Figure 2.1: The six EUROHYDROS stations that were used for δD observations.

The flasks used for sampling at Alert, Schauinsland and Neumayer (operated by UHEI-IUP) were conditioned by flushing with dry air (dewpoint of $-76\,^{\circ}$C) over two hours on two consecutive days. During sample collection the flask air was dried cryogenically, to a dewpoint of $-70\,^{\circ}$C for Alert and Neumayer and a dewpoint of $-40\,^{\circ}$C for Schauinsland. The flasks were flushed for at least 15 min and then pressurized to ≈ 2 bar (absolute pressure) with KNF Neuberger pumps (type N86KNDC with EPDM membrane).

The flasks used for sampling at Mace Head and Amsterdam Island (operated by LSCE) were evacuated and filled with dry air between each sampling round. At the measurement sites, they were flushed for 10 min and then filled to ≈ 2 bar (absolute pressure). For these flasks, more information can be found in (*Yver*, 2010).

The flasks used for sampling at Cape Verde (operated by MPI-BGC) were conditioned by evacuating at 70° C for three days, followed by flushing with 30 l of dried ambient air before the first use, and reconditioned between each sampling round by flushing with dried ambient air at 1.6 bar. They were pressurized to 1.6 bar before shipping to Cape Verde, and flushed with the sample air before pressurizing with a membrane pump. The sample air was dried with $Mg(ClO_4)_2$.

The samples were first shipped to the institute that operated the station, where mixing ratios of H_2 and other trace gases were measured. H_2 mixing ratios were determined with reduction gas analysers, either the RGA-3 (Trace Analytics Inc.) or the Peak Performer 1 RCP (Peak Laboratories) (*Hammer and Levin*, 2009; *Yver et al.*, 2009; *Jordan and Steinberg*, 2011). Reduction gas analysers separate reduced gases such as H_2 from the air matrix by gas chromatography, and then quantify them via a redox reaction with mercuric oxide and detection of the resulting mercury vapour by UV absorption. We give mixing ratios in units of "parts per billion" (ppb, equivalent to the SI-unit "nmole mole^{-1}"). All laboratories used laboratory working standards that are now on the MPI2009 scale, developed at the MPI-BGC (*Jordan and Steinberg*, 2011). The samples were then shipped to the isotope laboratory at the Institute for Marine and Atmospheric Research (IMAU) of Utrecht University. Typically, several months passed between sample collection and isotope analysis. A total of 480 flasks were analysed; the number of samples per station is listed in Table 2.2.

In Utrecht, a gas chromatography isotope-ratio mass spectrometry (GC-IRMS) system as described in (*Rhee et al.*, 2004) is used to separate H_2 from the air matrix and to determine its isotopic composition in a four-step procedure, as follows (see also Figure 1.12):

- A $\approx$ 750 ml glass sample volume is filled with sample air until pressure in the volume has reached $\approx$ 700 mbar. This sample air is then exposed to a Cold Head cooled by a liquid helium compressor to $\approx$ 40 K, so that all except the most volatile gases (H_2, He and Ne) condense.
- The remaining volatile gases are flushed with He carrier gas to a pre-concentration trap, consisting of a 1/8 inch (3.2 mm) stainless steel tube filled with 5 Å molecular sieve, immersed in liquid nitrogen, which is cooled down to the triple point of nitrogen (63 K) by pumping off the gas phase.
- After pre-concentration the trap is lifted from the liquid nitrogen and the trapped gases are flushed to a cryo-focus trap. This trap consists of a molsieve 5 Å capillary column, jacketed in a stainless steel tube and immersed in liquid nitrogen at ambient pressure (77 K). After focussing, the trap is lifted from the liquid nitrogen and the gases are injected into a 5 Å molsieve Gas Chromatography column kept in an oven at 50° C, where the H_2 is separated from any potential contaminants.
- The purified H_2 is then injected through an open split system into the IRMS (ThermoFinnigan Delta plus XL) for determination of the D/H ratio.

In the IRMS chromatogram, the sample peak was typically bracketed by seven H_2 laboratory working gas peaks of pure H_2 before and two H_2 working gas peaks after. By the same procedure as for the samples, comparable quantities of air from laboratory reference air bottles were typically measured twice a day. The H_2 mixing ratio in the laboratory reference bottle that was in use from March 2007 until February 2010 was determined by UHEI-IUP to be (546.2 ± 2.5) ppb, later confirmed by MPI-BGC to be (545.0 ± 0.5) ppb. Its δD ($(+73.0 \pm 1.8)$ ‰, where the error bar indicates one standard error from 5 different determinations) was calculated using mixtures of synthetic air with H_2 of known isotopic

composition ((-9.5 ± 0.5) ‰ and $(+205 \pm 2)$ ‰, certified by Messer Griesheim, Germany) that were measured on the GC-IRMS system on the same days as the laboratory reference bottle. When this laboratory reference air bottle became exhausted, it was replaced with two other mixtures of synthetic air and H_2 ((580.78 ± 0.03) ppb and (244.3 ± 0.8) ppb, as determined by BGC Jena) that were regularly measured from December 2008 onward. From measurements during the overlap period, the isotopic composition of these new reference gases was calibrated versus the old reference air bottle ($(+207.0 \pm 0.3)$ ‰ and $(+198.2 \pm 0.5)$ ‰). Inspection of these measurements also allowed a robust assessment of the reproducibility of our system yielding a standard deviation of 4.5 ‰ in δD. It should be borne in mind that the error estimates given here are estimates of the random error due to measurement scatter only. The determination of $\delta D(H_2)$ of the laboratory reference air bottle comprises additional systematic uncertainties, e.g. the correctness of the initially assigned $\delta D(H_2)$ values of the commercial calibration gases, changes of these values in the process of creating calibration mixtures with near-ambient $\chi(H_2)$, and the calibration measurements themselves. This may lead to an additional systematic error of a few ‰.

The measurements of the laboratory reference bottles were used to construct 5-day moving average values of measured δD values and the deviation of the measured from the assigned δD value for each measurement day. The moving average of the laboratory reference bottle measurements was replaced by the average of an adjusted selection of these measurements for those days around which a relatively sudden shift in the measured values seemed to occur. An empirical scale contraction factor (1.0613) was determined from the measurements of the mixtures of synthetic air with H_2 of known isotopic composition. This factor was used to determine the corrected δD value for the sample measurements by inter- or extrapolation from the 5-day moving average values of the reference gas results for that day. (It was assumed that the GC-IRMS follows a linear response curve.)

A blank measurement was usually performed once a day as well. The blank peak area was usually less than 4 % of a typical sample peak area. Due to the small peak area, the δD value of the blank could not be determined reliably from these measurements and could therefore not be taken into account in the calculation of the sample δD values. The contribution of the blank signal to the random scatter is included in the 4.5 ‰ reproducibility that is obtained for repeated measurements of the laboratory reference air bottle. However, the blank may cause an unquantified systematic error.

The laboratory reference bottle and blank measurements were used to calculate $\chi(H_2)$ for the samples as well. Mixing ratios determined by GC-IRMS measurement typically deviated less than 4 % from the determinations by RGA-3 or Peak Performer. They were used for quality assessment of the data, but are not considered further in this paper.

Despite these calibration measures, δD measurements from June 2010 onwards seemed to have a positive offset with respect to the previously measured samples and an increased scatter. By comparing the respective samples from stations with long data series (Alert and Neumayer) with measurements from previous years, the offset was empirically determined to be on average 9.5 ‰. Unfortunately, it could not be determined whether the offset was caused by simultaneous drift in the two laboratory reference bottles in use at that time or by the replacement of parts of the setup. At present the system is undergoing substantial rebuilding and further automation in order to be able to accommodate more reference gas measurements in the future.

The affected measurements of Alert and Neumayer samples still showed the same seasonal patterns as the previous measurements, and were therefore adjusted to fall on the same scale as the previous data by subtracting the empirically determined 9.5 ‰ offset.

The respective data are indicated with open symbols in Figure 2.2. Cape Verde samples that were also measured during this period showed a more erratic behaviour and were therefore omitted from the time series presented here. The Schauinsland samples collected after September 2009 showed strong pollution signatures (high mixing ratios, as determined by both RGA-3 and GC-IRMS measurements, and very low δD values), which coincided with CO_2 contaminations. As a leak or contamination in the sampling system was suspected, these data were also omitted.

Some of the $\chi(H_2)$ and δD data points seem to fall outside of the normal range of variation at the respective sampling station. For several of these outliers, we have looked into back-trajectory calculations (see section 2.3.1) to determine if the origin of these air parcels was unusual, but no clear conclusions could be derived from this analysis. Therefore, we have selected outliers based only on visual inspection of the time series. These data points are indicated with open stars in Figure 2.2. The data indicated with open symbols in Figure 2.2 (the outliers and the samples measured after June 2010) are not used in further calculations.

2.3 Results and discussion

2.3.1 Time series

The time series of $\chi(H_2)$ and δD for all six stations are shown in Figure 2.2, and will be discussed individually in the following subsections. Figure 2.3 shows the seasonal averages from which an annual average was calculated for each station. Using the seasonal averages rather than the raw data for calculation of the mean has the advantage that each of the seasons (DJF, MAM, JJA, SON) has equal weight, which avoids bias from having more samples from some seasons than from others.

Least-squares harmonic fits were applied to the $\chi(H_2)$ and δD data of the three stations that showed the clearest seasonal cycles in δD. We use the function:

$$y = a\cos(2\pi(x-\varphi)) + m \tag{2.2}$$

where x is the time in years and a (amplitude), φ (phase) and χ (average value) are the fitting parameters. A term for a possible temporal trend is not included in the fit function because our time series of $\chi(H_2)$ and δD are still relatively short. The results (listed in Table 2.3) were used to construct the ellipses in the phase diagrams in Figure 2.6.

Alert

Alert is the station with the largest number of analysed samples (Table 2.2) and about four full seasonal cycles of data. The annual average values are $\chi(H_2) = (496.9 \pm 1.2)$ ppb, and $\delta D = (124.1 \pm 0.5)$ ‰, where the error bar indicates the standard error of the mean (the standard deviation as a result of the variance in the measurements, divided by the square root of the number of measurements). A difference of 131 ppb is found between the highest and lowest $\chi(H_2)$ value, as well as a difference of 41 ‰ between the highest and lowest δD (excluding the measurements affected by the 9.5 ‰ offset and outliers for δD).

A distinct seasonal cycle is observed for both $\chi(H_2)$ and δD (Figure 2.2). The two quantities clearly increase and decrease out-of-phase. This out-of-phase timing results

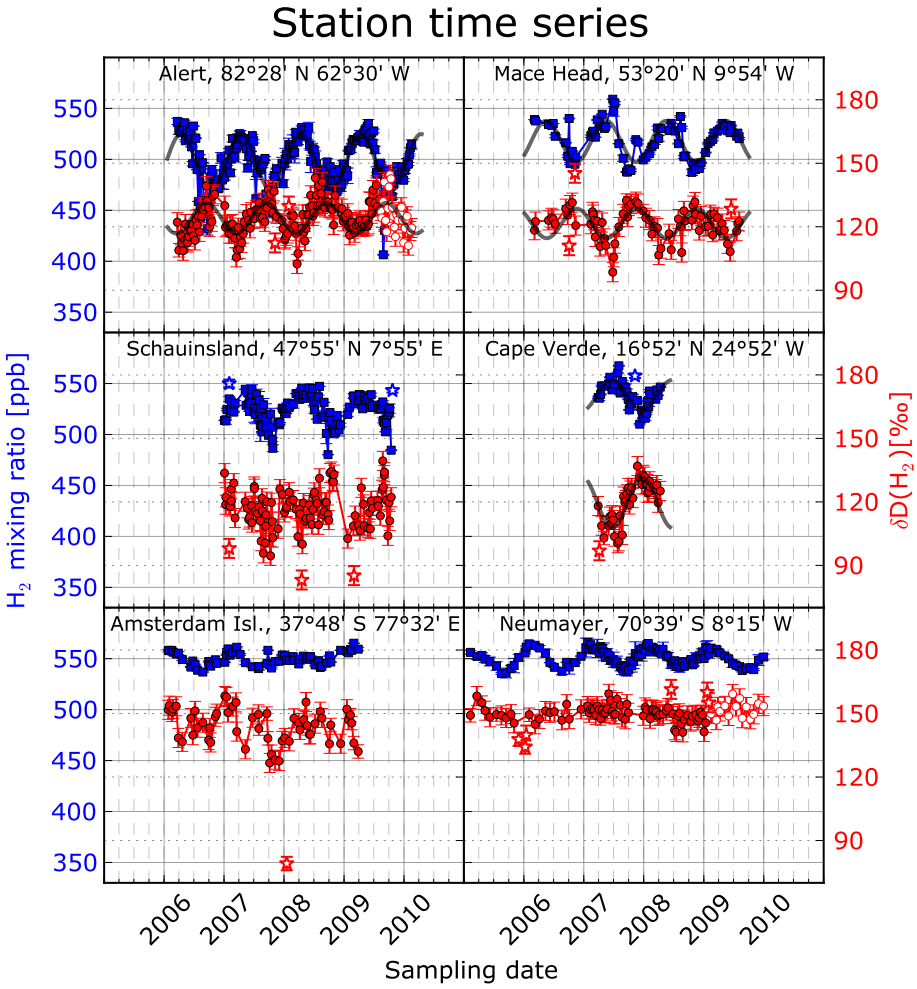

Figure 2.2: $\chi(H_2)$ (blue squares, measured by UHEI-IUP, LSCE and MPI-BGC) and δD (red circles) measured by IMAU on samples from the six stations. Solid grey lines represent a harmonic best fit to the data from Alert, Mace Head and Cape Verde. Error bars indicate one standard deviation for $\chi(H_2)$ determined from successive measurements, and one standard error for δD (the standard deviation of 4.5 ‰, as determined from repeated laboratory standard bottle measurements, divided by the square root of the number of repeat measurements of the same flask). Open red circles indicate the δD-values where an empirical value of 9.5 ‰ was subtracted to adjust for the bias that affected the GC-IRMS system from June 2010 onward. Open blue and red stars indicate other unexplained outliers in $\chi(H_2)$ and δD, respectively. None of the open-symbol data are used in any further calculations. Some outliers at Amsterdam Island are off the scale.

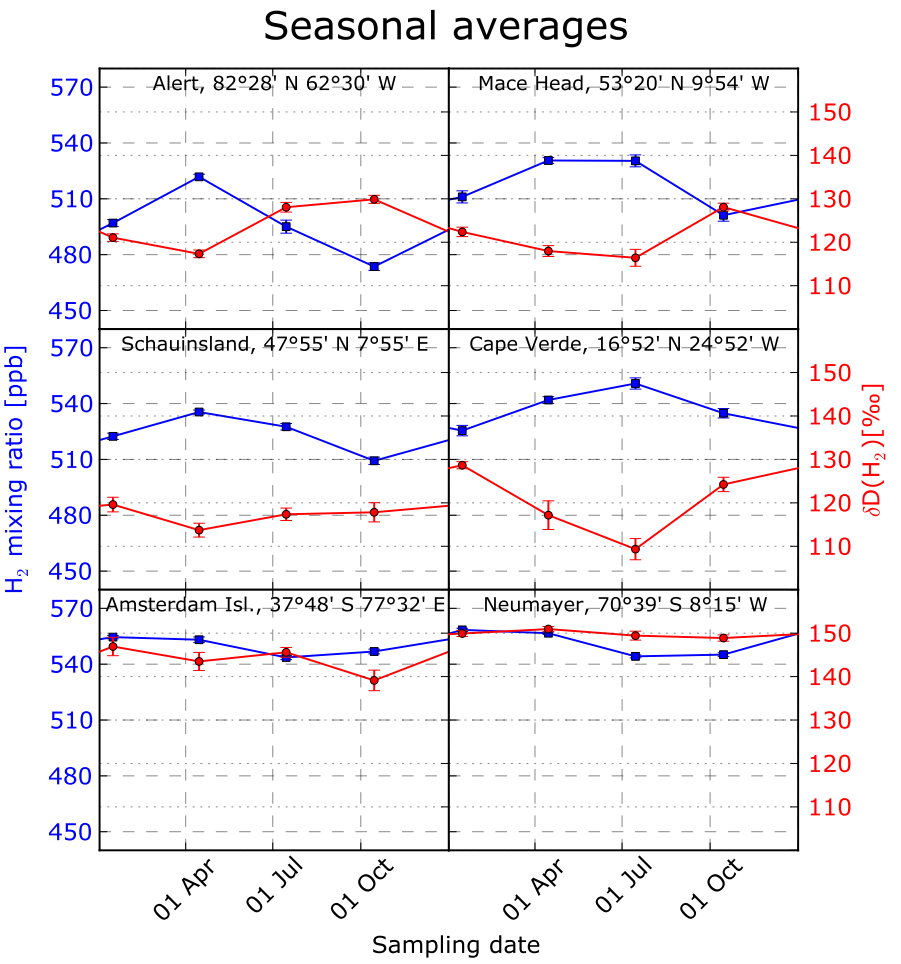

Figure 2.3: Seasonal averages of $\chi(H_2)$ (UHEI, LSCE and MPI-BGC) and δD (IMAU) plotted versus time of year. Error bars indicate one standard error, which is calculated purely from variance in the values obtained for one season.

from the seasonal variations of the mainly deuterium-depleted (combustion) sources and the deuterium-enriching removal processes. Photochemically produced H_2 can contribute to $\chi(H_2)$ changes, but contributes little to changes in δD, since its δD value is relatively close to ambient δD values. So, in winter, H_2 accumulates from depleted sources, leading to an $\chi(H_2)$ peak and a δD minimum in spring, while during summer, the removal processes are strong and the remaining H_2 becomes enriched, leading to an $\chi(H_2)$ minimum and δD maximum in autumn. The detailed study of the global H_2 isotope budget with the TM5 model (*Pieterse et al.*, 2011) shows that the soil sink contributes most to the seasonal cycle of the mixing ratio, while the smaller photochemical sink has a slightly

larger effect on the isotopic composition, due to the larger isotope fractionation. The emissions from combustion sources are not strongly seasonal. Photochemical production does have a seasonal cycle, but contributes little to the variations in δD.

The phase of the least-square harmonic fits to the Alert $\chi(H_2)$ data (Table 2.3) is similar to the phase reported by *Rhee et al.* (2006b) for the cycle of NH near-tropopause averages of $\chi(H_2)$ obtained from three flights with a passenger aircraft, whereas the phase found for the δD cycle is slightly different (the Alert δD-cycle is slightly ahead of the (*Rhee et al.*, 2006b) cycle). The average mixing ratio is lower. The most striking difference is in the amplitudes; the amplitudes of the seasonal cycles found at Alert are larger than for the (*Rhee et al.*, 2006b) NH near-tropopause averages, even more so since on visual inspection the harmonic fit seems to underestimate the amplitudes. The larger amplitudes can likely be attributed to the larger seasonality in the sinks at higher NH latitudes, due to the larger relative soil surface and the seasonal snow cover variation that modulates the soil sink. As we will show below, for the high-latitude NH stations, soil uptake dominates the seasonal cycle more than at lower NH latitudes. It seemingly also dominates the Alert seasonal cycle more than the NH high tropospheric average cycle. In a modelling study that focused on H_2 uptake by soil, *Yashiro et al.* (2011) found that the soil uptake flux for the latitude range north of 45° N has a much larger seasonal variation than for the 15° N to 45° N latitude range, which is in accordance with this finding. However, it should be noted that the analysis of *Rhee et al.* (2006b) is based on fitting a harmonic function to three data points only, whereas the Alert data series clearly captures the full seasonal evolution of the isotope signal.

Gerst and Quay (2000) published six δD measurements on samples from another high northern latitude station, Point Barrow, Alaska, collected in the period from February to August 1997. Unexpectedly, the δD values of $(+92 \pm 10)$ ‰, (one standard deviation) at Point Barrow are significantly lower than what we find at Alert and other NH stations (see below). The reason for this discrepancy is not understood, and the TM5 model (Pieterse et al., 2011) does not predict such a large difference either. It should be noted, however, that in-cylinder growth of H_2 is an issue in the early data from *Gerst and Quay* (2000). Specifically, four other samples from Point Barrow in the study from *Gerst and Quay* (2000) were considered contaminated since their mixing ratios differed by more than 3σ from a multi-year average of NOAA-CMDL data. All samples were measured more than one year after collection and the discrepancy to the new values from Alert may indicate that the six samples considered reliable may have been contaminated too. The isotopic composition of the cylinder grown contamination was determined by *Gerst and Quay* (2000) to be $\delta D = -614$ ‰, and thus only a few % of contamination from this source could lead to the observed depletions.

Mace Head

The time series for Mace Head span more than three years now. The maximum amplitudes are 72 ppb and 34 ‰ for $\chi(H_2)$ and δD, respectively and the annual averages are (518.3 ± 1.4) ppb and (121.2 ± 0.7) ‰. $\chi(H_2)$ shows a clear seasonal cycle; it increases steadily from autumn until summer, and then decreases rapidly. The δD time series in 2007 and 2008 shows a minimum in late spring or early summer, indicating a seasonal cycle in δD at Mace Head, which is also predicted by the TM5 model (*Pieterse et al.*, 2011). In general, the δD cycle moves in antiphase to the $\chi(H_2)$ cycle, as discussed above for Alert. However, it can be seen from the seasonal averages (Figure 2.3), as well

as from the phase obtained from the harmonic fit (Table 3), that the timing of the minimum is delayed with respect to Alert. The phase obtained from the harmonic fit to the Mace Head δD data is in fact closer to the phase found by *Rhee et al.* (2006b) than the phase obtained from the Alert cycle. Still, as at Alert, the amplitude is larger than that from *Rhee et al.* (2006b). Mace Head can still be considered to be in the higher latitude part of the NH (especially since it receives much air from regions to the North-West, see below), and this large seasonal variation can thus be attributed to the large seasonal variation in the soil uptake flux at high NH latitudes as well. That this isotopic seasonal cycle is not visible in the first year of the series (2006) may be due to the small number of samples in this year. In 2009, there is one high δD outlier right in the seasonal minimum. The δD seasonal cycles vary considerably between 2007 and 2009, but the same is true for $\chi(H_2)$, so what causes the interannual variations in $\chi(H_2)$ likely causes the interannual variations in δD.

To investigate the origin of the interannual variations, backward trajectories were calculated with the NOAA HYSPLIT model to investigate if the rather high $\chi(H_2)$ and low δD values in summer 2007 might have been a result of synoptic conditions that brought more polluted air than usual to the station. Such an effect was not found. The trajectories showed that most air masses that arrive at Mace Head come from either the north Atlantic or the NH northern temperate to boreal regions to the west, and air masses that were sampled in summer 2007 were no exception. *Grant et al.* (2010b) also showed that Mace Head rarely receives air masses from lower latitudes, supporting our limited trajectory study. Therefore, transport of H_2-rich and δD-depleted air from lower latitudes does not seem a very likely explanation. It is more likely that the full interannual variability in H_2 cannot be seen at this station due to the limited time period over which samples have been taken so far.

Schauinsland

In the time series from Schauinsland station, the maximum differences are 67 ppb and 45 ‰, and the seasonally weighted average values are (523.7 ± 0.8) ppb and (117.1 ± 0.9) ‰. This is relatively similar to the values from Mace Head, but the seasonal cycles show differences. At Schauinsland, a clear seasonal cycle is visible in the $\chi(H_2)$ data, but not in the δD data. In 2007, the δD signal seems to trend downward, while in 2008 and 2009 it appears to trend upward. These trends are not statistically significant, though, but they underline that no clear seasonal cycle in δD is present at Schauinsland.

Unlike Alert and Mace Head, Schauinsland is not a coastal but a continental location, close to anthropogenic sources, especially in the Rhine valley, and in the middle of a large land area where deposition to soil occurs. Possibly, significant nitrogen fixation by soil microbes takes place in the surrounding region as well. H_2 produced by nitrogen fixers has a very depleted source signature (Table 2.1), so only a small amount of this H_2 may have a significant effect on the isotopic signature of the total ambient H_2. Although this was not investigated in more detail, interannual variations in microbial production may thus contribute to the difference in seasonal patterns between years.

The station is usually above the boundary layer at night, and within the boundary layer during the day, particularly in summer (*Schmidt et al.*, 1996). The upper edge of the boundary layer generally passes the station altitude after 10:00 a.m. (CET), so samples collected after this time are potentially locally influenced; they may contain boundary layer air that has been in contact with local (anthropogenic) sources and the surface.

Most of the samples analysed for this record were sampled before 10:00 a.m.; about 10 % was collected later in the day. However, excluding these samples from the time series did not yield a more distinct seasonal cycle. This indicates that the deviations in the isotopic composition are not a product of local factors only. It should be noted that also the TM5 model predicts a considerably smaller seasonal cycle in δD for Schauinsland compared to Mace Head (*Pieterse et al.*, 2011), so a longer time series may be needed to clearly distinguish the cycle from the data scatter.

Cape Verde

Although the Cape Verde time series is the shortest (little more than one year), the data indicate a clearer seasonal cycle than at Mace Head. As at Alert and Mace Head, $\chi(H_2)$ and δD vary out-of-phase. The timing of the minima and maxima is closer to what is observed at Mace Head than at Alert. The mixing ratio peaked at 567 ppb in August and then decreased by 57 ppb to 510 ppb at the end of the year. From April until August the δD value was rather constant (minimum value of 100 ‰ in July) and after August it increased until the end of the year (maximum observed value 137 ‰ in November). Seasonally weighted annual averages of (538.3 ± 1.3) ppb and (119.9 ± 1.1) ‰ were observed.

The amplitude found with the harmonic fit to the data is remarkably large, larger than for Mace Head and Alert. This contrasts with the TM5 model results (*Pieterse et al.*, 2011) where the seasonal variation in δD at Cape Verde is somewhat smaller than for Mace Head and Alert. However, in Alert and Mace Head, the fit seems to underestimate the amplitudes of the seasonal variation due to differences between years. The amplitude obtained from the fit is apparently dependent on the presence of interannual variations that cannot be detected for Cape Verde (because of the limited length of the measurement record). Therefore, it seems more reasonable in the case of Cape Verde to compare the δD variation in the original data with the other stations (Figure 2.2 and Table 2.2). When these are compared, the seasonal δD variation does not seem exceptionally large in Cape Verde.

The cycles shift to later in the year when moving from Alert to Mace Head to Cape Verde. This can also be seen in the phases obtained from the cosine fits (Table 2.3). It is possible that seasonal variation in the sources (e.g. tropical biomass burning) or transport (e.g. interhemispheric exchange) contribute to these shifts. Due to the dominant NNW wind direction (trade winds), Cape Verde receives much air from Mauretania and surrounding countries. The biomass burning season in this region is in winter, but we do not see the expected $\chi(H_2)$ increase and concomitant δD decrease in this season. Most interhemispheric mixing occurs in summer, when Cape Verde is close to the edge of the ITCZ. Since δD values are higher in the SH (*Gerst and Quay*, 2000; *Rice et al.*, 2010, see also Figure 2.4 (b) below) , increased transport from the SH should result in higher δD values, but this is not observed. Therefore, we cannot identify individual source or transport signatures that cause the cycles in Cape Verde to be delayed with respect to the Alert cycles.

Amsterdam Island

The time series from Amsterdam Island does not show a very distinct seasonal cycle. H_2 mixing ratios only vary between 537 and 565 ppb, with seasonal maxima in austral summer, and no clear seasonal signal can be identified in the δD data. This may be due to the remoteness of this location; it is far removed from densely populated areas where

anthropogenic H_2 is produced, and far away from large land areas where deposition to soil can occur. Other $\chi(H_2)$ time series from locations in the Indian Ocean, such as the time series from the Seychelles (in (*Novelli et al.*, 1999)), also show very small seasonal cycles.

Yashiro et al. (2011) concluded from the timing of the $\chi(H_2)$ seasonal cycle that photochemical production is a dominant driver of the seasonality in $\chi(H_2)$ south of 30° S, which is in accordance with the conclusions that *Rhee et al.* (2006b) drew from δD observations. Since the δD value of photochemically produced H_2 is close to ambient values, this does not cause a large seasonality in δD. Nonetheless, in austral summer photochemical H_2 destruction will occur, with a D-enriching effect on the reservoir. That we see no seasonal cycle in δD implies that a D-depleting process compensates this enrichment. Transport of depleted H_2 from lower latitudes (from tropical biomass burning in SH spring and interhemispheric exchange) is a likely explanation. The budget calculations made by *Pieterse et al.* (2011) suggest that transport of depleted H_2 from lower latitudes is a significant contributor to the seasonal δD changes in the extratropical SH.

Some unexplained extreme outliers do occur in the measurements. Excluding these outliers, the maximal variability in mixing ratio is 28 ppb, and in the isotopic composition 32 ‰. The yearly average values are (549.5 ± 0.6) ppb and (143.8 ± 1.0) ‰.

Neumayer

At present, the Neumayer time series covers 5 full seasonal cycles, and average values are (551.1 ± 0.4) ppb and (149.8 ± 0.4) ‰. A clear seasonal variation can be distinguished in the mixing ratio data, but not in the isotope data. The mixing ratios vary by at most 30 ppb over the year, and the isotope values by at most 18 ‰, making Neumayer the station with the lowest variability in δD. A relatively sharp "dip" appears in the δD values at the end of 2005. This feature was not observed in the other years, so we suspect that this is an artefact rather than a real atmospheric signal and flagged these data points as outliers.

The variation in δD at Neumayer is remarkably small, considering that $\chi(H_2)$ does show a clear cycle. As in Amsterdam Island, there is an $\chi(H_2)$ maximum in austral summer, likely an effect of photochemical production. That no accompanying change in δD is observed can probably be attributed to the same processes that cause the lack of seasonality in δD at Amsterdam Island: a maximum in photochemical production produces H_2 without affecting the δD value much, and the D-enriching effect from photochemical destruction of H_2 in summer is balanced by a D-depleting process like transport of depleted H_2 from lower latitudes. The timing of these processes is, however, somewhat problematic. According to the TM5 model calculations (*Pieterse et al.*, 2011), horizontal transport has the largest depleting effect on the H_2 deuterium content south of 30° S in the months July, August and September. This is too early to compensate for the expected enriching effect of photochemical H_2 destruction in austral summer. The lack of seasonal variation at Neumayer, and to some extent Amsterdam Island, is therefore not fully explained and requires further study.

Table 2.2: The locations and operating institutes of the six EUROHYDROS flask sampling stations discussed here, and the length, average values and maximum variations of their $\chi(H_2)$ and δD sample records.

Station	Coordinates	Operating Institute	Samples	Record length (months)	Average $\chi(H_2)$ [ppb]	Max. $\chi(H_2)$ variation [ppb]	Average δD [‰ vs. VSMOW]	Max. δD variation [‰]
Alert	82°28′ N 62°30′ W	UHEI-IUP	194	47	496.9 ± 1.2	131	124.1 ± 0.5	41
Mace Head	53°20′ N 9°54′ W	LSCE	71	41	518.3 ± 1.4	72	121.2 ± 0.7	34
Schauinsland	47°55′ N 7°55′ E	UHEI-IUP	127	34	523.7 ± 0.8	67	117.1 ± 0.9	45
Cape Verde	16°52′ N 24°52′ W	MPI-BGC	42	12	538.3 ± 1.3	57	119.9 ± 1.1	36
Amsterdam Island	37°48′ S 77°32′ E	LSCE	63	38	549.5 ± 0.6	28	143.8 ± 1.0	32
Neumayer	70°39′ S 8°15′ W	UHEI-IUP	110	59	551.1 ± 0.4	30	149.8 ± 0.4	18

Table 2.3: The obtained fitting parameters for a least-square fit with a harmonic function to the data from Alert, Mace Head and Cape Verde ($y = a\cos(2\pi(x-\phi)) + m$).

	Alert		Mace Head		Cape Verde		(Rhee et al., 2006b) NH hemisphere average	
	$\chi(H_2)$ [ppb]	δD [‰]	$\chi(H_2)$ [ppb]	δD [‰]	$\chi(H_2)$ [ppb]	δD [‰]	$\chi(H_2)$[ppb]	δD [‰]
Amplitude (a)	27.8 ± 1.4	7.3 ± 0.7	20.3 ± 1.9	7.0 ± 1.0	15.0 ± 1.7	12.0 ± 1.2	18.2 ± 1.6	4.0 ± 0.9
Phase (ϕ)	0.24 ± 0.01	0.66 ± 0.02	0.33 ± 0.01	0.84 ± 0.02	0.43 ± 0.02	0.94 ± 0.02	0.28 ± 0.01	0.85 ± 0.05
Average (m)	497.0 ± 1.0	124.1 ± 0.5	517.6 ± 1.3	121.6 ± 0.7	538.4 ± 1.1	119.7 ± 0.8	543.4 ± 0.8	128.3 ± 0.7

Seasonal mean variations

Averages per season (December January February (DJF), March April May (MAM), June July August (JJA) and September October November (SON)) were calculated for each station and are shown in Figure 2.3. This averaging eliminates the scatter from analytical uncertainty and short-term natural variability and allows the general shape of the seasonal cycles to be compared between the stations. The anticorrelated seasonal cycles of δD and $\chi(H_2)$ at Alert can be seen very clearly. There is also an anticorrelation at Mace Head and Cape Verde, but the timing of the minima and maxima is different from the timing at Alert. Although it was not visible in the raw data in Figure 2.2, the seasonal averages of the Schauinsland data seem to show a weak anticorrelation, which is primarily caused by the δD value having a minimum in spring, when $\chi(H_2)$ shows a maximum. In comparison to the NH stations, the two SH stations have much smaller seasonal cycles in $\chi(H_2)$ and δD. The δD cycle at Neumayer does not seem well-correlated to the δD cycle at Amsterdam Island.

2.3.2 Latitudinal gradients

Figure 2.4 shows the latitudinal dependence of the seasonal averages. In all seasons, both mixing ratios and δD values are higher in the SH than in the NH. The lowest average mixing ratios are found for the highest-latitude NH station (Alert) in all seasons. The minimum in δD is, however, not found at Alert for any season, but either at one of the midlatitude stations, or, in summer (JJA), at Cape Verde. As anthropogenic H_2 emissions originate mainly from temperate latitudes (*Hauglustaine and Ehhalt*, 2002; *Price et al.*, 2007), and H_2 from anthropogenic source regions is usually depleted with respect to atmospheric H_2, the midlatitude minimum can be attributed to anthropogenic influence. This is also evident in the spatial δD distribution modelled in TM5 (*Pieterse et al.*, 2011).

Gerst and Quay (2000) concluded from their dataset, obtained from a Pacific Transect at the end of 1998 and two stations in North America, that there was a poleward decrease in δD. However, at their northernmost sampling point (Point Barrow, 71° N), the δD values seem to be exceptionally low. Whereas the rest of the data agree reasonably well with our measurements, their measurements from Point Barrow are more than 20 ‰ lower than our data from Alert. The potential problems with these Point Barrow measurements have been discussed above. We note that without this sampling point, also the data from *Gerst and Quay* (2000) show a δD minimum at temperate northern latitudes.

From Figure 2.4, it is clear that the latitudinal gradient varies with season. As the seasonal variation in both $\chi(H_2)$ and δD is much larger in the NH than in the SH, the size of the latitudinal gradient is for the largest part determined by the variation in the NH. Hence, the smallest pole-to-pole δD difference (19 ‰ between Neumayer and Alert) is found when δD is at its maximum in Alert, i.e., in SON. During this season, $\chi(H_2)$ is lowest in Alert, and therefore the $\chi(H_2)$ difference is largest (72 ppb). At that time, soil uptake in Alert is past its summer peak, so that H_2 mixing ratios are low and the remaining H_2 is isotopically enriched. Reversely, the largest δD pole-to-pole difference (34 ‰) is found when δD is at its minimum in Alert and $\chi(H_2)$ is at its maximum, namely in MAM, when over winter H_2 from depleted sources has accumulated without being absorbed by the snow-covered soil. This is accompanied by the smallest difference in $\chi(H_2)$ (35 ppb).

The interhemispheric difference reported by *Gerst and Quay* (2000) was about 15 ‰, and *Rice et al.* (2010) found a similar gradient, (16 ± 12) ‰. The interpolar difference from the EUROHYDROS stations is clearly larger, but we miss a station at low southern

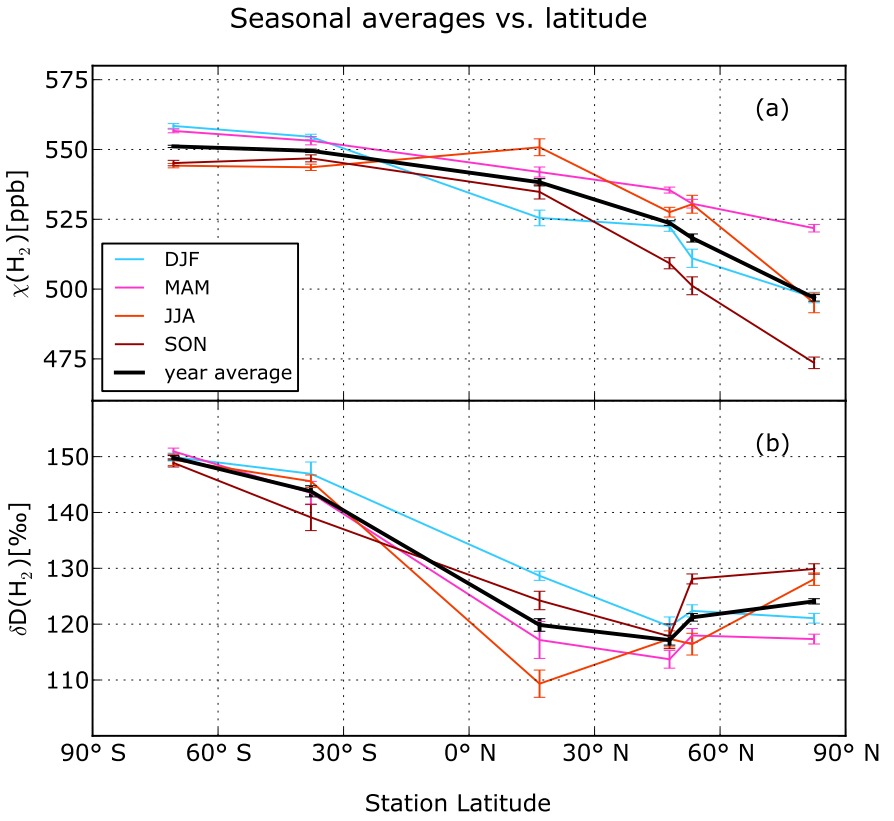

Figure 2.4: Seasonal averages and seasonally weighted yearly averages of $\chi(H_2)$ **(a)** and δD **(b)**.

latitudes to be able to make a reliable southern hemispheric average and to calculate a reliable difference between the two hemispheres.

2.3.3 Latitude dependence of the apparent fractionation factor

If it is assumed that the seasonal cycles of H_2 and its isotopic composition are primarily determined by the sink processes, the fractionation factor α, i.e., the ratio of the removal rate of the heavy isotope species (k_{HD}) to the removal rate of the light isotope species (k_{HH}), can be calculated from the time series as for a single stage Rayleigh fractionation process (see (*Rhee et al.*, 2006b)). In such a Rayleigh removal process, $\chi(H_2)$ and δD evolve as

$$(\alpha - 1) \ln \left[\frac{\chi(H_2)}{\chi(H_2,\ \max)} \right] = \ln(\delta D + 1) + c \tag{2.3}$$

where $\chi(H_2, \text{max})$ is the maximum value for $\chi(H_2)$ found in the series and c is a constant. The real situation at the measurement stations is more complex than this simple Rayleigh fractionation model, as will be discussed below. Still, an "apparent" fractionation factor was calculated for each station from the slope of a linear fit to the data in a Rayleigh fractionation plot (Figure 2.5). This apparent fractionation factor does not quantify the inherent isotope fractionation in one single reaction, but is calculated from atmospheric data collected in a complex situation that involves more than one sink reaction, as well as other processes such as mixing, and we denote this apparent fractionation factor by α_{app}. To make the straight-line fits, a Weighted Total Least-Squares (WTLS) fitting algorithm (*Krystek and Anton*, 2007) was used. This algorithm takes errors in both the x- and the y-direction into account. The squared correlation coefficient (R^2) and the F-test p-value were calculated for each station in the same way as they would be calculated for an "ordinary" least-squares fit of a straight line. The fits to the Amsterdam Island and Neumayer data yielded p-values above 0.05, suggesting a less than 95 % significance of the correlation. The fit to the Schauinsland data did yield a p-value that was slightly smaller than 0.05, but the R^2-value for this fit is very low, which indicates that only a very small part of the variation present in the dataset is described by the fit. This means that the simple Rayleigh fractionation model may not be adequate for evaluation of the time series from Schauinsland and the SH. This is not surprising, considering that no clear isotope seasonal cycles were found for these stations.

Of course, the isotopic composition of the H_2 at the measurement stations depends not only on the fractionation in the removal processes, but also on the isotopic composition of the sources that influence the sites and their variation over the year. Also the relative contribution of the two sink processes (atmospheric OH oxidation and uptake by soils) to the total sink could conceivably vary with season. In this light, it is illustrative to look at the phase diagrams (δD plotted against $\chi(H_2)$) of the monthly means that can be constructed from the three stations that show clear cycles (Figure 2.6). For Alert, it is clear that these points do not fall on a single straight fractionation line, but on the ellipse that is traced by the two harmonic functions that were fitted to the $\chi(H_2)$ and δD time series. This shows that in the fractionation plots in Figure 2.5, not all of the spread around the fractionation lines is random scatter; some of this spread is caused by the phase difference between the $\chi(H_2)$ and δD seasonal cycles. The largest part of this phase difference is probably caused by seasonal variation in the sources and sinks.

Allan et al. (2001) described such phase ellipses for model results of methane mixing ratio and the carbon isotopic composition of methane ($\delta^{13}C(CH_4)$). In their simulations with only one source and one sink process, the monthly means fell on a straight line. This line broadened into an ellipse when different sources with different seasonal cycles were combined, with the largest broadening effect for the sources of which the isotopic signature differed the most from the isotopic signature of the mean source. However, the differing phases of the different sources did not appreciably affect the slope of the major axis of the ellipse: this slope depended robustly on the fractionation factor assumed for the sink, suggesting that even if the phase diagram shows a broadened ellipse, this slope can provide a good estimate of the fractionation in the sink. The ellipse major axis coincided largely with a relationship the authors termed the "KIE line" after the Kinetic Isotope Effect, which is described by:

$$\Delta\delta^{13}C(CH_4) = \varepsilon(1 + \delta_0^{13}C(CH_4))\frac{\Delta m(CH_4)}{m_0(CH_4)} \tag{2.4}$$

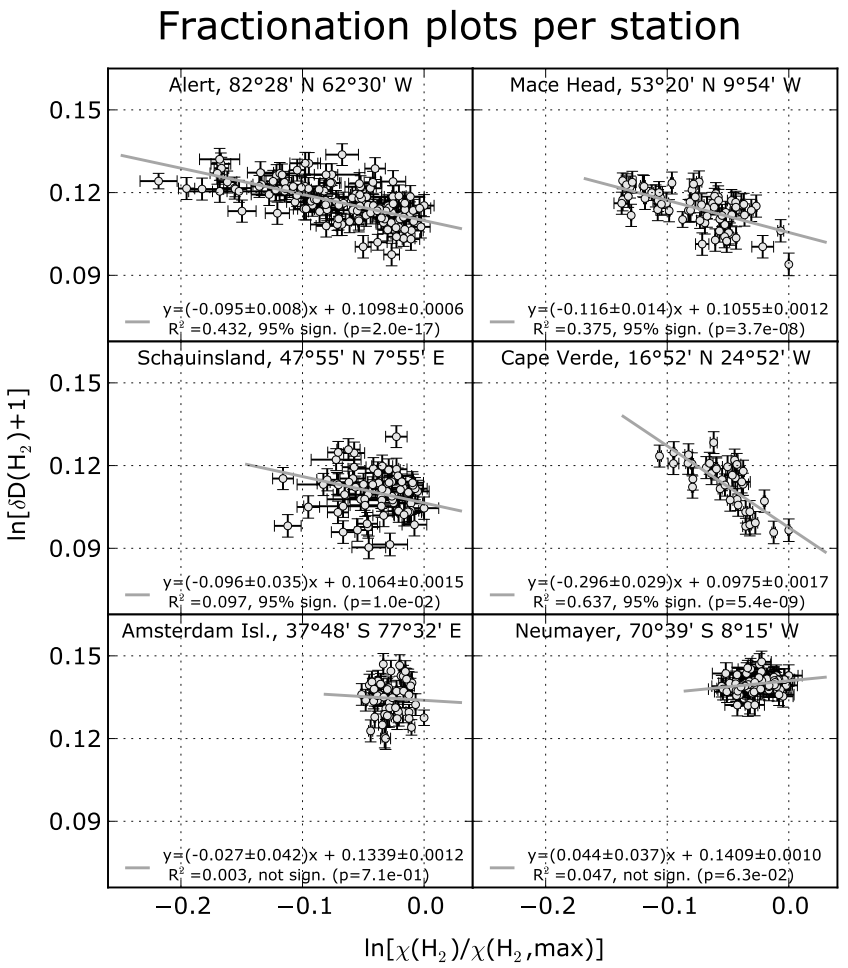

Figure 2.5: Fractionation plots of the datasets from the different stations. Plotted are ln(δD + 1) vs. ln(χ(H$_2$)/χ(H$_2$, max)) with χ(H$_2$, max) the maximum mixing ratio found. Grey lines are the fitted lines obtained from the Weighted Total Least-Squares fitting routine. Error bars indicate one standard deviation. Indicated errors in the fit parameters indicate one standard error. R^2 is the squared correlation coefficient and p is the p-value for the F statistic, both calculated as for an ``ordinary'' least squares fitted line.

with subscript zero indicating a mean value, Δ indicating the difference of a value from the mean, $\chi(CH_4)$ indicating methane mixing ratio, and $\varepsilon = \alpha - 1$.

In the case of H_2, seasonal variation in the sources and sinks contributes to the ellipse eccentricity, but *Rhee et al.* (2006b) showed that as long as the H_2 system is in isotopic equilibrium on an annual basis, the isotopic fractionation does not depend on seasonal changes in source emissions. Since there is no evidence for a tropospheric trend in either

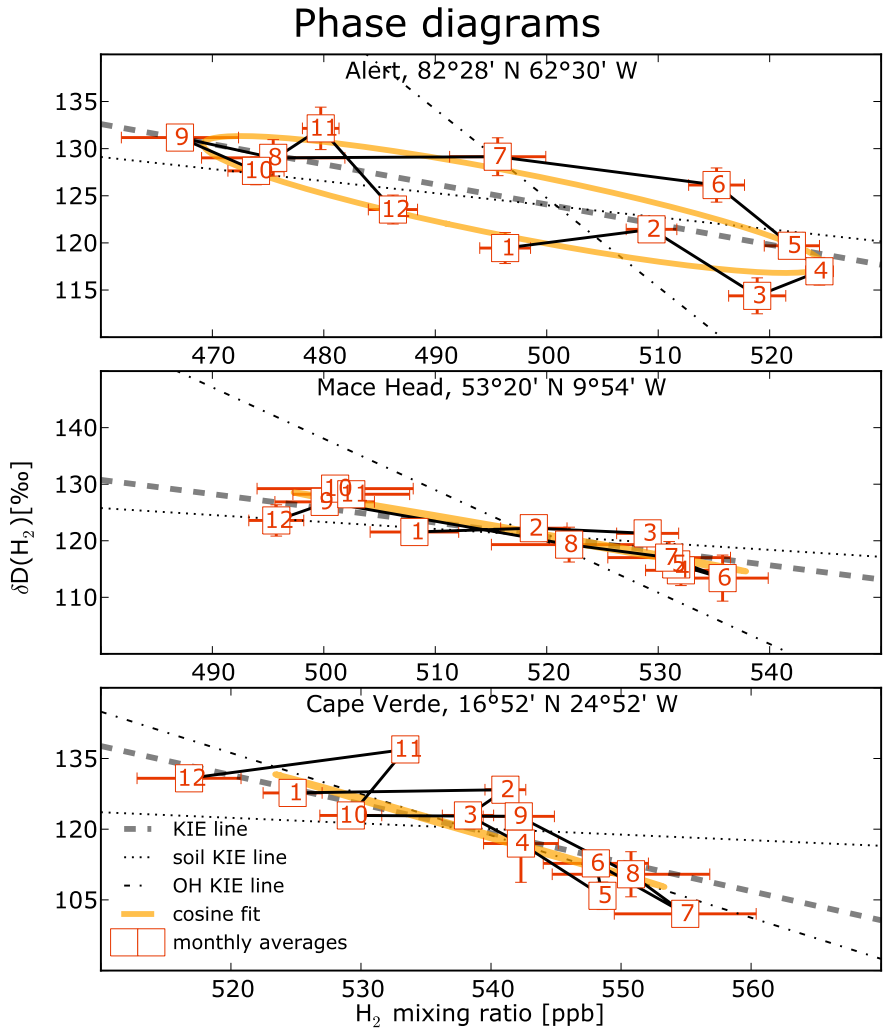

Figure 2.6: Phase diagrams (δD vs. $\chi(H_2)$) of the monthly averages (labelled with month number) of the three stations that show clear seasonal cycles. The orange ellipses are derived from the sinusoidal fits to the time series. The thick grey dashed line is the ``KIE'' line for the apparent fractionation factor determined from the fractionation plot for the respective station as defined in (Allan et al., 2001). The dotted and dash-dotted lines are the KIE lines for the two different sink processes, with values for α from (Rhee et al., 2006b). Note that the determined KIE line at Alert and Mace Head is closest to the soil uptake KIE line, while the determined KIE line at Cape Verde is closer to the OH oxidation KIE line.

$\chi(H_2)$ or δD, it is reasonable to assume isotope equilibrium for the years over which the data presented here were collected.

A factor that could still affect the analysis is a seasonally varying contribution of the two main sinks. However, especially in Alert, any variations in the relative contributions of the two sinks over the year are expected to be small, because even if soil uptake and atmospheric OH oxidation do not follow the exact same seasonal pattern, their patterns are expected to share the main characteristics, with a minimum in winter, and a peak in summer. Hence, although the Rayleigh fractionation model does not represent the full complexity of reality at the stations, the apparent fractionation constants determined with this model provide a good estimate of the total sink fractionation.

For Alert, Mace Head and Cape Verde, KIE lines were calculated with the hydrogen α_{app} obtained for the different stations, as well as with the fractionation constants *Rhee et al.* (2006b) for the two H_2 sink processes and added to Figure 6. Clearly, for Alert and Mace Head the KIE line of the fit lies closest to the KIE line of soil uptake, whereas in Cape Verde it lies closest to atmospheric OH oxidation. For these three stations, α_{app} is plotted versus station latitude in Figure 2.7 (a). The apparent fractionation factor can be interpreted as a combination of the fractionation factors of the main sink processes. For Alert and Mace Head, the α_{app} values (0.905 ± 0.008 and 0.884 ± 0.014, respectively) are close to the fractionation factor assigned to soil uptake ($\alpha = 0.943 \pm 0.007$). *Rhee et al.* (2006b) also concluded from a similar analysis on a small set of upper tropospheric air samples that the seasonal cycle of H_2 in the NH is largely driven by soil uptake. Closer to the equator, at Cape Verde, α_{app} (0.704 ± 0.029) is lower and closer to the value for oxidation by OH ($\alpha = 0.58 \pm 0.07$). This indicates that the relative importance of the uptake by soil with respect to the destruction by OH increases with latitude.

Figure 2.7 (b) shows the relative contribution of both sinks processes to the total destruction of H_2, as can be calculated from these isotope data if α_{app} is assumed to be a simple mass weighted average of the fractionation factors of soil removal and reaction with OH. This calculation yields that OH destroys more than half ($(66 \pm 15)\,\%$) of the H_2 at Cape Verde, but that at Alert, $\approx 90\,\%$ of the H_2 is destroyed by soil uptake. This finding of a latitudinal trend in the data presented here depends heavily on the Cape Verde station, where the formal application of the Rayleigh fractionation model yields a very low α_{app} and therefore a large contribution of OH oxidation to the total sinks. As discussed in section 2.3.1, the $\chi(H_2)$ and δD cycles at Cape Verde are shifted in time with respect to Alert and Mace Head, which indicates that the way the source, sink and transport processes drive the seasonal variations is somewhat different between these stations. But although α_{app} may be underestimated in Cape Verde, the general trend towards a higher OH fraction with decreasing latitude is in accordance with expectation and model results. In the TM5 model study, H_2 destruction is clearly dominated by the soil sink in the high northern latitude band (30° N–90° N), whereas the two sinks are of comparable magnitude in the tropical latitude band (30° N–30° S) (Figure 8 in Pieterse et al., 2011). Therefore, our findings indicate that the NH average α_{app} of 0.90 ± 0.02 found by *Rhee et al.* (2006b) for a limited number of samples in the tropopause region and the associated $(87 \pm 7)\,\%$ relative contribution of the soil sink may be overestimates. This also means that their H_2 lifetime estimate of (1.4 ± 0.2) years may be too short. To investigate this further, it would be useful to analyze samples from subtropical northern latitudes, for example the Iberian Peninsula, the Canary Islands or Morocco.

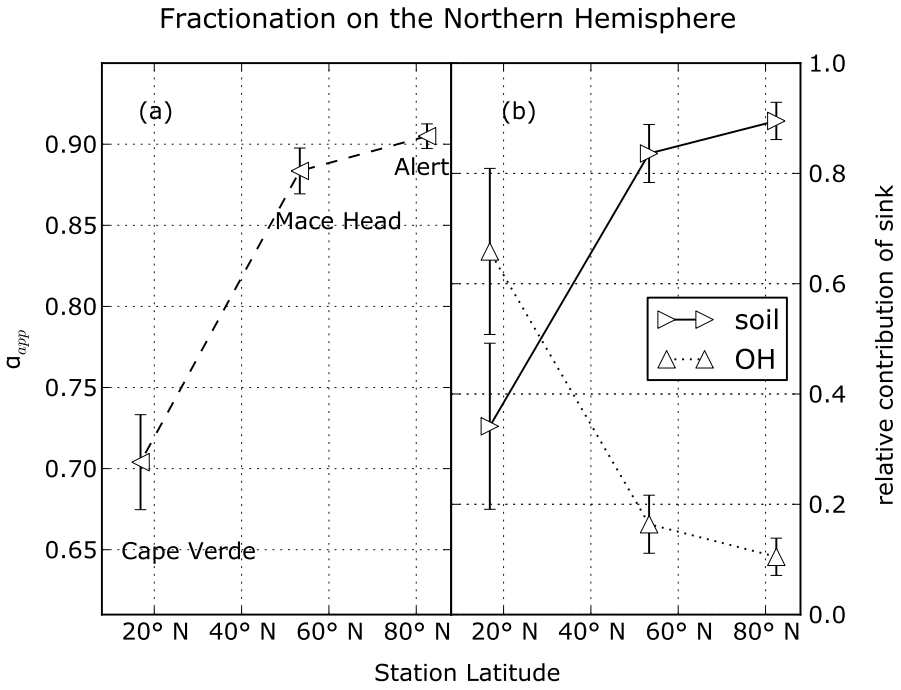

Figure 2.7: (a): Apparent fractionation factors for the NH, calculated from a least-squares fit to a Rayleigh plot, plotted as a function of station latitude. **(b):** Relative contributions of uptake by soils and atmospheric oxidation by OH to the total sinks, calculated from the apparent fractionation factors and the values for the fractionation processes used by *Rhee et al.* (2006b). Error bars indicate one standard error.

2.4 Conclusions

Air samples from six EUROHYDROS stations have been analysed regularly for $\chi(H_2)$ and δD, which allows analysis of the temporal and latitudinal distribution of H_2 and its isotopic composition. These data greatly expand the existing δD dataset, and can be used to constrain the global and regional H_2 budgets with the help of global and regional models.

The out-of-phase behaviour of $\chi(H_2)$ and δD that was proposed for the NH by *Rhee et al.* (2006b) is seen at Mace Head and Cape Verde, and particularly clearly at Alert, but not at Schauinsland, which is a continental station and closer to anthropogenic source regions. The SH stations show very little variation in δD, even when $\chi(H_2)$ exhibits a small seasonal cycle. The δD data show a clear latitudinal gradient with higher values in the SH than in the NH. This gradient varies with season, mainly driven by the seasonality in the NH. The observed pole-to-pole differences are larger than observed on ship cruises (*Gerst and Quay*, 2000; *Rice et al.*, 2010). The lowest annual average δD value is not found at the highest NH latitude station, but at lower NH latitudes, where the influence

of the anthropogenic fossil fuel combustion source is strongest. If it is assumed that the seasonality of the $\chi(H_2)$ and δD time series is mainly determined by the removal processes, the relative changes of $\chi(H_2)$ and δD can be used to provide information on the relative sink strengths of soil deposition and atmospheric oxidation. The data then indicate that at high NH latitudes, the removal processes are almost completely dominated by deposition to soil, whereas in the tropics, soil deposition and atmospheric oxidation by OH are of similar importance. Our findings imply that the previously reported average value of α_{app} for the NH and the large relative contribution of the soil sink derived from it may be overestimates.

Chapter 3

δD(H_2) in the tropopause region probed by the CARIBIC aircraft

This chapter is based on:

Batenburg, A. M., Schuck, T. J., Baker, A. K., Zahn, A., Brenninkmeijer, C. A. M., and Röckmann, T.: *The stable isotopic composition of molecular hydrogen in the tropopause region probed by the CARIBIC aircraft*, Atmos. Chem. Phys., **12**, 4633–4646, doi: 10.5194/acp-12-4633-2012, 2012. URL: `www.atmos-chem-phys.net/12/4633/2012/acp-12-4633-2012.html`

Abstract

More than 450 air samples that were collected in the upper troposphere - lower stratosphere (UTLS) region by the CARIBIC aircraft (Civil Aircraft for the Regular Investigation of the atmosphere Based on an Instrument Container) have been analyzed for molecular hydrogen (H_2) mixing ratios ($\chi(H_2)$) and H_2 isotopic composition (deuterium content, δD).

More than 120 of the analyzed samples contained air from the lowermost stratosphere (LMS). These show that $\chi(H_2)$ does not vary appreciably with O_3-derived height above the thermal tropopause (TP), whereas δD does increase with height. The isotope enrichment is caused by competing H_2 production and destruction processes that enrich the stratospheric H_2 reservoir in deuterium (D); the exact shapes of the profiles are mainly determined by mixing of stratospheric with tropospheric air. Tight negative correlations are found between δD and the mixing ratios of methane (CH_4) and nitrous oxide (N_2O), as a result of the relatively long lifetimes of these three species. The correlations are described by $\delta\mathrm{D}[‰] = -0.35 \cdot \chi(\mathrm{CH_4})[\mathrm{ppb}] + 768$ and

$\delta D[‰] = -1.90 \cdot \chi(N_2O)[ppb] + 745$. These correlations are similar to previously published results and likely hold globally for the LMS.

Samples that were collected from the Indian subcontinent up to 40° N before, during and after the summer monsoon season show no significant seasonal change in $\chi(H_2)$, but δD is up to 12.3 ‰ lower in the July, August and September monsoon samples. This δD decrease is correlated with the $\chi(CH_4)$ increase in these samples. The significant correlation with $\chi(CH_4)$ and the absence of a perceptible $\chi(H_2)$ increase that accompanies the δD decrease indicates that microbial production of very D-depleted H_2 in the wet season may contribute to this phenomenon.

Some of the samples have very high $\chi(H_2)$ and very low δD values, which indicates a pollution effect. Aircraft engine exhaust plumes are a suspected cause, since the effect mostly occurs in samples collected close to airports, but no similar signals are found in other chemical tracers to support this. The isotopic source signature of the H_2 pollution seems to be on the low end of the signature for fossil fuel burning.

3.1 Introduction

3.1.1 Atmospheric Molecular Hydrogen (H_2)

Molecular hydrogen (H_2) has been a relatively little studied atmospheric trace gas for some time, but over the last decades, there has been a steep increase in research efforts into the global H_2 cycle. These efforts have undoubtedly been spurred by the possible future use of H_2 as an energy carrier. It is expected that when this technology comes into wide use, it will lead to leakage of H_2 into the atmosphere, which may lead to considerably increased atmospheric H_2 levels. This may affect the atmosphere's oxidative capacity and stratospheric ozone levels (*Schultz et al.*, 2003; *Warwick et al.*, 2004; *Tromp et al.*, 2003; *Feck et al.*, 2008). A number of global H_2 budget estimates have been made (*Novelli et al.*, 1999; *Hauglustaine and Ehhalt*, 2002; *Sanderson et al.*, 2003; *Rhee et al.*, 2006b; *Price et al.*, 2007; *Xiao et al.*, 2007; *Ehhalt and Rohrer*, 2009; *Yashiro et al.*, 2011; *Yver et al.*, 2011a; *Bousquet et al.*, 2011; *Pieterse et al.*, 2011, 2012). These estimates agree that the largest source of H_2 to the atmosphere is oxidation of hydrocarbons, followed by combustion of fossil fuels and biomass (see Table 3.1). Production of H_2 during N_2-fixing by microbes on land or in the ocean constitutes a minor source. These source terms are balanced by two sink processes, uptake by soils (and subsequent destruction by enzymes) and atmospheric oxidation by the hydroxyl radical (OH), of which soil uptake is the largest. Together, these processes result in typical atmospheric H_2 mixing ratios ($\chi(H_2)$) of around 548 ppb (nmole/mole) at ground level (*Novelli et al.*, 1999, converted to the latest $\chi(H_2)$ scale established by *Jordan and Steinberg* (2011)), with on average 3 % higher values in the Southern Hemisphere. Model results indicate that $\chi(H_2)$ may increase slightly with height, especially in the Northern Hemisphere extratropics (*Hauglustaine and Ehhalt*, 2002; *Price et al.*, 2007; *Pieterse et al.*, 2011). Despite the qualitative agreement, the uncertainties in the estimates of the magnitudes of the different terms in the budget are large.

Table 3.1: The global H_2 budget and isotope budget as estimated by *Pieterse et al.* (2011) in a model study with global model TM5. The estimated magnitudes, isotopic signatures and uncertainties (super- and subscript numbers) of the different surface sources were based on previous studies. For biomass burning, the estimated source signature was based on measurements that were later published in (*Röckmann et al.*, 2010a). The magnitudes and isotope effects of the photochemical processes and the soil uptake were calculated from the model output; in this first H_2 study with TM5, no estimates of the uncertainties associated with these terms were made yet. At the bottom of the table are estimates by different authors of the global average $\chi(H_2)$ and $\delta D(H_2)$.

Sources	Magnitude (Tg H_2 yr^{-1})	δD (‰)
Fossil fuel combustion	17.0^{+3}_{-6}	-196^{+10}_{-74}
Biomass burning	15.0^{+5}_{-5}	-260^{+60}_{-60} [a]
Ocean N_2 fixation	5.0^{+1}_{-2}	-628^{+0}_{-72} [b]
Land N_2 fixation	3.0^{+3}_{-3}	-628^{+0}_{-72} [b]
Photochemical production	37.3	+116
Total sources	**77.3**	
Sinks	Magnitude (Tg H_2 yr^{-1})	Fractionation coefficient ($\alpha = \frac{k_{HD}}{k_{HH}}$)
Photochemical removal (mainly by OH)	22.1	0.542
Deposition to soils	55.8	0.925
Total sinks	**77.9**	
Global averages	$\chi(H_2)$	δD(H)2)
	547 ppb [c]	+124 to +150 ‰ [d]

[a] Results from *Vollmer et al.* (2010) indicate that this source signature may be lower for modern cars and certain driving conditions. Results from a polluted station in the Netherlands also indicate this (*Batenburg et al.*, 2012).
[b] *Walter et al.* (2011) found this source signature to be (-741 $\pm$ 13) ‰.
[c] *Novelli et al.* (1999)
[d] Depending on latitude, *Batenburg et al.* (2011)

3.1.2 Stable isotope studies of H_2

Studies of the stable isotopic composition of H_2 ($\delta D(H_2)$, or henceforth, δD) can provide independent information to constrain the H_2 budget. The isotope effects associated with sources and sinks of H_2 (Table 3.1) are particularly large due to the large relative mass difference between deuterated hydrogen (HD) and 'ordinary' hydrogen (HH). We define

δD as:

$$\delta\mathrm{D} = \delta\mathrm{D}(\mathrm{H_2}) = \left(\frac{R_{Sample}}{R_{VSMOW}} - 1\right) \cdot 1000‰ \tag{3.1}$$

where R_{Sample} is the ratio of the number of deuterium atoms (D) to protium atoms ("ordinary" hydrogen atoms, H) in the sample H_2, and R_{VSMOW} is this D/H ratio in Vienna Standard Mean Ocean Water. Recently, isotope effects in the production processes of H_2 have been studied (*Gerst and Quay*, 2001; *Rahn et al.*, 2002b, 2003; *Röckmann et al.*, 2003; *Rhee et al.*, 2006a; *Feilberg et al.*, 2007; *Rhee et al.*, 2008; *Röckmann et al.*, 2010a,b; *Vollmer et al.*, 2010; *Walter et al.*, 2011; *Haumann et al.*, 2012), as well as the isotope effects in the H_2 uptake by soils (*Gerst and Quay*, 2001; *Rahn et al.*, 2002a; *Rice et al.*, 2011).

Two chemical transport models have been adapted to incorporate the stable isotopic composition of H_2, namely GEOS-CHEM (*Price et al.*, 2007) and TM5 (*Pieterse et al.*, 2009, 2011, 2012), and many more δD data have become available for the validation of such models (*Rice et al.*, 2010; *Batenburg et al.*, 2011). However, for obvious practical reasons, most of these data were collected at ground level, and yield little information about processes higher up in the atmosphere, particularly in the Upper Troposphere-Lower Stratosphere (UTLS) region. This is problematic since Stratosphere-Troposphere Exchange (STE) in the UTLS may be one of the main processes that enrich the global tropospheric H_2 reservoir. Both *Price et al.* (2007) and *Pieterse et al.* (2011) estimated that STE contributes several tens of ‰ to the global tropospheric δD average. Furthermore, *Pieterse et al.* (2011) found that the magnitude of the contribution was highly sensitive to the δD value assumed for the stratosphere. A good parameterization of the isotope effects of STE is therefore necessary to reduce the uncertainties in the modeled isotope budget, which is, in turn, necessary to be able to use the isotopes to constrain the global H_2 budget. A number of investigations have been conducted in the stratosphere (*Rahn et al.*, 2003; *Röckmann et al.*, 2003; *Rhee et al.*, 2006a), but only three of the samples analyzed for these studies were sampled below 14 km altitude. *Rhee et al.* (2006b) presented data from three previous CARIBIC (Civil Aircraft for the Regular Investigation of the atmosphere Based on an Instrument Container) flights, but focused only on the tropospheric samples, and actually omitted those samples near the tropopause (TP) or in the lowermost stratosphere (LMS) from further analysis.

Not only are some altitudes underrepresented in the published δD data, also some regions of the world are not well covered. Previously published data were mostly from samples collected at two stations at the west coast of North America and on Pacific Ocean transects (*Gerst and Quay*, 2000; *Rice et al.*, 2010), or at stations in Europe and the polar regions (*Batenburg et al.*, 2011). Data from other regions, such as South Asia, are scarce. The aim of analyzing data from the CARIBIC program is to close both the altitudinal and the regional gap in the observations.

The CARIBIC project uses a passenger aircraft to make in-situ measurements and to sample air and aerosol at aircraft cruise altitude, generally between 9 and 11 km. At this altitude, the aircraft intercepts both upper troposphere (UT) and lowermost stratosphere (LMS) air masses in similar quantities at mid-latitudes. CARIBIC is therefore a very suitable platform to study the UTLS region. The obtained information is somewhat Eurocentric, because the aircraft is based at Frankfurt airport (Fig. 3.1). Nevertheless, a large region of the globe is covered, including the Indian subcontinent where air was sampled before, during and after the summer monsoon season. To our knowledge, this paper presents the first δD observations that have been made in or over India. The results of measurements of

greenhouse gases (GHGs) in the South Asian samples discussed here have been published previously by *Schuck et al.* (2010). These revealed an increase in greenhouse gas mixing ratios during the monsoon season, especially for methane (CH_4). This was attributed to increased CH_4 emissions from rice paddies and wetlands, and increased convective transport that brought the CH_4 to aircraft cruising altitude. The δD data from these samples provide a unique opportunity to study possible δD effects in the convective monsoon system.

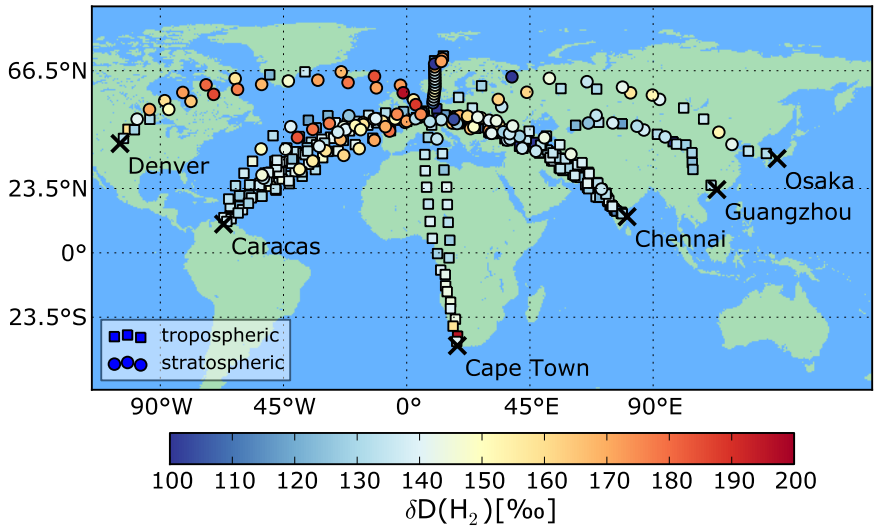

Figure 3.1: Sampling locations of all samples. The color scale indicates the measured value of δD. The destination airports of the flights are indicated with black crosses and names. Marker type indicates if the sample is tropospheric (□) or stratospheric (○), as determined by the O_3-derived height above the tropopause (TP) (*Sprung and Zahn*, 2010). Some polluted samples are off the scale ($\delta D < 100‰$).

3.1.3 δD in the stratosphere

H_2 mixing ratios vary little in the stratosphere, but isotope information reveals that H_2 is involved in stratospheric reactions. Deuterium enrichments of more than 250 ‰ above typical tropospheric values ($\approx$ +130 ‰) were found during a stratospheric research aircraft campaign (*Rahn et al.*, 2003) and stratospheric balloon campaigns (*Röckmann et al.*, 2003; *Rhee et al.*, 2006a). These are evidence that production and destruction of H_2 do take place; that $\chi(H_2)$ remains unchanged means that H_2 production (by methane oxidation) and destruction (by its own oxidation) are of almost equal magnitude. Since

δD varies much more in the stratosphere than $\chi(H_2)$, it contains much more information about the stratospheric cycles of H_2 and other H-containing compounds (CH_4, HCHO, H_2O, ...) than $\chi(H_2)$.

Plumb (2007) found that compact correlations between stratospheric species are common, as the time scales for stratospheric transport are shorter than the chemical lifetimes of (relatively) long-lived trace gases. Due to this, all the data from *Rahn et al.* (2003), *Röckmann et al.* (2003) and *Rhee et al.* (2006a) show a compact inverse correlation between δD and methane (CH_4) mixing ratios ($\chi(CH_4)$). So, as the air ages, CH_4 is destroyed, and H_2 is both produced and destroyed by processes that cause a net D-enrichment.

H_2 removal by OH has a strong preference for removal of HH over removal of HD (*Talukdar et al.*,1996, see also Table 3.1) and therefore enriches the remaining H_2 reservoir. However, to explain the total observed enrichments, also the H_2 produced from CH_4 must be D-enriched. The first step in the chain of reactions that leads from CH_4 to H_2 is the abstraction of an H atom from CH_4, and the last step is photolysis of the intermediate product formaldehyde (HCHO). Both these steps proceed more slowly for the deuterated than for the non-deuterated species (*Sander et al.*, 2006; *Feilberg et al.*, 2007; *Rhee et al.*, 2008; *Röckmann et al.*, 2010b), but these effects are offset by D-enriching effects in the other reactions in the chain (*Nilsson et al.*, 2007). For the total process, stratospheric (δD) source signatures between +130 and +370 ‰ were reported (*Rahn et al.*, 2003; *Röckmann et al.*, 2003; *Rhee et al.*, 2006a). Results from the TM5 model indicate that the source signature is likely in the low end of this range (*Pieterse et al.*, 2011, see also Table 3.1). Also, a lab study by *Nilsson et al.* (2010) showed that the isotope effects are pressure dependent.

McCarthy et al. (2004) presented parametrizations of δD and the mixing ratio of deuterated hydrogen (χ(HD)) relative to $\chi(CH_4)$, based on the data from *Rahn et al.* (2003). *Pieterse et al.* (2011, 2012) used this to obtain the first results with the TM5 model, but had to apply a large correction to keep the model results close to observed tropospheric δD values. The CARIBIC data presented here allow us to calculate a new correlation between δD and $\chi(CH_4)$. As this new correlation is based on samples collected close to the TP, we would consider it a very suitable choice for parameterizing δD from $\chi(CH_4)$ in the LMS in models.

3.2 Experimental

3.2.1 Sampling and in-situ measurements

The CARIBIC Airbus A340-600 is equipped with a 35 cm tall inlet system with several intake probes, which is located underneath just in front of the belly fairing (*Brenninkmeijer et al.*, 2007). Air from the trace gas inlet probe passes through heated PFA-lined stainless steel tubing ($\approx$ 40° C) to the equipment in the automated CARIBIC measurement container. Here, whole air samples are collected by the so-called TRAC (Triggered Retrospective Air Collector) (*Brenninkmeijer et al.*, 2007; *Schuck et al.*, 2009). This system consists of a pumping unit and two separate sample units, controlled by a computer unit. Each sample unit contains 14 glass cylinders with a volume of 2.67 l each that during sampling are pressurized to an effective pressure of 3.5 to 4.2 bar. During flight, sampling starts after a pressure cutoff level (450 mbar) is reached to avoid sampling of low-level polluted air in the vicinity of airports. By flushing, the air within each flask is replaced approximately ten times before the actual sample is taken. The pressurization of the sample

to the final pressure then takes from 0.5 to 1.5 min, which corresponds to a flight distance of 7 to 21 km (this varies as it takes longer to fill the samples to the required minimum final pressure at higher altitude). A flask is filled every hour or half hour at points evenly distributed over the expected flight time. On arrival back in Frankfurt, one of the sample units usually contains samples from the first flight leg (Frankfurt to destination) and the other contains samples from the return flight (destination to Frankfurt). With this method of regular, automated, non-event-driven sampling, the distribution of samples is likely representative of the different air masses encountered by the aircraft. *Schuck et al.* (2009) showed that this was the case for carbon dioxide mixing ratios ($\chi(CO_2)$) in these samples.

Ozone (O_3) mixing ratios ($\chi(O_3)$) and carbon monoxide (CO) mixing ratios ($\chi(CO)$) are measured in-flight. $\chi(O_3)$ is measured with a custom made UV-photometer (*Brenninkmeijer et al.*, 2007), and $\chi(CO)$ is measured with a vacuum ultraviolet fluorescence instrument (*Scharffe et al.*, 2012). These measurements are integrated over the TRAC sampling times to obtain the $\chi(O_3)$ and $\chi(CO)$ value for each TRAC sample. The ozone values are then used to estimate the height above the thermal TP with the method of *Sprung and Zahn* (2010).

Meteorological plots and trajectory calculations are routinely produced for each CARIBIC flight by the KNMI (*van Velthoven*, 2009), based on European Centre for Medium Range Weather Forecasts (ECMWF) data. For the calculation of the mean trajectory parameters for each sample, 15 five-day trajectories are generated that start at the same time, but at slightly different locations or pressures. These are combined into one mean trajectory by averaging at each one-hour timestep; the parameters are then calculated from the mean trajectory.

3.2.2 GHG analysis

The samples that are collected in the TRAC units are routinely analyzed for CH_4, CO_2, nitrous oxide (N_2O) and sulfur hexafluoride (SF_6)) mixing ratios ($\chi(CH_4)$, $\chi(CO_2)$, $\chi(N_2O)$ and $\chi(SF_6)$) at the Max Planck Institute for Chemistry in Mainz on a gas chromatography system. This uses an HP 6890 gas chromatograph with two simultaneously operated channels: one to measure $\chi(CO_2)$ and $\chi(CH_4)$ with a Flame Ionization Detector (FID) and one to measure $\chi(N_2O)$ and $\chi(SF_6)$) with an Electron Capture Detector (ECD). Four injections are made for each sample, and the repeatability for each datapoint is determined from the standard deviation of the four injections. The measurement of each sample is bracketed by the measurement of a laboratory working gas to detect any instrument drift. These laboratory working gases are calibrated against NOAA standards. $\chi(CH_4)$ values reported in this paper are on the NOAA 2004 scale, and $\chi(N_2O)$ values are on the NOAA 2006 scale.

3.2.3 Analysis of $\chi(H_2)$ and $\delta D(H_2)$

A subset of the samples collected by the TRAC, 490 in total, was sent to the isotope laboratory of the Intitute for Marine and Atmospheric Research Utrecht (IMAU). Here, air samples are routinely analyzed for $\chi(H_2)$ and δD with a Gas Chromatography Isotope Ratio Mass Spectrometry (GC-IRMS) system as described by *Rhee et al.* (2004) following a day-to-day procedure as described by *Batenburg et al.* (2011). Briefly, in each acquisition the H_2 is separated from the air matrix and isotopically analyzed in the following 4 steps.

1. *Trapping of all air components* except helium, hydrogen, neon and a trace of ni-

trogen in an $\approx$ 0.5 L (STP) aliquot of sample air by exposure to a $\approx$ 40 K cold head.

2. *Pre-concentration* of the H_2 from the head space of the cold head by flushing it with helium through a trap filled with 5 Å molecular sieve kept at $\approx$ 63 K by submersion in liquid nitrogen at reduced pressure.
3. *Focussing* of the H_2 pulse in a cryo-focus trap consisting of a steel-jacketed 5 Å molecular sieve capillary submersed in liquid nitrogen (77 K) and *final purification* on a 5 Å molecular sieve gas chromatography column kept at 323 K.
4. *Injection* of the purified H_2 through an open split interface into an IRMS (ThermoFinnigan Delta plus XL) for determination of the D/H ratio.

469 samples were successfully analyzed for $\chi(H_2)$ and δD. 10 of these samples were collected below 6 km altitude during a special flight to investigate the plume of the 2010 Eyjafjallajökull eruption and are left out of further analysis.

Measurements of air from laboratory reference air bottles, as well as blank measurements, were typically performed every operational day following the same procedure as for the samples. The 5-day moving average values of these reference measurements were used to calculate the corrected $\chi(H_2)$ and δD for each sample. From measurements of other samples on this system it was concluded that measurements performed from June 2010 onwards had a positive bias in δD (*Batenburg et al.*, 2011). An empirically determined offset of 9.5 ‰ was therefore subtracted from all CARIBIC δD datapoints measured after this time. To the $\chi(H_2)$ data a linear empirical correction formula was applied that was derived from a comparison of the GC-IRMS results with results from collaborating laboratories within the EUROHYDROS project. The estimated standard deviation (σ) in the measurements of $\chi(H_2)$ is 2.5 % (relative), and the estimated standard deviation in δD is 4.5 ‰ (absolute).

3.2.4 Selection of stratospheric and polluted samples

Sprung and Zahn (2010) presented a method to translate the observed $\chi(O_3)$ for a sample to an estimate of the vertical distance above the thermal TP by interpolation from vertical $\chi(O_3)$ profiles observed during balloon soundings at 12 ground stations (*Sprung and Zahn*, 2010). This estimate can be made for any sample with a $\chi(O_3)$ higher than at the local thermal TP. All 123 TRAC samples for which this estimate could be made are considered 'stratospheric', the 336 others are considered 'tropospheric'. This selection criterion was chosen to accurately resolve the chemical fine structure of the TP.

For some samples, often taken close to take-off and landing of the aircraft, the GC-IRMS analysis yielded very high $\chi(H_2)$ and very low δD values, indicating that these samples were affected by pollution. Samples were flagged as polluted by an iterative process that was applied separately to the tropospheric and stratospheric samples, as follows: samples that were more than three standard deviations below the (unweighted) average value of δD or three standard deviations above the (unweighted) average $\chi(H_2)$ were filtered out of a list of the data, after which new averages and standard deviations were calculated. This was repeated until no new outlying samples were found, and the resulting averages were used to label each sample that showed a δD value more than three standard deviations below the new δD average, or an $\chi(H_2)$ value more than three standard deviations above the new $\chi(H_2)$ average as polluted. Three (out of 123) stratospheric and 25 (out of 336) tropospheric samples were labelled as polluted by this process.

3.3 Results and discussion

The geographical distribution of the analyzed samples is shown in Fig. 3.1. The color scale indicates the measured δD, and the type of marker indicates whether the sample is tropospheric or stratospheric. It can be seen that due to the use of one base airport, the area that is covered is not global, although it is large. Only one of the analyzed stratospheric samples was collected in the Southern Hemisphere, and no samples were collected over the Pacific Ocean. Europe and the North Atlantic are the best covered regions, and also the Middle East and Central Asia are reasonably well covered. Except the samples that were collected below 6 km altitude and left out of the analysis, all samples were collected between 6.9 and 12.3 km altitude, with an average altitude of 10.9 (σ = 0.8) km. The months in which the largest number of analyzed samples were collected are May, July and September, whereas none of the samples were collected in December, January and February.

As an illustration of the features that are typically observed in the CARIBIC dataset, Fig. 3.2 shows the $\chi(H_2)$ and δD values that were measured on those samples that were collected on flights to Caracas (Venezuela). The flights from April 2009 and September 2009 show the pollution phenomenon discussed above; in both return flights, one sample that is taken close to Frankfurt airport (50.1° N) shows very high $\chi(H_2)$ and very low δD values (off the scales). Another feature that is illustrated by these plots is that the stratospheric samples (shown with open symbols) often show a marked elevation in δD with respect to the tropospheric samples as a result of stratospheric processing, whereas no difference in $\chi(H_2)$ can be noted by eye.

Averaged over the whole unpolluted dataset, the tropospheric $\chi(H_2)$ and δD averages and standard errors (SEM) are (550.5 $\pm$ 0.9) ppb (311 samples, σ = 16.6 ppb) and (132.8 $\pm$ 0.4) ‰ (σ = 7.1 ‰), respectively. For the stratosphere, these values are (559.8 $\pm$ 1.5) ppb (120 samples, σ = 16.1 ppb) and (151.8 $\pm$ 1.6) ‰ (σ = 17.4 ‰). The difference between troposphere and stratosphere is larger for δD, but for both $\chi(H_2)$ and δD, the difference is significant with 95 % confidence.

3.3.1 Pollution signatures

In the total dataset of 459 successful measurements, 28 samples were labeled as polluted by the iterative selection procedure. Nine of these samples were in the first canister (number 1 or 15) of a TRAC sample unit, and eight were in the last (number 14 or 28). These two endcanisters are filled closest to the departure or destination airport (of the total of 14 canisters in a TRAC sample unit). Clearly, this pollution effect has a very strong tendency to occur there. Typically, the first sample in the sample unit is collected at the lowest altitude, as the aircraft usually follows a slightly upward sloping flight route. Therefore, pollution from the boundary layer was a suspected cause. However, a study of the calculated backward trajectories of these samples showed that only a minority of the outlying samples (eight, of which five in the first TRAC sample unit canister) had possible boundary layer influence.

Because of this, and because of the strong tendency to occur in the vicinity of airports where a large concentration of airplanes are present, we consider the interception of exhaust plumes of other aircraft in the flight corridor a possible cause. As exhaust plumes are occasionally seen by equipment in the container as sharp spikes in NO_x and NO_y (*Ziereis et al.*, 2000), we inspected all data to see if the finding of polluted H_2 values

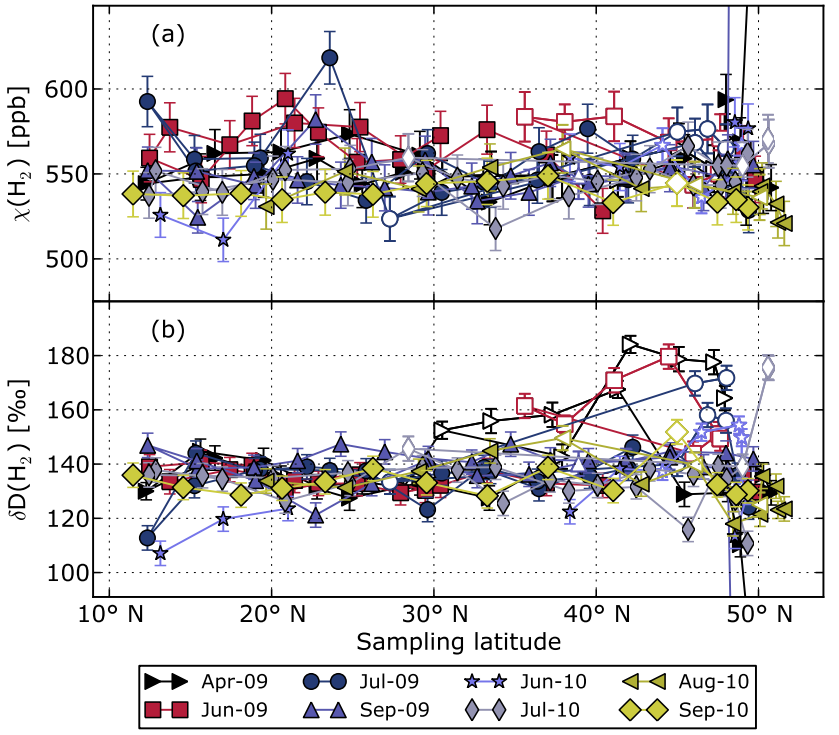

Figure 3.2: Latitudinal distribution of $\chi(H_2)$ **(a)** and δD **(b)** data from samples that were collected on flights to Caracas, Venezuela. Stratospheric samples are indicated with open symbols. Two (polluted) samples are off the scales.

coincided with NO_x and NO_y spikes. Unfortunately, the NO_x/NO_y measurements often began (just) after the first canister was filled, and ended before the last, so for the polluted samples in the first and last canisters of the TRAC sampling unit this information was often not available. For the polluted samples for which NO_x/NO_y measurements were available, a clear relation between polluted samples and NO_x/NO_y spikes was not found. Aerosol data were more often available (*Brenninkmeijer et al.*, 2007), but no clear relation was found with either N4-12, N12 or N18 particle numbers (numbers indicate particle size in nm). Because of this lack of correlation with other species, the origin of these pollution signatures cannot be definitively established.

An artifact in the measurement system is unlikely, because the measurements of these samples proceeded without peculiarities. The TRAC samples are kept in glass flasks connected to Valco multiposition valves with stainless steel tubing. *Gerst and Quay* (2000) found that D-depleted H_2 can form in metal cylinders, possibly associated with water vapor in the sample. However, the surface area of stainless steel in the TRAC tubing and valves is very small. So although the formation of H_2 from water vapor on the metal

parts could explain why the phenomenon so often occurs at the beginning and the end of flights, where the water vapor levels are (much) higher than during the rest of the flight (as the flight altitude is lower), it is not a likely process. Moreover, the occurrences of such pollution effects in intermediate canisters were not associated with water vapor peaks.

To determine the isotopic signature of the pollution source, a so-called Keeling plot was made (δD plotted against inverse $\chi(H_2)$) of the datapoints that met the pollution criterion (Fig. 3.3). One sample that was taken close to Cape Town and had both an elevated $\chi(H_2)$ and an elevated δD value was left out of this plot. The marker type indicates to which category of can (closest to takeoff, closest to touchdown or intermediate) the sample belongs, and the marker color indicates sampling altitude. It can be observed that the samples that have the clearest pollution signatures were in the endcanisters. We also note that the samples closest to takeoff are usually collected at lower altitudes (color scale), but that there is no clear relation between sampling altitude and the degree of pollution.

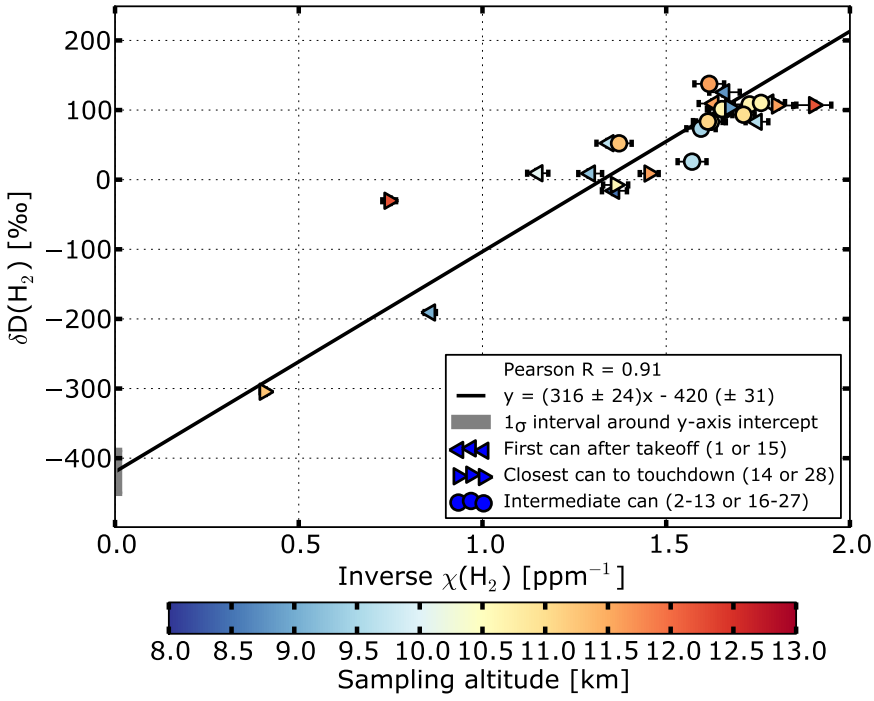

Figure 3.3: Keeling plot (δD vs. inverse $\chi(H_2)$ for those samples that were labeled as polluted with the iterative selection procedure. The solid line is a linear fit through all the data with the `Williamson-York' (W-Y) algorithm that takes the variance and the estimated errors in both the x- and y-direction into account (*Cantrell*, 2008). The 1×SEM (standard error) interval around the axis intercept of the fit is indicated in grey on the vertical axis. The marker type indicates in which part of a flight the sample was taken; the marker color indicates sampling altitude.

The linear fit to this Keeling plot was made using the Williamson-York (W-Y) algorithm described by *Cantrell* (2008). In contrast to a simple least-squares fit, this algorithm takes the variance and the estimated uncertainties in both the x- and the y-values of the data into account. This fit yields a very depleted source signature ((-420 ± 31) ‰, y-axis intercept) for the H_2 produced by the pollution source. This is very low compared to the commonly accepted values for fossil fuel or biomass burning emissions (see Table 3.1). Omission of the three most polluted data points in the fit increased the source signature to (-364 ± 60) ‰, which is still quite low. No data on the isotopic composition of H_2 produced by combustion of kerosine in jet engines are available, and whether the deuterium signature of H_2 produced by jet engines may be lower than that of H_2 from other fossil fuel combustion sources is unknown.

3.3.2 The stratosphere

The sampling location of each of the 123 selected stratospheric samples is indicated in Fig. 3.1 by circles, with the color representing δD according to the color scale. Most of the stratospheric samples that are at the high end of this scale were taken on a flight to Denver (USA) in May 2009. The aircraft reached high latitudes ($> 70°$ N) en route to this destination. Samples collected at higher latitudes have on average higher δD values, firstly because the TP slopes down with latitude and the aircraft therefore penetrates more deeply into the stratosphere at higher latitudes, and secondly because the average degree of stratospheric processing of the air masses is higher at higher latitudes due to the general poleward pattern of stratospheric circulation (*Holton et al.*, 1995).

The average degree of stratospheric processing of air generally increases with distance above the TP, and therefore stratospheric δD values also increase with altitude. For all stratospheric samples, an O_3-derived estimate of the height above the TP was available (in fact, this is how these samples were selected, see subsection 3.2.4). The O_3-derived altitude is not the same as the instantaneous altitude above the TP. Instead, it can be considered as a measure of the degree of mixing between low-O_3 air from the troposphere and high-O_3 air from the stratosphere. As detailed by *Sprung and Zahn* (2010), it is a robust method to quantify a "chemical" vertical coordinate around the tropopause. When $\chi(H_2)$ and δD are plotted against mean trajectory latitude and this O_3-derived height above the TP (Figure 3.4 (a) and (b)) it is clearly visible that δD increases with distance to the TP, whereas $\chi(H_2)$ does not. These figures also show that with the CARIBIC sampling method, the samples collected at the largest distance above the TP are generally collected at the highest latitudes. Figure 3.4 (c) shows the seasonal variation in the $\chi(CH_4)$ profile in the measured samples. In Northern Hemisphere (NH) spring subsidence occurs of air masses with low $\chi(CH_4)$. This pattern is almost exactly inversely mirrored in the seasonal variation in the δD profiles in Figure 3.4 (d); in NH spring, subsidence occurs of air with D-enriched H_2.

Both N_2O and CH_4 have sinks in the stratosphere. CH_4 has no stratospheric sources; N_2O may have a very small stratospheric source (*Estupiñán et al.*, 2002). $\chi(CH_4)$ and $\chi(N_2O)$ can therefore be used as an indicator of average degree of stratospheric processing that an air parcel has undergone. Plotting δD against $\chi(N_2O)$ and $\chi(CH_4)$ (Figure 3.5) shows very compact negative correlations for δD and these two greenhouse gases. There are no correlations with $\chi(H_2)$ (not shown); no systematic spatial or temporal $\chi(H_2)$ variation is observed in these data. So as the air ages, N_2O and CH_4 are destroyed, and H_2 becomes progressively D-enriched while its mixing ratio remains almost unchanged.

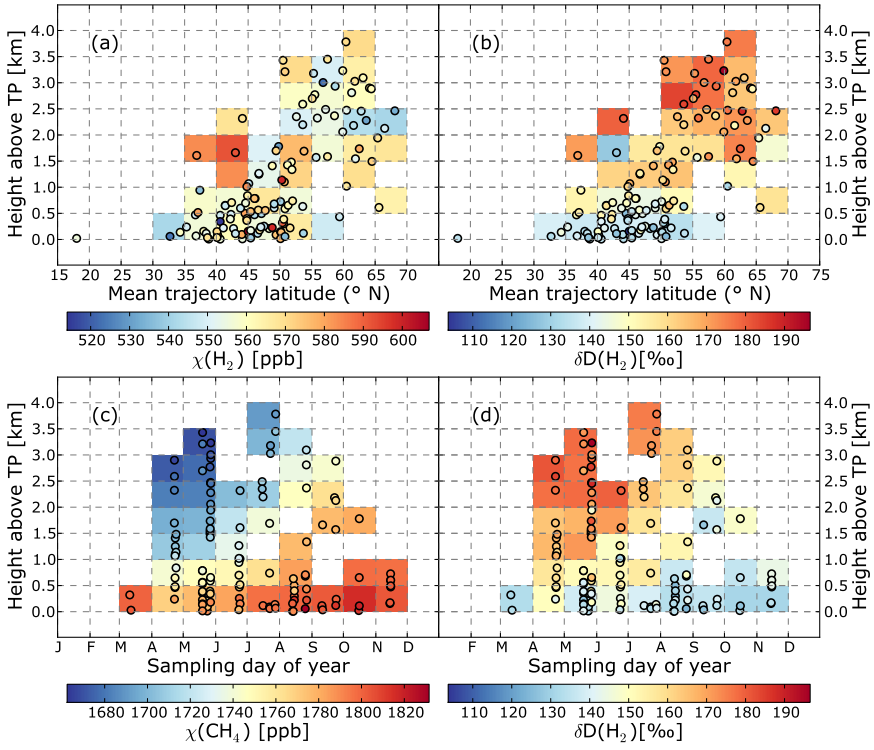

Figure 3.4: Distributions of $\chi(H_2)$ **(a)**, $\delta D(H_2)$ **(b)**, $\chi(CH_4)$ **(c)** and $\delta D(H_2)$ **(d)** in the stratospheric samples plotted against height above the thermal TP (calculated from the $\chi(O_3)$ measurements following the method of *Sprung and Zahn* (2010)) and mean trajectory latitude (calculated from the 15 five-day trajectories) **(a,b)** or time of year **(c,d)**. The squares are colored according to the averages of the samples in the squares.

Plumb (2007) showed that tight correlations exist between many long-lived stratospheric species. H_2, CH_4 and N_2O all have chemical lifetimes that are longer than the transport times in the lower stratosphere, and as a result their distributions are determined by transport and/or mixing processes rather than by chemistry. This explains the tightness of the observed correlations for both CH_4, which has a chemical link with H_2, and N_2O, which has none. We note that these correlations show that δD has potential for use as a tracer for stratospheric oxidation reactions of H-containing species (H_2, CH_4, H_2O, HCHO).

Correlations between δD and mixing ratios of other stratospheric species were previously found by *Rahn et al.* (2003), *Röckmann et al.* (2003) and *Rhee et al.* (2006a). Comparisons of the CARIBIC data to the data from *Rahn et al.* (2003) and *Röckmann et al.* (2003) are shown in Table 3.2 and Figure 3.6. Methane mixing ratio data from *Rahn et al.* (2003) and *Röckmann et al.* (2003) were multiplied by a factor of 1.0124 to convert them to the NOAA2004 scale. In the δD vs. $\chi(CH_4)$ correlation plot (Figure 3.6), a small offset

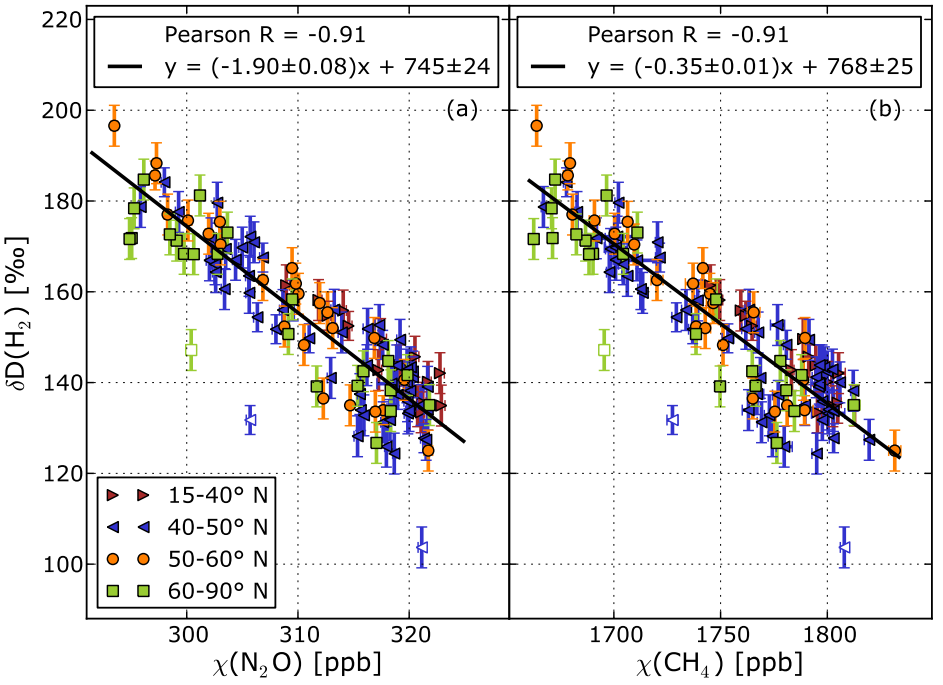

Figure 3.5: δD plotted against $\chi(N_2O)$ **(a)** and $\chi(CH_4)$ **(b)**. Solid lines are W-Y fits (*Cantrell*, 2008). Different colors and markers indicate different sampling latitude bands. Open symbols denote outlying datapoints that were left out of the fitting procedure.

occurs between the data from *Rahn et al.* (2003) and the new data presented here. From 2000 to 2009, the globally averaged $\chi(CH_4)$ increased by $\approx$ 15 ppb (*Duglokencky et al.*, 2009). The offset between the CARIBIC correlation and the correlation from *Rahn et al.* (2003) seems considerably larger than that, and therefore it is likely that the largest part of the offset is caused by inter-laboratory differences. A possible but speculative explanation for part of the offset is that *Rahn et al.* (2003) sampled "older" stratospheric air than CARIBIC, as they sampled higher in the stratosphere with a stratospheric research aircraft. The air masses that they sampled may have been introduced into the stratosphere before 2000, when tropospheric methane levels were even lower, whereas CARIBIC probably samples air masses that were more recently imported into the stratosphere. The slope of the CARIBIC correlation is outside of the 2×SEM interval of the slope of the *Rahn et al.* (2003) correlation, and vice versa.

The agreement between the data from *Röckmann et al.* (2003) and the CARIBIC data is slightly better. At 130 ‰, close to the tropospheric average, the difference in $\chi(CH_4)$ between the two correlation lines is $\approx$ 37 ppb, which is still more than twice the tropo-

spheric CH_4 increase. This may again be partly due to stratospheric age differences in the sampled air. The slopes, however, agree within one standard error of the CARIBIC fit.

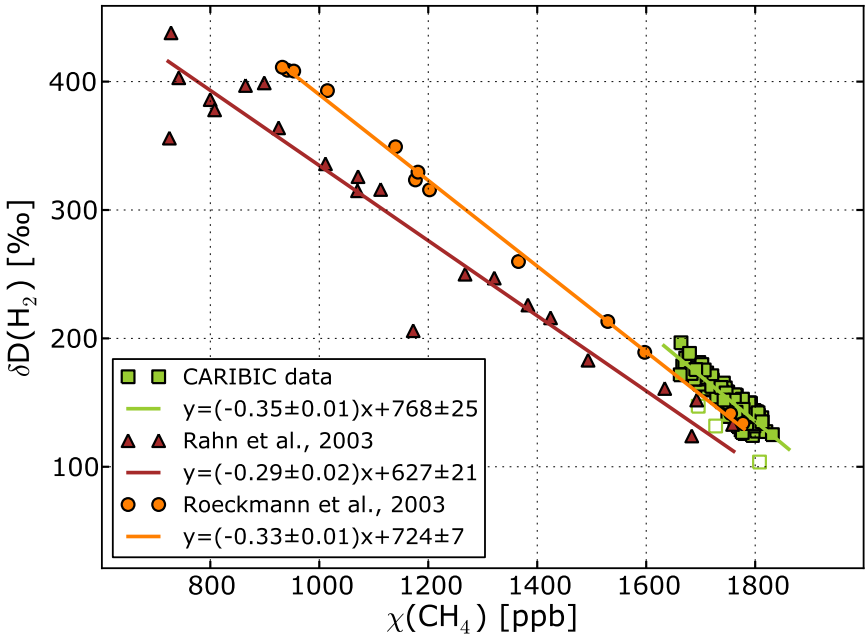

Figure 3.6: δD plotted against $\chi(CH_4)$, together with values from *Rahn et al.* (2003) and *Röckmann et al.* (2003) for comparison. Literature values were multiplied by a factor of 1.0124 to convert them to the NOAA2004 scale. Fits are made with the W-Y algorithm (*Cantrell*, 2008), without error estimates of the individual measurements for the literature values. Open symbols denote outlying datapoints that were left out of the fitting procedure.

That relatively good agreement between the slopes of the correlations of δD with $\chi(CH_4)$ is found in samples of two very different platforms, at different altitudes and in different regions of the globe (see Table 3.2), indicates that these very likely hold globally. We expect, therefore, that the approach to approximate δD from an empirical correlation with another species (as, for example, in (*Pieterse et al.*, 2011), where the relation from (*McCarthy et al.*, 2004) is used) should give reasonable results as long as the parametrization that is used is appropriate.

When the average value of $\chi(H_2)$ for the dataset ((559.2 ± 1.5) ppb, without the outliers shown in Fig. 3.5) is used to calculate χ(HD) from the δD data and a straight-line (W-Y) fit is applied, the CARIBIC data yield:

$$\chi(\mathrm{HD})[\mathrm{ppb}] = (-6.07 \cdot 10^{-5} \pm 2.5 \cdot 10^{-6}) \cdot \chi(CH_4)[\mathrm{ppb}] + 0.307 \pm 4.4 \cdot 10^{-3} \quad (3.2)$$

Table 3.2: Campaign description and correlations between δD or χ(HD) and methane from different publications. Methane mixing ratio data ($\chi(CH_4)$) from *Rahn et al.* (2003) and *Röckmann et al.* (2003) were multiplied by a factor of 1.0124 to convert them to the NOAA2004 scale. All fits were made with the Williamson-York algorithm described by *Cantrell* (2008). No error estimates for the individual measurements were taken into account for the literature values.

Author	Campaign description	$\delta D(H_2)$[‰] -$\chi(CH_4)$[ppb] correlation	χ(HD)[ppb] -$\chi(CH_4)$)[ppb] correlation
Rahn et al., 2003	Research aircraft 11-21 km 65-80° N 11-63° E Jan-Mar 2000	$y =$ $(-0.29 \pm 0.02)x$ $+627 \pm 21$	$y =$ $(-4.5 \cdot 10^{-5} \pm 3 \cdot 10^{-6})x$ $+0.260 \pm 0.003$
Röckmann et al., 2003	Balloon 12-33 km 43.7° N 0.3° W Okt 2002	$y =$ $(-0.33 \pm 0.01)x$ $+724 \pm 7$	$y =$ $(-5.55 \cdot 10^{-5} \pm 8 \cdot 10^{-7})x$ $+0.287 \pm 0.001$
This work	Commercial aircraft 6.5-12.5 km ≈ global 2007-2010	$y =$ $(-0.35 \pm 0.01)x$ $+768 \pm 25$	$y =$ $(-6.1 \cdot 10^{-5} \pm 3 \cdot 10^{-6})x$ $+0.307 \pm 0.004$

The slope of the relation proposed by *McCarthy et al.* (2004) is (just) in the 1×SEM interval of the slope of this correlation. We suggest that the relation found in the CARIBIC data discussed here may be the most appropriate choice for parameterizing the δD of the H_2 that is mixed into the troposphere from the stratosphere, since all CARIBIC data are collected close to the region of interest for STE (i.e., just above the TP).

3.3.3 Indian summer monsoon

Six of the analyzed flights had Chennai (formerly Madras, India) as the destination airport. Of these flights, three took place in the summer monsoon season of 2008. *Schuck et al.* (2010) noted a marked increase in the mixing ratios of greenhouse gases over the Indian subcontinent in the summer monsoon period. This increase was most prominent in $\chi(CH_4)$ and was attributed to increased microbial production of CH_4 in the wet season and increased transport of boundary layer air to cruising altitude by convection.

These $\chi(CH_4)$ data are plotted in Fig. 3.7 (a); the increase of methane levels in the wet season (blue tones) with respect to the dry season (red tones) can be seen clearly. The χ(CO), $\chi(H_2)$ and δD data are plotted in Fig. 3.7 (b), (c) and (d). χ(CO) shows an increase of up to ≈ 30 ppb in the monsoon. An increase in $\chi(H_2)$ is not apparent in these data, but a clear shift occurs in δD. Monsoon samples seem at least 10 ‰ more depleted than non-monsoon samples. Fig. 3.8 (a) shows the δD plotted against $\chi(CH_4)$ values for the three monsoon flights. A remarkably strong correlation is found between

the two quantities. The correlation is not as strong as in the stratosphere, but clearly significant. The strong connection between the increase in $\chi(CH_4)$ and the decrease in δD suggests that the processes that cause the D-depletion coincide in time and space with the processes that cause the $\chi(CH_4)$ increase.

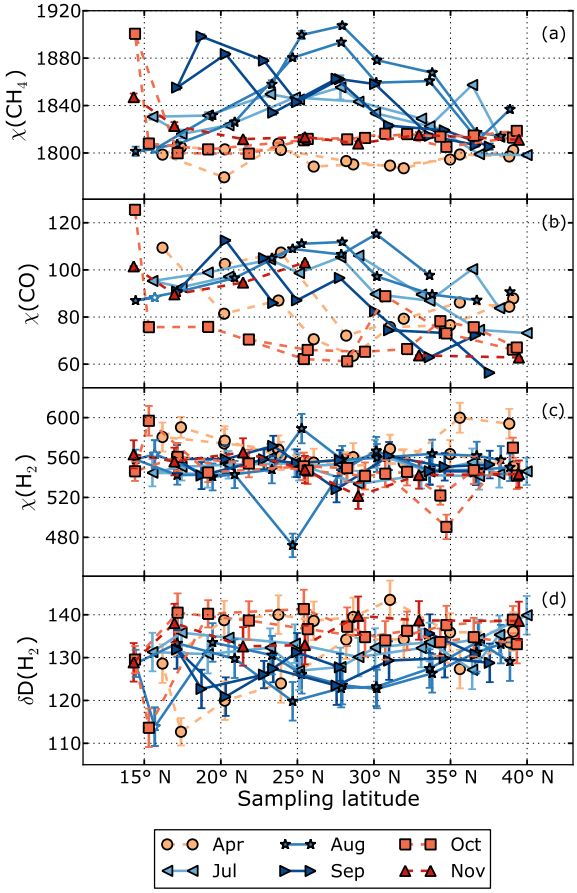

Figure 3.7: $\chi(CH_4)$ **(a)**, $\chi(CO)$ **(b)**, $\chi(H_2)$ **(c)** and δD **(d)** for the samples taken on flights to Chennai south of 40° N in the monsoon season (blue tones) and outside the monsoon season of 2008 (red tones). The open symbol (16° N) indicates a sample with a back trajectory originating outside of the monsoon system that was not taken into account in the fits.

Changes in δD at cruise altitude can be caused by changes in different variables, most importantly the strength and isotopic composition of H_2 emissions at the ground and the efficiency of upward convective transport. Since there are no measurements of δD at the

surface in India during this season, it is not possible to fully calculate how much each process contributes to the upper troposphere D-depletion. Nevertheless, we next explore the most likely scenarios.

Rhee et al. (2006b) argued that in biomass burning plumes from forest fires δD could be depleted while $\chi(H_2)$ remains almost the same if a sink process such as soil uptake compensates for the mixing ratio effect of the source. Neither increased biomass burning nor increased soil uptake are likely in the Indian summer monsoon. The biomass burning maximum in India is in winter rather than summer (*van der Werf et al.*, 2003), and the uptake of H_2 is hindered in very wet soils, as the reactive H_2-destroying sites in the soil pores are then covered by layers of water. *Schmitt et al.* (2009) reported that soil moisture is the major parameter controlling H_2 uptake by soils, with a secondary role for temperature; it is therefore unlikely that an increased enzymatic activity due to increased temperatures in the monsoon could compensate for the decrease in diffusion of H_2 to the reactive sites.

A second possible explanation is that H_2 from fossil fuel combustion or household biomass burning emissions, that are not expected to vary much with season, is transported much more efficiently to cruise altitude due to the monsoon increase in convection. This would be in line with the observed increase in CO, which is co-emitted with H_2 in combustion processes. To assess this possibility we use the mass balance equation for mixing of polluted air with $\chi_p(H_2)$ and δ_pD with background air with $\chi_{bg}(H_2)$ and δ_{bg}D, resulting in a mixture with $\chi_{p+bg}(H_2)$ and δ_{p+bg}D:

$$\chi_{p+bg}(H_2)\delta_{p+bg}D = (\chi_p(H_2) + \chi_{bg}(H_2))\delta_{p+bg}D = \chi_p(H_2)\cdot\delta_pD + \chi_{bg}(H_2)\cdot\delta_{bg}D \quad (3.3)$$

If the combustion emissions are assumed to have an average δD of -230 ‰ (Table 3.1), and background values are assumed to be 556.4 ppb and +134.1 ‰ (the averages of the samples taken over India south of 40° N outside the monsoon season), it can be estimated from this mass balance equation that the observed 12.3 ‰ depletion (the average of the five most depleted samples in the monsoon system) would in this case be accompanied by an $\approx$ 19.5 ppb increase in $\chi(H_2)$. We note that this value is of the order of magnitude that would be expected from the increase in χ(CO), since typical H_2/CO emission ratios of combustion processes are between 0.3 and 0.5 (*Popa et al.*, 2011; *Haumann et al.*, 2012). This increase is, however, not observed in $\chi(H_2)$. For the same reason as discussed above for forest fires, it is unlikely that soil uptake is compensating for the increase.

A third explanation is that extremely depleted H_2 from microbial production is added to the mixture. Microbially produced H_2 has a source signature of (-741 $\pm$ 13) ‰ (*Walter et al.*, 2011). With this, it can be calculated that if the observed depletion were caused exclusively by microbial production, it would be accompanied by a $\chi(H_2)$ increase of 8.0 ppb, which is within the error range of our $\chi(H_2)$ measurements. Also the correlation between δD and $\chi(CH_4)$ is in agreement with production of H_2 in the same wet soils, rice paddies or wetlands where CH_4 production takes place.

If we assume that all of the D-depletion is caused by H_2 from microbial production, we can use the mass balance equation (eqn. 3.3) to estimate the $\chi(H_2)$ increase that would be necessary to cause it, $\Delta\chi(H_2)_{microbial}$. Fig. 3.8 (b) shows $\Delta\chi(H_2)_{microbial}$ plotted against $\chi(CH_4)$. A linear (W-Y) fit shows that in this case, the $\frac{H_2}{CH_4}$ emission ratio is 0.073 $\pm$ 0.009. According to the EDGAR database (V4.2, edgar.jrc.ec. europa.eu/datasets_list.php?v=42), 8.50 Tg of CH_4 was produced in India in 2008 by rice cultivation and wastewater treatment. Our emission ratio estimate would then imply a concomitant production of 0.62 Tg H_2. This is a large number compared to the 3 Tg estimate for the global annual H_2 production from N_2 fixation that is often assumed in H_2 budgets (Ta-

ble 3.1), but the uncertainty estimate for this term is also large (3 Tg). It should also be noted that the estimates for this term are largely based on a study by *Conrad and Seiler* (1980) where H_2 production measurements at two stations in Germany were scaled up to a global estimate. Little is known about the variation in H_2 production between regions and ecosystems.

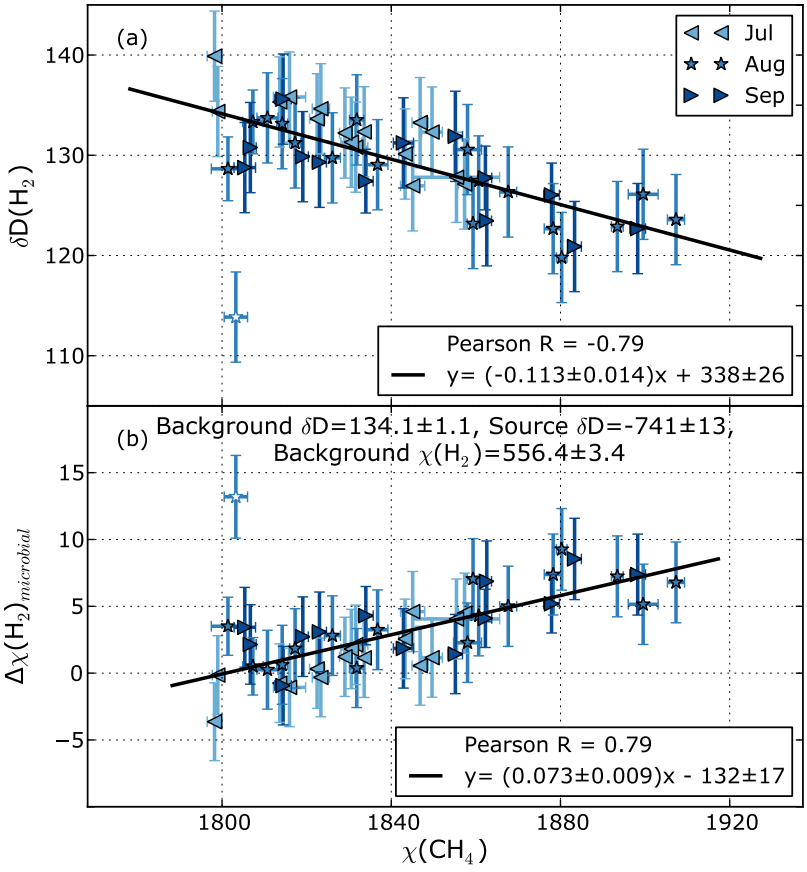

Figure 3.8: (a): δD plotted against $\chi(CH_4)$ for the samples taken on flights to Chennai south of 40° N in the summer monsoon season. **(b):** Estimated amount of H_2 (as a $\chi(H_2)$ increase) produced by monsoon-related microbial processes ($\Delta\chi(H_2)_{microbial}$) that would be required to explain the observed isotope depletions, plotted against $\chi(CH_4)$. Calculations are done under the assumption that all D-depletion is caused by microbially produced H_2 with a source signature of δD of (-741 $\pm$ 13) ‰ (*Walter et al.*, 2011). Solid lines indicate W-Y fits (*Cantrell*, 2008). The open symbol indicates a sample with a back trajectory originating outside of the monsoon system that was not taken into account in the fits.

3.4 Conclusions

The large suite of measurements of $\chi(H_2)$ and δD on samples taken onboard the CARIBIC aircraft demonstrates the usefulness of studying δD of H_2 in the UTLS region. A few samples had unexpectedly high $\chi(H_2)$ and low δD values. This tends to occur close to the departure or destination airports. We hypothesize that some of these events may be caused by the interception of exhaust plumes from other aircraft. The source signature of this pollution (-420 $\pm$ 31) ‰ is on the low end of what is expected for the combustion of fossil fuels. However, no relation is found with species that are usually expected in aircraft exhaust plumes. Measurement or sampling artifacts are unlikely since the measurements of these samples proceeded without other peculiarities.

More than 120 datapoints were obtained from the LMS, which greatly expands the existing δD dataset from this region. The δD data show a tight correlation with $\chi(N_2O)$ and $\chi(CH_4)$. The relation with $\chi(CH_4)$ follows the line $\delta D[‰] = (-0.35 \pm 0.01) \cdot \chi(CH_4)[ppb] + 768 \pm 25$, which is close to the relation found by *Röckmann et al.* (2003), but somewhat steeper than the (*Rahn et al.*, 2003) results. Since the correlations presented in this paper are compact and based on samples from many different locations around the world in the LMS, they are suitable for parameterizing STE in models.

A δD depletion by up to 12.3 ‰ was found in samples collected above India during the monsoon season, without an accompanying increase in $\chi(H_2)$. Increased convective transport in the monsoon season transports D-depleted H_2 from surface sources in the boundary layer more effectively to cruise altitude. If only combustion sources were responsible for the deuterium depletion, then either a concomitant increase in $\chi(H_2)$ should be observed, or this increase would need to be compensated by increased soil uptake. Alternatively, increased microbial production of H_2 in the monsoon could lead to the observed deuterium depletions, which would also explain the absence of a simultaneous (perceptible) increase in $\chi(H_2)$. This requires further study, and we recommend investigations into possible H_2 production in wet South Asian soils. Also, regular observations at a ground station in India would close a geographical gap in the ground station observations and could provide useful comparison material for the data presented here.

Continuation of the δD measurements on CARIBIC samples would provide the global coverage needed to validate global models, and could also resolve the seasonal and latitudinal variation of δD in the upper troposphere and the lowermost stratosphere better.

Chapter 4

$\chi(H_2)$ and $\delta D(H_2)$ observations at the Cabauw tall tower

This chapter is based on:

Batenburg, A. M., Popa, M. E., Vermeulen, A. T., van den Bulk, W. C. M., Jongejan, P. A. C., Fisher, R. E., Nisbet, E. G., Röckmann, T.: *Hydrogen mixing ratio and stable isotopic composition observations at the Cabauw tall tower*, to be submitted, 2012

Abstract

Measurements of the stable isotopic composition ($\delta D(H_2)$ or δD) of atmospheric molecular hydrogen (H_2) are a useful addition to mixing ratio ($\chi(H_2)$) measurements to improve our understanding of the atmospheric H_2 cycle. We complement the set of published δD data, which consists mostly of observations at background locations, with observations from the Cabauw tall tower, located in a densely populated region of the Netherlands. These measurements show a large anthropogenic influence on the local H_2 cycle, with frequently occurring pollution events that are characterized by large $\chi(H_2)$ and low δD values. An isotopic source signature analysis yields a value between -350 and -300 ‰, which is more D-depleted than the isotope signature commonly used in budget studies for H_2 production from fossil fuel combustion. Similar results are found for two diurnal cycles that were sampled at a suburban site near London. This indicates that the source signature of the Northwest European vehicle fleet may have shifted to lower values due to developments in vehicle technology and changes in average driving conditions. An added advantage of tower measurements is the possibility to sample vertical profiles. We find no significant difference in the median values of $\chi(H_2)$ measured in samples from different heights (20, 60, 120 and 200 m). Median δD values, however, are sig-

nificantly lower at the 20 and 60 m levels than at the 120 and 200 m levels. This confirms the limited role of soil uptake around Cabauw, and indicates possible differences in vehicle fleet and driving conditions between the footprint areas of the different sampling levels.

4.1 Introduction

Atmospheric molecular hydrogen (H_2) is the second most abundant reduced gas in the atmosphere. It is formed by the oxidation of hydrocarbons, by combustion processes and by nitrogen-fixing microbes in soils and in the ocean. Globally, uptake by soils removes roughly three quarters of this H_2, leaving a quarter to be oxidized by hydroxyl radicals (OH). Despite increasing methane levels and increased combustion of fossil fuels, there is no evidence for a long-term trend in H_2 mixing ratios ($\chi(H_2)$) (*Ehhalt and Rohrer*, 2009; *Grant et al.*, 2010b). This may change when H_2 comes into wider use as an energy carrier and leaks into the atmosphere during transport and storage. The associated increase in H_2 levels would have consequences for the stratospheric ozone chemistry and an indirect climate effect through a decrease in the oxidative capacity of the atmosphere (*Schultz et al.*, 2003; *Warwick et al.*, 2004; *Tromp et al.*, 2003; *Feck et al.*, 2008). Because of this impending disturbance of the H_2 cycle, the global H_2 budget has received increased attention in recent years, with several new budget estimates published very recently by *Bousquet et al.* (2011); *Yashiro et al.* (2011); *Yver et al.* (2011a) and *Pieterse et al.* (2011, 2012), but considerable uncertainties remain.

Investigation of the stable isotopic composition of H_2 can provide additional information about the sources and sinks of H_2 (*Gerst and Quay*, 2001; *Rahn et al.*, 2002b) and put extra constraints on models that describe the H_2 cycle (*Price et al.*, 2007; *Pieterse et al.*, 2009, 2011, 2012). The stable isotopic composition of H_2 is generally expressed in isotopic "δ" notation:

$$\delta\mathrm{D} = \delta\mathrm{D}(\mathrm{H_2}) = \left(\frac{R_{\mathrm{Sample}}}{R_{\mathrm{VSMOW}}} - 1 \right) \cdot 1000‰ \tag{4.1}$$

where R_{Sample} is the atomic ratio of deuterium (D) to "light" hydrogen atoms (H) in the H_2 of the sample, and R_{VSMOW} is the atomic ratio in the international VSMOW (Vienna Standard Mean Ocean Water) standard.

The different production and destruction processes of H_2 have very different effects on the δD value of the H_2 reservoir. Photochemical oxidation of methane and other hydrocarbons yields H_2 that has a positive δD value, i.e. is enriched in D with respect to VSMOW (*Gerst and Quay*, 2001; *Rahn et al.*, 2003; *Rhee et al.*, 2006a, 2008; *Feilberg et al.*, 2007; *Röckmann et al.*, 2003; *Pieterse et al.*, 2009; *Röckmann et al.*, 2010b). This δD value, with estimates ranging from +116 ‰ (*Pieterse et al.*, 2011) to +190 $\pm$ 50 ‰ (CH_4 only, (*Rhee et al.*, 2006a)), is similar to the δD value of the ambient H_2 reservoir, which is on average +124 to +150‰, depending on latitude (*Batenburg et al.*, 2011). For this reason, photochemical H_2 production has generally little influence on ambient δD variability, despite being the largest global source of H_2 (*Pieterse et al.*, 2011).

H_2 produced in combustion processes has negative δD values. Estimates of the source signature (δD) of biomass burning range between -290 ‰ (*Gerst and Quay*, 2001) and -90 ‰ (*Rhee et al.*, 2006b); more recent studies indicate that the more negative of these estimates is the more likely (*Röckmann et al.*, 2010a; *Haumann et al.*, 2012). *Gerst and*

Quay (2001) reported a source of -196 ‰ for fossil fuel combustion based on samples collected in environments with different degrees of pollution, the most polluted being a parking garage. *Rahn et al.* (2002b) reported a source signature of -270 ‰ based on a set of samples that included samples of car exhaust. Emissions from vehicles constitute $\approx$ 60 % of the total fossil fuel source (*Ehhalt and Rohrer*, 2009). In the study of *Rahn et al.* (2002b), the car exhaust samples alone showed a similar source signature as the other, environmental, samples that contained H_2 from the total fossil fuel source. This suggests that the the source signature of the vehicles alone was similar to the source signature of the total fossil fuel combustion source. Recent work by *Vollmer et al.* (2010) shows that the source signature can decrease to -370 ‰ in vehicles equipped with modern catalytic converters. The contribution of microbial production to the global H_2 production is small, but it may have a strong isotopic effect on local scales due to its extremely depleted source signature of (-712 $\pm$ 13) ‰ (*Walter et al.*, 2011).

Both destruction processes of H_2, uptake by soil and photochemical oxidation by the hydroxyl (OH) radical, are associated with isotopic fractionations, as the "light" form of H_2 (HH) is destroyed faster than the deuterated form (HD). The strength of an isotopic fractionation effect is often expressed as a fractionation factor α, which is the ratio of the removal rate of the heavy species to the removal rate of the light species. The H_2 isotope fractionation is much stronger for the photochemical removal (α = 0.57 at 298.15 K (*Talukdar et al.*, 1996)) than for the uptake by soils ($\alpha = 0.943 \pm 0.024$, (*Gerst and Quay*, 2001; *Rahn et al.*, 2002a; *Rice et al.*, 2011)).

The first environmental observations of $\delta D(H_2)$ in the troposphere were already made in the 1950s (see (*Kaye*, 1987) for an overview), but difficult and time-consuming measurements limited the application until new techniques became available at the start of this century (*Rahn et al.*, 2002b; *Rhee et al.*, 2004). Especially in the last few years, many more tropospheric observations were published (*Rhee et al.*, 2006b; *Rice et al.*, 2011; *Batenburg et al.*, 2011, 2012). These recent observations were mostly done at "background" locations, either from ships, from aircraft in the upper troposphere or at predominantly remote surface stations. This paper presents δD results from the Cabauw tall tower station in the Netherlands. This tower is located in an agricultural area in the centre of the Netherlands, but within 20 to 50 km from the four largest Dutch cities. One of the reasons to do these measurements was to complement the existing dataset of mostly background observations with data from a more anthropogenically polluted site.

Very few δD data from polluted regions exist, but an increasing number of observations of H_2 mixing ratios were made at such places in recent years. Semicontinuous measurements were performed at suburban sites near Zürich (Dübendorf) (*Steinbacher et al.*, 2007), Paris (Gif-sur-Yvette) (*Yver et al.*, 2009), and Heidelberg (*Hammer et al.*, 2009) , at an urban site in Bristol (*Grant et al.*, 2010a), and also at the Cabauw tall tower (*Popa et al.*, 2011) and Royal Holloway, a suburban site near London (*Fowler et al.*, 2011). A common feature in the published time series from these stations is that $\chi(H_2)$ is very variable and shows large excursions to high values superposed on a seasonally changing baseline. During these H_2 peaks, $\chi(H_2)$ can increase to two or, in the case of Dübendorf and Bristol, even three times its background value.

An additional advantage of sampling from the Cabauw tower is that air can be sampled from different sampling heights. Measurements of $\chi(H_2)$ have been performed at different heights at the Cabauw tower (*Popa et al.*, 2011) and at the Trainou television tower near Orléans (*Yver et al.*, 2011b). The measurement of vertical gradients is useful in the study of H_2 uptake by soil. Also, by measuring at different heights, it is possible to probe different

"footprint" areas, i.e. differently weighted combinations of local and more remote sources and sinks (*Vermeulen et al.*, 2011). To our knowledge, this paper presents the first vertical profiles of δD in the boundary layer.

4.2 Methods

4.2.1 Tower location and continuous on-site measurements

The Cabauw tall tower is a 213 m steel construction dedicated to meteorological research (*Popa et al.*, 2011; *Vermeulen et al.*, 2011). Its location (51° 58′ N, 4°55′ E, 2 m a.s.l.) is in the so-called "Green Heart" of the Netherlands, a relatively rural region surrounded by the "Randstad" conurbation. The area directly surrounding the tower is relatively sparsely populated and mainly used for agriculture (mostly grassland), but population and road density increase steeply further away from the tower. The distance from the tower to the city of Utrecht is $\approx$ 20 km, to Rotterdam $\approx$ 30 km, to the Hague $\approx$ 40 km and to Amsterdam $\approx$ 45 km; an estimated seven million people inhabit the Randstad conurbation that consists of these four big cities and their many neighboring settlements.

The tower is equipped with a tubing system to measure greenhouse gas mixing ratios in air sampled at 20, 60, 120, and 200 m (*Vermeulen et al.*, 2011). Air is continuously drawn from the different heights and lead through Decabon® tubing to the laboratory in the base of the tower. There, 400 ml min^{-1} air streams are separated from the bulk air flow (which is flushed outside), dried in cryogenic water traps to a dew point of $\approx$ -50° C, divided and analysed on either a CO_2 analyser ($\approx$ 150 ml min^{-1}) or on a GC system for other GHGs ($\approx$ 80 ml min^{-1}). In 2007, a reduction gas analyser (RGA-3) for the measurement of H_2 and CO mixing ratios was added in series after the GC system. The RGA-3 measures a vertical profile every half hour (*Popa et al.*, 2011). The $\chi(H_2)$ measurements of the RGA-3 are calibrated to the recently defined WMO scale (*Jordan and Steinberg*, 2011). These continuous measurements were used to assess the quality of the flask sample data presented in this work.

Due to the often high wind speeds in the region and the large variability in wind direction, the Cabauw site has a large "footprint" or influence region, especially at the highest sampling height where it covers roughly a 500 by 700 km area (*Henne et al.*, 2010; *Vermeulen et al.*, 2011). The soil in the surrounding area is a combination of peat and clay layers with a high water table. These soil characteristics may be one of the reasons that *Popa et al.* (2011) found low H_2 deposition velocities at this location.

4.2.2 Collection of Cabauw flask samples

The flasks used for the sampling at Cabauw were Normag borosilicate 3.3 glass flasks with Kel-F (PCTFE) O-ring sealed stopcocks. Most samples were collected in 1 L flasks; a minority was collected in 2 L flasks of the same type. All flasks were covered with a black shrink hose and stored in closed boxes to avoid photochemical alteration. Many trace gases have been shown to be stable in these flasks (*Rothe et al.*, 2004); with the exception of a few outliers, this is also true for H_2 [*A. Jordan, personal communication*].

The air for the flask samples was drawn in through the same tubing system as was used for the greenhouse gas and semicontinuous H_2 and CO measurements. The streams of dried air that the on-site measurement system measures are vented every half hour when measurements of working tank and target tank gases are performed. This venting flow

goes through the sampling flasks; the flasks are always filled during this venting period. The flasks were filled up to ≈ 1.5 bar of absolute pressure.

During the sampling period, from July 2008 to August 2011, 91 individual samples were taken from the 200 m level around midday, resulting in more than two samples per month that are representative of the daytime conditions in Cabauw. In the same period, 18 complete and 15 incomplete vertical profiles were sampled additionally. The vertical profiles were mostly sampled under stable atmospheric conditions, when the real-time raw data from the RGA showed a positive or negative vertical gradient in $\chi(H_2)$. The vertical profiles are therefore biased towards stable conditions, and not fully representative of the H_2 climatology at Cabauw. Flask samples were stored between between 1 and 20 months before analysis because of delays in the automation of the isotope measurement system.

4.2.3 Collection of Royal Holloway flask samples

The samples of the Royal Holloway diurnal cycles were collected on the Royal Holloway campus of the University of London in Egham, located 30 km WSW of central London (*Fowler et al.*, 2011). One set of eight samples was collected in July 2008, another set of 12 was collected in January 2009. Both were collected under conditions where the Royal Holloway site received urban air masses from the Greater London area and an overnight $\chi(H_2)$ variation of more than 100 ppb (nmole mole^{-1}) was observed in the continuous measurements at the site.

The sample air was dried, collected in 3 L stainless steel tanks and subsequently analyzed on an Peak Performer 1 (Peak Laboratories) for $\chi(H_2)$ and χ(CO). The tanks were stored for 1-2 months before isotopic analysis. The isotopic analysis of two of the 20 tanks yielded unreliable results (as was confirmed by a large difference between the mixing ratio measured by the GC-IRMS system and the mixing ratio measured by the Peak Performer 1 in the tanks as well as in the continuous measurements at the site). These were left out of all further analysis.

4.2.4 Analysis of the flask samples

The analysis of the flasks was performed with an online Gas Chromatography - Isotope Ratio Mass Spectrometry (GC-IRMS) setup as developed by *Rhee et al.* (2004), with adaptations described by *Röckmann et al.* (2010b). This setup isolates the H_2 from the air matrix and analyzes it for $\chi(H_2)$ and δD in four steps:

1. *Cryogenic separation* of the main components of an ≈ 0.5 L aliquot of air from a headspace containing only the most volatile components (H_2,He, Ne and a trace of N_2) by exposure to a cold head kept at ≈ 40 K.
2. *Pre-concentration* of the H_2 in a stainless steel trap filled with 5 Å molecular sieve, submerged in liquid nitrogen at reduced pressure to keep it at ≈ 63 K.
3. *Cryo-focussing* of the H_2 on a steel-jacketed 5 Å molecular sieve gas chromatography column submerged in liquid nitrogen and *gas chromatographic purification* on a 5 Å molsieve gas chromatography column kept at 323 K.
4. *Injection* of the purified H_2 into the IRMS (ThermoFinnigan Delta plus XL) through an open split interface for analysis.

In the final chromatogram, the sample peak is bracketed with H_2 laboratory working gas peaks before and after. At the start of this research project, the GC-IRMS system was semi-automated to enable automated measurement of one aliquot of air. In the summer of 2011, the system was automated further to enable the fully automated measurement of up to 25 aliquots in one measurement sequence. The sample calibration procedures differ slightly for the two measurement periods.

Before the full automation, one blank measurement and two measurements of air from laboratory reference air bottles were typically performed every measurement day. A bottle containing a compressed whole air sample with $\chi(H_2)$ (545.0 $\pm$ 0.5) ppb (MPI-BGC Jena) and δD (+73.0 $\pm$ 1.8) ‰ was used until it was used up in the spring of 2010. It was replaced with two other bottles containing mixtures of pure H_2 with synthetic air with the values (580.78 $\pm$ 0.03) ppb and (+207.0 $\pm$ 0.3) ‰, and (244.3 $\pm$ 0.8) ppb and (+198.2 $\pm$ 0.5) ‰, respectively (error bars indicate standard errors). 5-day moving average values obtained from these laboratory reference bottles were used to correct the $\chi(H_2)$ and δD values for each sample for instrument drift. A 9.5 ‰ offset was subtracted from the δD values for samples measured between June 2010 and the full automation in the summer of 2011, to correct for an empirically observed bias. This procedure is more fully described in (*Batenburg et al.*, 2011, 2012)

The full automation of the system increased the measurement capacity of the system such that measurements of laboratory reference air bottles could be made much more often. In addition, two bottles were added to the set of reference bottles. From comparison of their measurements with the measurements of the bottles that were already in use before the automation, their values were determined to be (765.4 $\pm$ 1.4) ppb and (-116.1 $\pm$ 0.4) ‰, and (862.0 $\pm$ 2.6) ppb and (-200.0 $\pm$ 0.8) ‰. Typically, the 765 ppb/-116 ‰ bottle was measured after each two samples, and some measurements of the other three bottles were performed at the end of the measurement sequence. Each of the bottles was measured at least 4.5 times per week on average. A blank was typically performed once per measurement day. As before, the 5-day moving average of the blanks and the laboratory reference air bottles were used to correct the sample measurements for instrument drift.

Where available, the continuous measurements of $\chi(H_2)$ at the Cabauw tower (*Popa et al.*, 2011, and unpublished measurements) were used for quality assessment of the flask sample measurements, as follows: 2 hr averages of the continuous data were made per sampling height. The flask $\chi(H_2)$ data were compared to these averages. For datapoints where the difference exceeded 50 ppb, the measurement logs and the time evolution of the $\chi(H_2)$ signal were inspected to make an expert judgement to flag the datapoint as “good”, “suspect” or “contaminated”.

4.3 Results and Discussion

4.3.1 Time series

Figure 4.1 shows all the $\chi(H_2)$ (a) and δD (b) flask data for the Cabauw tower as a function of sampling time. Flask data that were collected from the EUROHYDROS station Mace Head by *Batenburg et al.* (2011) in a similar fashion are shown for comparison, as well as cosine fits to these data. Mace Head is located on the west coast of Ireland (53 ° 20′ N, 9° 54′ E) and is considered a clean background station. Because of its location and the

dominant westerly winds in this latitude band, the measurements performed there can be used as a background for continental Europe (*Grant et al.*, 2010b).

It can be seen in the upper panel (a) of this figure that the Mace Head $\chi(H_2)$ data form the lower bound for the Cabauw $\chi(H_2)$ data. In Cabauw, very large excursions occur above this baseline, especially during winter. During these excursions, $\chi(H_2)$ is often highest at the lower sampling heights. It seems that due to these excursions, the seasonal cycle at Cabauw is shifted with respect to Mace Head; whereas in Mace Head the maximum in $\chi(H_2)$ is observed in April/May, in Cabauw the 2009 and 2010 maxima appear shifted towards the earlier winter. For the the 2011 maximum, this cannot be seen so clearly due to increased scatter since the summer of 2010. The general behavior of the $\chi(H_2)$ time series is in good agreement with the results of *Popa et al.* (2011) at Cabauw. They found a large $\chi(H_2)$ variability, with especially large peaks in winter, and as a result, a seasonal cycle with a maximum in winter. This maximum was slightly earlier and higher for the lower sampling heights. The occurrence of these large winter excursions was attributed to the decrease in atmospheric mixing in winter, which leads to large accumulations of pollution in the boundary layer. Similar features were also seen in the results of *Steinbacher et al.* (2007) for the Dübendorf site.

The δD time series (Figure 4.1 (b)) looks like a mirrored image of the $\chi(H_2)$ time series. Here, the Mace Head data form the higher bound of the Cabauw data. It can be seen that the $\chi(H_2)$ peaks are accompanied by δD dips, and that during these dips, the lower sampling heights often have lower δD values than the higher sampling heights. The δD cycle also seems shifted with respect to Mace Head; the April/May Mace Head minimum is shifted to the earlier winter in 2009 and 2010. From the opposite behavior of the Cabauw $\chi(H_2)$ and δD time series and from the D-depletion in Cabauw with respect to Mace Head, it can already be concluded that the H_2 that makes up the large, mostly wintertime peaks originates from sources with a D-depleted source signature. Because of the location and frequent pollution events observed at the Cabauw site, fossil fuel combustion is the most likely explanation for these excursions. In the warmer seasons, microbial H_2 production might also contribute. In the next section, the isotopic composition of the source mix that affects Cabauw is investigated in detail.

4.3.2 Source signature studies

δ values are linear with regard to mixing of different reservoirs, and therefore the effect of mixing a background reservoir of a gas with mixing ratio χ_{bg} and isotopic composition δ_{bg} with a "polluted" airmass with mixing ratio χ_s and δ_s is described by a simple mass balance equation:

$$\delta_{obs}\chi_{obs} = \delta_{bg}\chi_{bg} + \delta_s\chi_s \tag{4.2}$$

where the "obs" superscript indicates observed values. This can be rewritten to

$$\delta_{obs} = \frac{\chi_{bg}}{\chi_{obs}}\left(\delta_{bg} - \delta_s\right) + \delta_s \tag{4.3}$$

This relation is the basis of the use of the traditional "Keeling" plot, where observed δ values are plotted against the inverse observed mixing ratios and the y-axis intercept returns the isotopic signature of the source(s). Figure 4.2(a) shows a Keeling plot of all Cabauw H_2 data that were labelled "good" in the data quality assessment (the rejected datapoints are shown as open symbols). The linear fit to this Keeling plot was made with the Williamson-York fit algorithm described by *Cantrell* (2008), and yielded a source signature estimate of (-336 $\pm$ 14) ‰ (error indicates one standard error, 1 SEM).

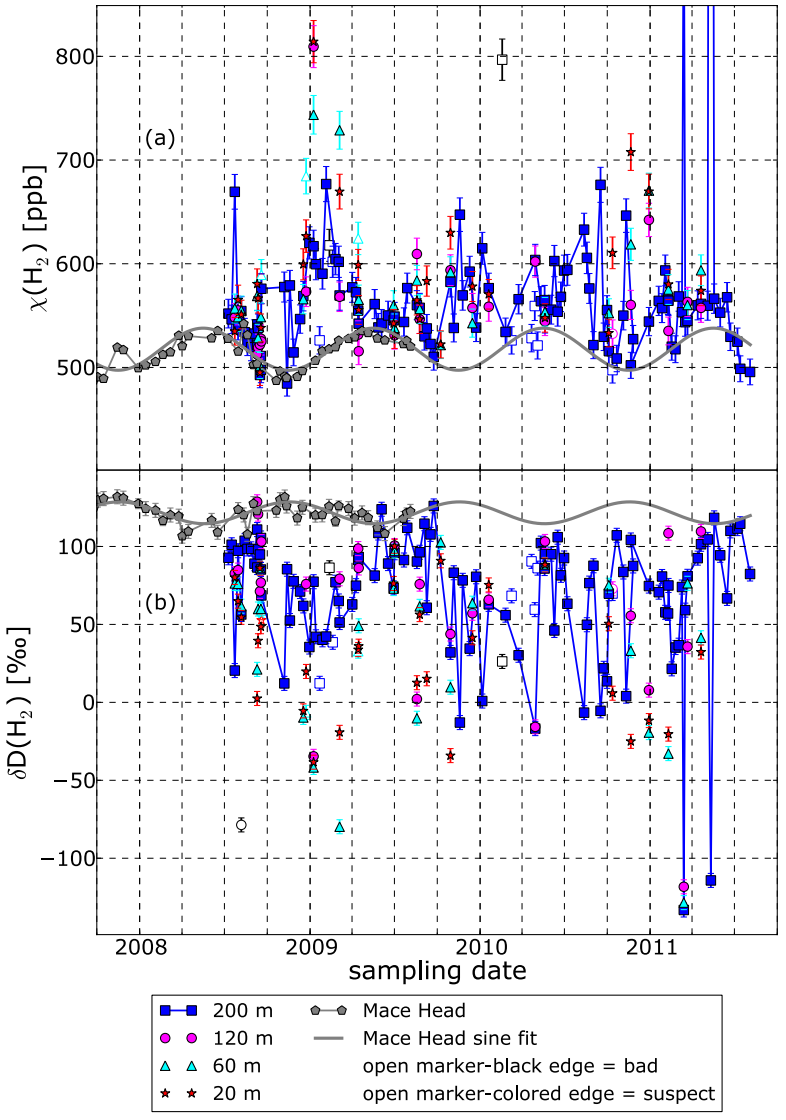

Figure 4.1: Time series of **(a)** $\chi(H_2)$ and δD **(b)** measured in samples from the Cabauw tower. Data from the background station Mace Head and a sine fit to the Mace Head data (*Batenburg et al.*, 2011) are plotted for comparison. Open symbols indicate Cabauw measurements that were deemed ``contaminated" (black edge) or ``suspect" (colored edge) in the data quality assessment. Some samples fall outside the scale limits of this plot.

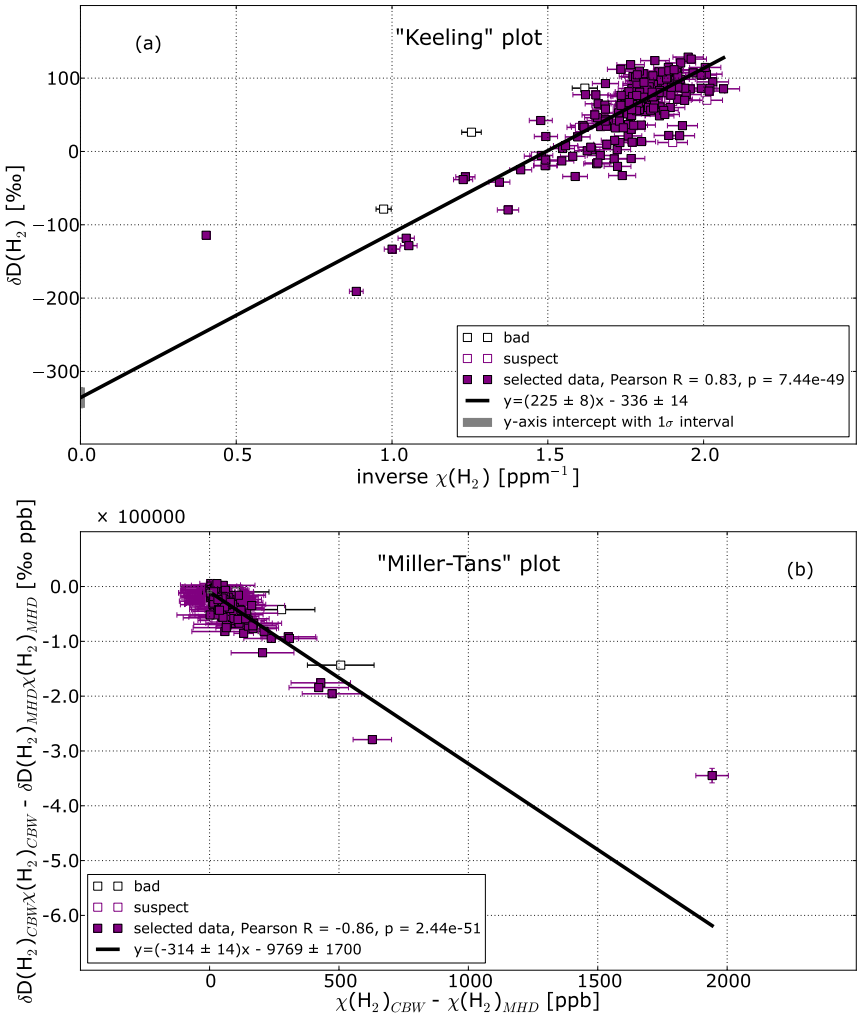

Figure 4.2: (a): ``Keeling" plot ($\delta$D plotted against 1/$\chi(H_2)$) of all Cabauw samples. The y-intercept gives an indication of the isotopic source signature. **(b):** ``Miller-Tans" plot ($\delta D_{obs}\chi(H_2)_{obs}$-$\delta D_{bg}\chi(H_2)_{bg}$ plotted against $\chi(H_2)_{obs}$-$\chi(H_2)_{bg}$) of the Cabauw samples. The slope gives an indication of the isotopic signature (*Miller and Tans*, 2003). The cosine function that describes the seasonal cycle in Mace Head found by *Batenburg et al.* (2011) was used to calculate the background values. Only samples with $\chi(H_2)$ above the background value were taken into account. All linear fits were made with the Williamson-York fitting algorithm described by *Cantrell* (2008). Samples labelled ``contaminated" or ``suspect" are indicated with open symbols and are not taken into account in the fits. The stated errors are one standard error (1 SEM).

An implicit assumption of this Keeling plot method is that the background mixing ratio and δ value are constant. Figure 4.1 shows that this is not the case for H_2 at Cabauw. For such cases, *Miller and Tans* (2003) proposed another formulation of the mass balance equation. If the mixing ratio and isotopic composition of the background reservoir are known (which is not necessary for the application of the Keeling plot, see above), it can be written as:

$$\delta_{obs}\chi_{obs} - \delta_{bg}\chi_{bg} = \delta_s\left(\chi_{obs} - \chi_{bg}\right) \tag{4.4}$$

This equation shows that the slope of a plot of $\delta_{obs}\chi_{obs} - \delta_{bg}\chi_{bg}$ against $\chi_{obs} - \chi_{bg}$ can be interpreted as the source signature. A plot following this method for Cabauw is shown in Figure 4.2(b). The cosine-shaped seasonal cycles that were found for $\chi(H_2)$ and δD at Mace Head by *Batenburg et al.* (2011) were used as background values. A linear Williamson-York fit yields an isotopic source signature estimate of (-314 $\pm$ 14) ‰.

The 1 SEM error ranges of this value and the estimate from the Keeling plot overlap, so the outcomes of both methods are not significantly different. Apparently, it does not make a large difference for the source signature estimate at Cabauw if the changing background is taken into account or not. A likely explanation for this is that the amplitude of the background seasonal cycle is small compared to the total variation (see Figure 4.1). The observed values are determined more by short-timescale pollution events than by seasonal variation in the background. Perhaps, too, the amplitude of the seasonal cycle at Mace Head is slightly underestimated by the cosine fit (*Batenburg et al.*, 2011).

Both estimates are more depleted than previous estimates of the total isotopic source signature of fossil fuel combustion of (-196 $\pm$ 10) ‰ by *Gerst and Quay* (2001) and -270 ‰ by *Rahn et al.* (2002b). *Vollmer et al.* (2010) found δD values between -270 ‰ and -370 ‰ for H_2 in the exhaust of a modern engine setup with a three-way catalytic converter (TWC). The TWC, fuel-rich driving conditions and certain operating modes were observed to lower the δD values. The Northwest European car fleet consists for a large part of modern vehicles (*UNECE*, 2012) with catalytic converters, and traffic conditions in the Netherlands are often jammed, leading to fuel-rich driving conditions. For these reasons, the isotopic signature of Northwest European traffic emissions may well be more depleted than previously reported signatures, and this may result in a more depleted signature for the total European fossil fuel source.

A contribution of H_2 emitted by N_2 fixing microbes in soil (in the root nodules of legumes) is an alternative explanation. The isotopic signature of microbially produced H_2 is depleted as much as (-712 $\pm$ 13) ‰ (*Walter et al.*, 2011), so only a small quantity from this source can affect the local isotope budget considerably and make the apparent isotopic signature of the source mix more depleted. Some types of legumes, especially types of clover, are common around the Cabauw tower; it is likely that some microbial production of H_2 occurs. This production is, however, very likely limited to the growth season. *Conrad and Seiler* (1980) reported that the production peaked from April to June, and that very little production occurred in the rest of the year. Flasks sampled in April, May or June constitute less than a quarter of the data in Figure 4.2(b). Omitting these data from the fit (not shown), yields a source signature that is even lower (-445 $\pm$ 16 ‰). Omitting the data from an even larger potential growth period (March-October) yields a similar result (-425 ‰). Hence, it is not likely that microbial sources are the most important cause for the low apparent source signature at the Cabauw tower.

4.3.3 Diurnal cycles at the Royal Holloway site

For comparison to the Cabauw data, two diurnal series of observations at Royal Holloway are shown in Figure 4.3 (a)-(b). The figure shows an anticorrelation between $\chi(H_2)$ and δD. The afternoon rush hour peak, with elevated $\chi(H_2)$ values and a simultaneous decrease in δD values, can be distinguished clearly around 7 PM.

A Keeling plot of these data is shown in the lower panel (c) of Figure 4.3. Linear Williamson-York fits were made to the separate diurnals and to the combined set of data. All three fits indicate a source signature lower than -260 ‰. This shows that also in the UK, the present isotopic source signature of H_2 from fossil fuel combustion sources might be lower than has been assumed based on earlier observations.

4.3.4 Height profiles

In Figure 4.1, inspection by eye suggests that pollution signals are often stronger at lower sampling heights than at the 200 m level. This is, for example, the case for the profiles sampled on 8 January 2009, 5 March 2009, 20 November 2010 and 29 December 2010. To investigate such differences between the sampling heights, the vertical profiles are plotted in Figure 4.4. They are overplotted with a boxplot that indicates the median, quartile and 95^{th} percentile values. From this plot, it seems that the median $\chi(H_2)$ value is slightly higher and the median δD value somewhat lower at the lower sampling heights than at the higher sampling heights. To determine if these differences are significant, pairwise Kruskal-Wallis H-tests were performed on the data from the different heights. The resulting p-values are listed in Table 4.1. A p-value below 0.05 indicates that the medians of the two datasets are different with more than 95% confidence. No significant differences between the different levels were found for $\chi(H_2)$, but for δD, significant differences were found for four of the pairs, each combining one of the lower sampling altitudes (20 or 60 m) with one of the higher sampling levels (120 or 200 m). So, it appears there is a shift in δD between the 60 m and 120 m level, with lower δD values below, and higher δD values above.

As noted, the sampling of the vertical profiles is biased towards stable, and therefore polluted conditions. Hence, it is not representative for the full year-round variability in $\chi(H_2)$ and δD. However, some general interpretations can be made. At locations where uptake by soils dominates the H_2 cycle, the expected vertical profile has lower $\chi(H_2)$ values and higher δD values at the bottom than at the top, since the uptake of H_2 by soils has a D-enriching effect on the remaining H_2 reservoir (*Gerst and Quay*, 2001; *Rahn et al.*, 2002a; *Rice et al.*, 2011). This is clearly not the case for Cabauw; there is no $\chi(H_2)$ depletion observed at the bottom, and δD is lower there, not higher. This indicates that not soil uptake, but source processes drive the H_2 variability at Cabauw. This is in agreement with the low uptake speeds found by *Popa et al.* (2011).

Vermeulen et al. (2011) reported that the footprint area for the 200 m sampling level (covering the Benelux, the north of France, the north and middle of Germany and the southeast of England) is considerably larger than that of the 20 m level (covering the Benelux and bits of northern France and western Germany). It is likely that the change in footprint area causes the 20 and 60 m sampling levels to experience a more D-depleted H_2 source mix than the 120 and 200 m levels. There is a number of possible explanations for this observation.

The first is that pollution from further away has travelled longer before reaching the tower. In an aging polluted airmass, oxidation processes can take place that both produce

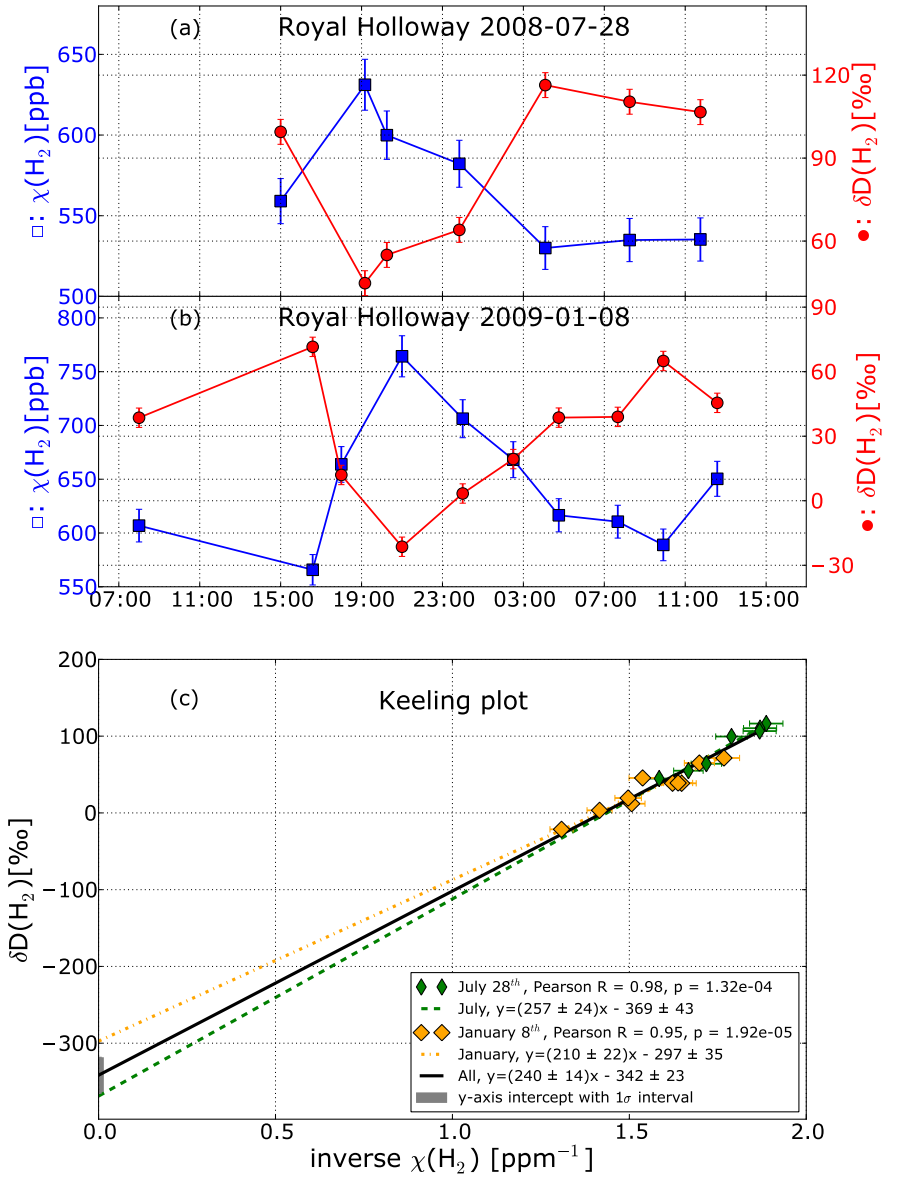

Figure 4.3: (a)-(b): Diurnal cycles of δD and $\chi(H_2)$ sampled at Royal Holloway. **(c):** Keeling plot of these data, with Williamson-York fits to the separate diurnal cycles and to the whole dataset.

Table 4.1: Resulting p-values from pairwise comparisons of the datasets from different sampling heights with the Kruskal-Wallis H-test, which tests the null hypothesis that the medians of the datasets are equal. It is assumed that the datasets are independent, and that the Kruskal-Wallis H-statistic has a χ^2 distribution. A p value below 0.05 (bold font) indicates that the medians are different with 95% confidence. The used data are the same as shown in Figure 4.4, i.e. all data from profiles with non-suspect data from at least two sampling heights.

p values for pairwise Kruskal-Wallis tests of $\chi(H_2)$ data

	20 m	60 m	120 m	200 m
20 m	-	0.9673	0.1056	0.0750
60 m	0.9673	-	0.1821	0.1099
120 m	0.1056	0.1821	-	0.9865
200 m	0.0750	0.1099	0.9865	-

p values for pairwise Kruskal-Wallis tests of δD data

	20 m	60 m	120 m	200 m
20 m	-	0.6759	**0.0063**	**0.0003**
60 m	0.6759	-	**0.0188**	**0.0034**
120 m	**0.0063**	**0.0188**	-	0.9462
200 m	**0.0003**	**0.0034**	0.9462	-

H_2 (from hydrocarbons) and remove it. Both the production of H_2 from the oxidation of hydrocarbons and the removal of H_2 by oxidation by OH radicals have a D-enriching effect on the H_2 reservoir. Therefore, it is possible that these processes cause δD in polluted airmasses to increase with average age, which then causes the higher median δD values at the 120 and 200 m sampling levels. But considering that these processes are relatively slow compared to the transport times, this explanation does not seem likely. H_2, for example, has a lifetime of $\approx$ 8 years with respect to oxidation by OH.

Another explanation is the local production of extremely D-depleted H_2 by N_2-fixing microbes. As noted before, it is likely that some microbial H_2-production occurs in the vicinity of the tower. Because of the different footprints, the 20 an 60 m levels are more sensitive to these processes than the higher levels, explaining their lower median δD values. This effect should be strongest in the April-May growing season, but only 6 of the 33 profiles were sampled in this period. In these profiles, the δD difference between the sampling levels is not more significant than during the rest of the year. For this reason, microbial production does not seem a satisfactory explanation to account for the overall difference between the median δD values for the different sampling levels.

The third and most likely explanation is that there is a difference in the fossil combustion source of H_2 between the different footprint areas. While we expect the whole Northwest European vehicle fleet to be very modern, subtle differences may exist between the fleets of the the Netherlands, Belgium, France, Germany and the United Kingdom. The

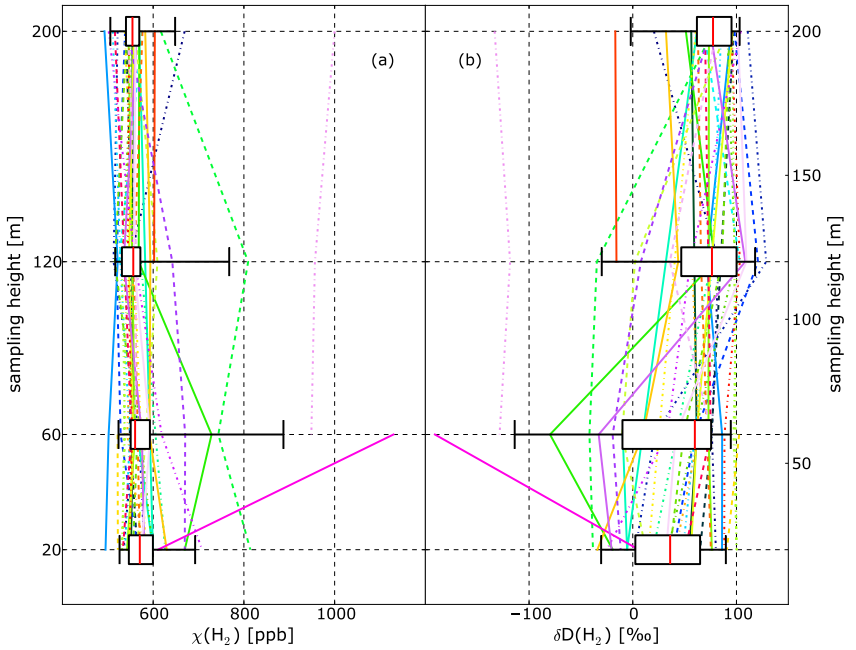

Figure 4.4: Vertical profiles of δD **(a)** and $\chi(H_2)$ **(b)**, overplotted with a box plot of the same data. All profiles with (non-suspect) data from at least two heights are included in this figure. In the boxes, the red lines indicate medians, the box edges indicate lower and upper quartiles and the whiskers indicate lower and upper 95^{th} percentiles.

driving conditions may differ as well, as the Dutch road system is notorious for its many congestions. The road networks of the Netherlands and the UK have the largest percentage of main network links that exhibit daily congestions in Northwestern Europe (*Bovy and Salomon*, 1999). These congestions may lead to more fuel-rich driving conditions in the Netherlands than in most surrounding countries, and according to the results of *Vollmer et al.* (2010), this may lead to lower δD values. As the lower sampling levels are more sensitive to local to regional emissions, this lower source signature may affect the lower levels more than the higher levels.

4.4 Conclusions and outlook

The set of $\chi(H_2)$ and δD data presented here shows that the H_2 cycle at Cabauw is under heavy anthropogenic influence. The time series show that the excursions to high $\chi(H_2)$ values already observed by *Popa et al.* (2011) are accompanied by low δD values, implying a large role for depleted sources such as fossil fuel combustion. Further analysis shows that the apparent δD source signature is lower than the signature often assumed for fossil fuel combustion, which may be due to the modernization of the Northwest Eu-

ropean vehicle fleet and the often congested driving conditions in the Netherlands. The results of the Royal Holloway observations so far indicate that the isotopic signature of the source mix there may be similar, but more observations are needed to obtain a year-round picture.

In the vertical profiles, median δD values were significantly lower at the 20 and 60 m than at the 120 and 200 m levels. We hypothesize that this difference is caused by differences in car fleets and in driving conditions between the varying footprint areas of the different sampling heights. Differences in the average age of pollution that reaches the different levels of the tower and microbial H_2 production in the vicinity of the tower seem less likely explanations, although they cannot be ruled out completely.

These results show that the assumption in global models of a uniform δD source signature for H_2 emissions from vehicles may be an oversimplification. It may be more appropriate to allow for differences between regional vehicle fleets, with more D-depleted source signatures for the more modern fleets in more congested situations. In addition, the magnitude of the microbial H_2 production term and the regional variations therein need further study. *Conrad and Seiler* (1980) estimated its global magnitude from a set of observations in Germany, but since then very little work has been done to study possible regional differences and refine the estimate. Microbial production may only constitute a small part of the global H_2 budget, but due to its extreme D-depletion (*Walter et al.*, 2011) its effect on the isotope budget may be considerable.

Observations like those presented here complement previous observations made at background locations or in the free troposphere. They provide more information on the H_2 cycle in densely populated areas such as the Netherlands, and can therefore help in assessing the climate and air quality impacts of future H_2 emissions in such regions with regional models. The measurements at different sampling heights can help in distinguishing local from long-range influences.

Chapter 5

Conclusions and outlook

The aim of this dissertation work was to contribute to the understanding of the global, regional and local cycles of atmospheric molecular hydrogen (H_2). Although H_2 has no direct effect on climate, ozone or public health, it is chemically linked to chemical species that do have such effects. And with the prospect of having parts of our vehicle fleet replaced by hydrogen-powered vehicles, which will inevitably be associated with H_2 leakage, it has now become extra important to understand the H_2 cycle. Our approach to this subject was to study the stable isotopic composition (δD) of H_2, in addition to observations of H_2 mixing ratio ($\chi(H_2)$). The stable isotopic composition of a substance contains information about the processes that have acted upon it, and it can serve as an extra constraint in models. However, to make optimal use of the stable isotopes, we need accurate knowledge of the isotope effects caused by different source and sink processes, and a good characterization of the spatial and temporal variations in δD. The research questions that we have tried to answer in this thesis are all related to this.

To find answers to these questions, we analyzed samples collected at different locations for $\chi(H_2)$ and δD with a Gas Chromatography - Isotope Ratio Mass Spectrometry GC-IRMS setup (*Rhee et al.*, 2004; *Röckmann et al.*, 2010a). In this thesis, we have presented three new datasets of environmental δD observations, and (semi-)quantitative analyses of their features. In the section, we relate the results to the original scientific questions posed in the introduction.

5.1 How does δD vary with latitude and season, and which processes drive these variations?

To investigate the global scale spatial and temporal variability of $\chi(H_2)$ and δD and answer this first question, samples were collected from six background stations that were part of the EUROHYDROS network for H_2 observations and analyzed for $\chi(H_2)$ and δD. The results are discussed in Chapter 2. For the stations Alert (Arctic Canada), Mace Head (Ireland) and Cape Verde (African archipelago in the Atlantic) , clear seasonal cycles were found in both $\chi(H_2)$ and δD. The δD cycles were five to six months out-of-phase with the $\chi(H_2)$ cycles, similar to the average cycles that *Rhee et al.* (2006b) found from fits to samples in the Northern Hemisphere (NH) upper troposphere. This pattern is the result

of sources that produce D-depleted H_2 (combustion of fossil fuels and biomass), which accumulates in winter, and strong sinks with D-enriching effects on the H_2 reservoir that are much stronger in summer than in winter (mostly deposition to soil, with a smaller contribution of oxidation by OH). The seasonal variation in both $\chi(H_2)$ and δD is larger in Alert than in Mace Head or Cape Verde, likely because the soil sink in Alert is more strongly seasonal. Despite the presence of clear $\chi(H_2)$ seasonal cycles in Schauinsland (Southern Germany) and Neumayer (Antarctica), no seasonal cycle was observed there in δD. In Amsterdam Island, the $\chi(H_2)$ cycle was weak and no δD cycle was found. The absence of observable δD cycles at these stations is not fully understood.

The averages of the six stations show latitudinal gradients, with higher values for both $\chi(H_2)$ and δD in the Southern Hemisphere (SH) than in the NH. This gradient is larger than gradients found in ocean cruises (*Gerst and Quay*, 2000; *Rice et al.*, 2010), but we do not have enough spatial coverage in the SH to make a reliable SH average and compare the NH - SH difference. Remarkably, the minimum in the latitudinal gradient of δD was not found in the Arctic, as reported by *Gerst and Quay* (2000), but at the NH midlatitudes, which is likely an effect of anthropogenic combustion sources (which are depleted in D). The seasonal variation in this gradient is largely determined by seasonal variations in the NH. Hence, the smallest pole-to-pole (= Neumayer - Alert) difference in $\chi(H_2)$ is found in March–May, when $\chi(H_2)$ is at its seasonal maximum in Alert after a winter with only small sinks. The pole-to-pole difference in δD is then at its largest, as δD is at its minimum in Alert at that moment, after H_2 from D-depleted combustion sources has accumulated during the winter in the absence of strong and fractionating sinks. During the summer, $\chi(H_2)$ decreases and δD increases under the influence of the active, fractionating sinks, resulting in a $\chi(H_2)$ minimum and a δD maximum in September–November (SON); the pole-to-pole difference in $\chi(H_2)$ is then the largest, and the difference in δD the smallest.

With the assumption that the seasonal cycles are mostly driven by variations in the sink processes, apparent fractionation factors (α_{app}) were calculated for Alert, Mace Head and Cape Verde. These show an increase with latitude, which leads us to conclude from this tentative analysis that the relative contribution of the soil sink ($\alpha = 0.943 \pm 0.007$) to the total removal of H_2 increases with latitude, while the relative contribution of oxidation by OH ($\alpha = 0.58 \pm 0.07$) decreases. With simple calculations, we have thus obtained qualitative and (semi-)quantitative information from these data about the spatial and temporal variability of δD, and the sources that drive the variability. These data also provide good constraints for background δD values in models.

5.2 What is the optimal way to describe the δD value of H_2 that is imported into the troposphere by Stratosphere - Troposphere Exchange (STE)?

To find out how the isotopic composition of H_2 that is imported from the stratosphere into the troposphere can best be described, we have collected $\chi(H_2)$ and δD observations from samples that were collected in the Upper Troposphere - Lower Stratosphere region (UTLS) by the commercial CARIBIC aircraft (Chapter 3). The CARIBIC aircraft regularly crosses the tropopause (TP), with the result that approximately 40% of the analyzed samples could be classified as stratospheric. These stratospheric samples show a small elevation in $\chi(H_2)$ with respect to the tropospheric samples, and a marked elevation in δD. The D-enrichment

increases with O_3-derived altitude above the TP, while no clear gradient is observed in $\chi(H_2)$. The enrichment, observed earlier by *Rahn et al.* (2003), *Röckmann et al.* (2003) and *Rhee et al.* (2006a), is caused by stratospheric oxidation processes. These have D-enriching effects on the H_2 reservoir, but produce and destroy H_2 at similar rates and thus leave $\chi(H_2)$ almost unchanged. We note that δD has therefore more potential than $\chi(H_2)$ as a tracer for stratospheric oxidation reactions of H-containing species. Tight correlations exist between many stratospheric species (*Plumb*, 2007), and were also found for δD and CH_4 by *Rahn et al.* (2003), *Röckmann et al.* (2003) and *Rhee et al.* (2006a). We find a tight correlation for δD and $\chi(CH_4)$ that agrees reasonably well with the results of *Röckmann et al.* (2003). There is a small offset between the two datasets, which is perhaps due to a difference in age of the sampeled air masses, but the slopes agree within one standard error. We also find a tight correlation between δD and N_2O. In models, δD of H_2 that is imported from the stratosphere to the troposphere by STE can be parameterized relative to CH_4 or N_2O with such correlations. The relations that are found in the stratospheric CARIBIC data presented here are very likely the most appropriate choice for parameterizing STE, since all these data are collected close to the region of interest for STE (i.e., just in the lowermost stratosphere).

The samples from CARIBIC also display unexpected features. A few of the samples show hydrogen pollution effects, with high $\chi(H_2)$ and low δD. This effect has a tendency to occur close to takeoff and landing and is therefore possibly related to the interception of exhaust plumes of other aircraft in the flight corridor, but no definitive proof for this could be given.

Samples from a suite of flights to India offered the opportunity to study $\chi(H_2)$ and δD over the Indian subcontinent before, in and after the summer monsoon. In the monsoon season, a decrease of δD was found that was not accompanied by a change in $\chi(H_2)$. The δD decrease was correlated with the increase in CH_4 that was found previously in these samples by *Schuck et al.* (2010). Due to a lack of hydrogen observations at the ground in the same region and season, the cause of this could not be definitively established, but some scenarios were explored. Increased convection in the monsoon system transports species emitted at the ground more effectively to cruise altitude. If the δD-decrease were caused by H_2 from combustion sources that was effectively transported upwards, a measurable, concomitant increase is expected in $\chi(H_2)$ from isotopic mass balance considerations. Such a $\chi(H_2)$ increase was not observed, so the combustion source would have had to be compensated by a sink. An increased soil sink does, however, not seem likely in the monsoon season. An increased microbial production of H_2 in wet soils in the monsoon season seems a more plausible explanation, as the source signature of microbial production is so extremely D-depleted that the observed depletion would be expected to be accompanied by such a small $\chi(H_2)$ increase that it cannot be detected with our measurement precision.

5.3 What is the source signature of the fossil fuel combustion source of H_2 in Northwest Europe, and how does this source affect the local to regional H_2 cycle?

To investigate the anthropogenic (fossil fuel burning) sources in Northwest Europe, three years of $\chi(H_2)$ and δD observations were collected at the Cabauw tall tower in the Netherlands. These are presented in Chapter 4, as well as two diurnal cycles sampled at the Royal Holloway suburban site near London. The Cabauw tower is located in an agricultural area in the middle of the Randstad conurbation (*Vermeulen et al.*, 2011). The $\chi(H_2)$ data from Cabauw show excursions to high $\chi(H_2)$ values, especially in winter, just as in the (semi-)continuous $\chi(H_2)$ data measured at the tower (*Popa et al.*, 2011). In the δD data, it is seen that these excursions are accompanied by large D-depletions. These features show up especially clearly when the Cabauw data are compared to the data from the background station Mace Head that were presented in Chapter 2. The seasonal cycles at Cabauw also seem shifted: the spring $\chi(H_2)$ maximum and δD minimum of Mace Head seems shifted earlier towards winter at Cabauw. The δD data indicate that the $\chi(H_2)$ peaks at Cabauw are caused by sources that emit D-depleted H_2, most likely for the largest part anthropogenic combustion of fossil fuels. An investigation of the combined mixing ratio and isotope variations yields a source signature of (-314 $\pm$ 14) ‰, which is lower than found previously for the fossil fuel combustion H_2 source (*Gerst and Quay*, 2001; *Rahn et al.*, 2002b). The diurnals from Royal Holloway indicate a similarly low source signature. An explanation may lie in the modernization of car engines (including the introduction of catalytic converters) and congested traffic conditions that can lower the δD value of the produced H_2 (*Vollmer et al.*, 2010). The measurements at the Cabauw tower offer interesting comparison material with the data from the background stations described in Chapter 2. These data illustrate how humans alter the local and regional H_2 cycle, and can be used in models of the impact of H_2 emissions in populated regions.

5.4 Can we find and characterize the signal of H_2 deposition to soil by measuring vertical gradients of $\chi(H_2)$ and δD in the Netherlands?

To find a soil uptake signal, we used the possibility to sample at four different heights (20, 60, 120 and 200 m) that the Cabauw tower offers. This has yielded the first vertical profiles of δD in the boundary layer at a polluted location, which are also presented in Chapter 4. In a situation with strong soil uptake, lower $\chi(H_2)$ values and higher δD values are expected at the lower sampling levels. However, we find no significant difference in $\chi(H_2)$ between the levels, and δD values are even significantly lower at the 20 and 60 m levels. This means that we have not detected a soil deposition signal, which indicates that soil uptake does not play a large role at Cabauw. *Popa et al.* (2011) also found low uptake speeds, which which may have been caused by the local soil type (peat/clay) and high soil moisture.

The significant decrease in δD at the lower sampling levels is nevertheless interesting.

By sampling at the different heights, differently sized footprint regions are probed (*Vermeulen et al.*, 2011), and the observed differences in δD may thus indicate differences in the average sources between the different footprint regions. Differences in vehicle fleets and traffic conditions between the different Northwest European countries may cause different average source signatures of the fossil fuel combustion source.

5.5 Use of these observations in model studies

The $\chi(H_2)$ and δD data presented in this thesis have, by themselves, already provided qualitative and (semi-)quantitative insights into H_2 cycle on global, regional and local scales. However, to obtain full insight into the H_2 cycle, models are indispensable. So far, two studies with the TM5 model (*Pieterse et al.*, 2011, 2012) have made use of the data presented here. The TM5 model output was compared to the ground station data presented in Chapter 2 of this thesis, and the parameterization of the deuterium content of H_2 that is imported from the stratosphere to the troposphere was adapted according to the relation that was found between δD and $\chi(CH_4)$ in the upper troposphere, presented in Chapter 3.

A recent change by *Jordan and Steinberg* (2011) in the calibration scale of $\chi(H_2)$ increased $\chi(H_2)$ values by $\approx 3.5\%$. As a result, the H_2 scheme described in (*Pieterse et al.*, 2011) would lead TM5 to underestimate the updated mixing ratios. Therefore, *Pieterse et al.* (2012) investigated different changes that could be made to the budget terms within their uncertainties to re-close the gap between model and measurements. Two scenario's were investigated: a 5 Tg yr^{-1} reduction in dry deposition velocity and a 5 Tg yr^{-1} increase in the fossil fuel source. The best fit between modeled and measured $\chi(H_2)$ was obtained with the scenario with reduced soil uptake. The increased fossil fuel source did not resolve the bias, and a further increase would move the estimate out of it's uncertainty band. The reduced deposition scenario was further supported by a comparison of the modeled latitudinal gradients with the latitudinal gradients found in the EUROHYDROS project presented in Chapter 2 (Figure 5.1). The isotope data have thus provided information that helps to distinguish between different model scenarios and to constrain the budget. Also, adapting the stratospheric boundary conditions with the correlation between δD and $\chi(CH_4)$ that was presented in Chapter 3 has contributed to making the modeled H_2 budget more consistent.

5.6 Remaining questions

In interpreting the observations in this dissertation, we have encountered several areas where more research is desirable. We discuss these here.

The relative sink contribution analysis in Chapter 2, and in fact, any isotopic approach to constrain the H_2 budget, relies on the knowledge of the fractionation factors for the different sinks. For the fractionation factor of the soil sink α_{soil}, average values of 0.943 ± 0.024 (*Gerst and Quay*, 2001), 0.94 ± 0.01 (*Rahn et al.*, 2002a) and 0.943 ± 0.005 (*Rice et al.*, 2011) have been reported. These values seem in good agreement. However, *Rice et al.* (2011) reported considerable variability between individual experiments, that may have been associated with soil moisture, temperature and the microbial population that was present. Furthermore, all these experiments were performed at only three different sites, namely the Washington Park Arboretum in Seattle, the Univer-

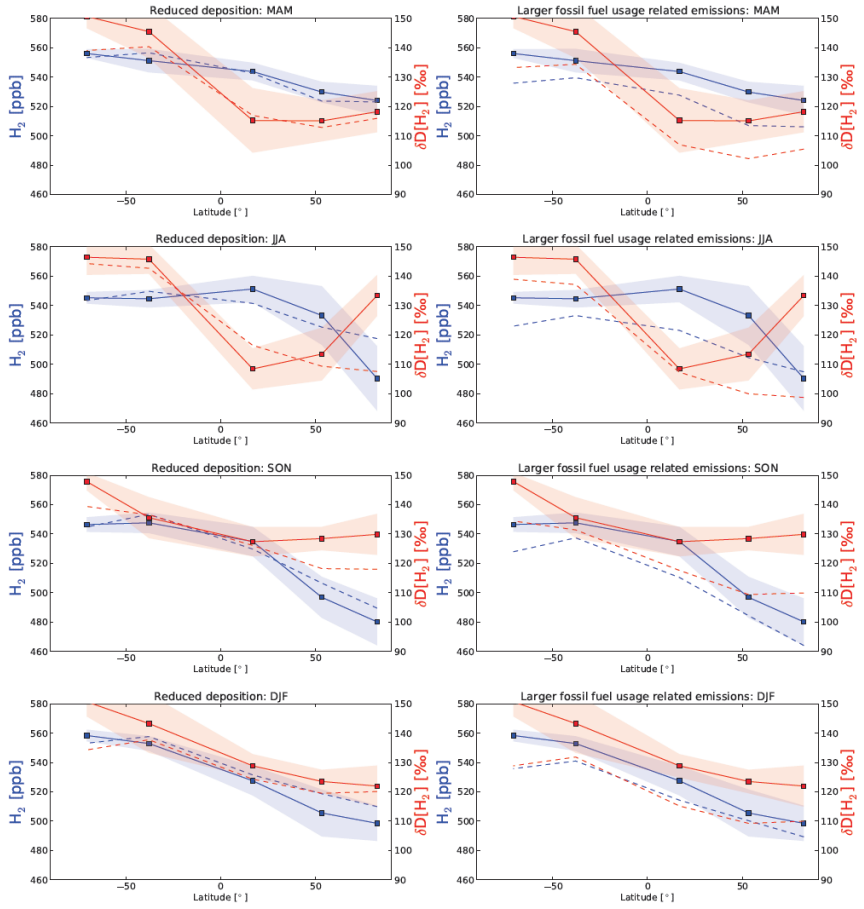

Figure 5.1: Comparisons by *Pieterse et al.* (2012) of the modeled seasonal mean latitudinal gradients (dashed lines) of $\chi(H_2)$ (blue) and δD (red) with the seasonal mean latitudinal gradients measured at the EUROHYDROS stations (solid lines) discussed in Chapter 2. The shading indicates one standard deviation of the measured values. The panels on the left depict the results of the reduced deposition scenario, and the panels on the right depict the results of the increased fossil fuel scenario.

sity of Washington campus in Seattle, and the Delta Junction boreal forest site in Alaska. It is safe to say that the geographical extent of these studies is very limited. Especially since deposition to soils is the largest sink in the budget, this situation is unsatisfactory. More soil uptake experiments are needed to verify the found fractionation factors in other regions of the world.

The datasets presented in this thesis have greatly expanded the existing set of environ-

mental δD observations, but the geographical extent is still limited. As far as we know, no ground level δD data were ever collected in South America, Australia, continental Africa and continental Asia. The data from the upper troposphere (Chapter 3) indicate that there may be unstudied, microbial sources of H_2 in South Asia, which would make it an interesting region to study next. The interpretation of the δD data collected over this region was limited by the lack of knowledge about the simultaneous situation at the ground. A ground station could at least provide comparison material that could be helpful with this. The observation in Chapter 2 that the relative contribution of soil uptake to the total sinks increases with latitude is in accordance with expectation and model results, but nevertheless it is based on only three stations. A time series from a station in the NH subtropics (for example on the Iberian Peninsula or the Canary Islands) could be useful to verify this trend. Extension of the CARIBIC project could increase the geographic extent too. So far, only one of the flights of which the samples were analyzed for δD reached the SH, and none of the analyzed samples were collected over the Pacific Ocean. Depending on the Lufthansa flight schedule, this could be remedied, at least for the SH (as the aircraft is based in Frankfurt, it is not likely to cross the Pacific often). Also, none of the analyzed flights took place in winter. With data from winter flights, the seasonal cycles in the upper troposphere could be characterized.

The estimates of global H_2 production by microbes on land are based on a very limited body of research, as they are largely based on observations by *Conrad and Seiler* (1980). *Conrad and Seiler* (1980) performed chamber measurements at two field stations around Mainz (Germany), and scaled their findings up to an estimate of 2.4–4.9 Tg yr^{-1} for the global source strength of microbial production, which still forms the basis of many estimates of this term in budget studies. Although this was valuable pioneering work, the question of whether the results from this area are globally representative remains open. The δD data obtained from the flights to India indicate that South Asian microbial emissions may be larger than previously thought (Chapter 3), although this is hard to verify without measurements at the ground. Microbial production may not be a large term in the global budget, but as the δD source signature is extremely depleted, it can be a significant term in the isotope budget. It could therefore be important to have a more precise knowledge of this process if isotope modeling is to be used to constrain the budget.

Recently, *Vollmer et al.* (2010) found that for modern cars with catalytic converters, the emitted H_2 could be more D-depleted than previously found by *Gerst and Quay* (2001) and *Rahn et al.* (2002b). The results from the Cabauw tower that are presented in this thesis (Chapter 4) confirm that the source signature of fossil fuel combustion may have decreased over the years. *Vollmer et al.* (2010) also found a considerable variation in de δD values in the exhaust gas that depended, among other parameters, on the temperature of the catalytic converter and on driving conditions. This means that there may be a geographical variation in the source signature of fossil fuel combustion, depending on the local vehicle fleet and other factors, that should be taken into account in models. This could be investigated with δD measurements in populated regions, ideally at different locations that differ in traffic conditions, climate, or age of the vehicle fleet.

As a closing note, it is clear that in the last few years, H_2 research has benefited from a close interaction between observational scientist and modelers. We would identify this as a key factor for success, and recommend that in future research efforts this interaction be continued.

Bibliography

Ahrens, C. D.: *Meteorology today: An introduction to weather, climate and the environment*, Thomson Brooks/Cole, eight edn., ISBN 0-495-10581-3, 2007.

Allan, W., Manning, M., Lassey, K., Lowe, D., and Gomez, A.: *Modeling the variation of $\delta^{13}C$ in atmospheric methane: Phase ellipses and the kinetic isotope effect*, Glob. Biochem. Cy., **15** (2), 467–481, doi:10.1029/2000GB001281, 2001.

Batenburg, A. M., Walter, S., Pieterse, G., Levin, I., Schmidt, M., Jordan, A., Hammer, S., Yver, C., and Röckmann, T.: *Temporal and spatial variability of the stable isotopic composition of atmospheric molecular hydrogen: observations at six EUROHYDROS stations*, Atmos. Chem. Phys., **11**, 6985–6999, doi:10.5194/acp-11-6985-2011, 2011.

Batenburg, A. M., Schuck, T. J., Baker, A. K., Zahn, A., Brenninkmeijer, C. A. M., and Röckmann, T.: *The stable isotopic composition of molecular hydrogen in the tropopause region probed by the CARIBIC aircraft*, Atmos. Chem. Phys., **12**, 4633–4646, doi:10.5194/acp-12-4633-2012, 2012.

Begemann, F. and Friedman, I.: *Tritium and deuterium content of atmospheric hydrogen*, Z. Naturforsch. A, **14**, 1024–1031, 1959.

Bond, S. W., Alvarez, R., Vollmer, M. K., Steinbacher, M., Weilenmann, M., and Reimann, S.: *Molecular hydrogen (H_2) emissions from gasoline and diesel vehicles*, Sci. Total Environ., **408**, 3596–3606, doi:10.1016/j.scitotenv.2010.04.055, 2010.

Bottinga, Y.: *Calculated fractionation factors for carbon and hydrogen isotope exchange in the system calcite - carbon dioxide - graphite - methane - hydrogen - water vapor*, Geochim. Cosmochim. Ac., **33**, 49–64, doi:10.1016/0016-7037(69)90092-1, 1969.

Bousquet, P., Yver, C., Pison, I., Li, Y. S., Fortems, A., Hauglustaine, D., Szopa, S., Rainer, P. J., Novelli, P., Langenfelds, R., Steele, P., Ramonet, M., Schmidt, M., Foster, P., Morfopoulos, C., and Ciais, P.: *A three-dimensional synthesis inversion of the molecular hydrogen cycle: Sources and sinks budget and implications for the soil uptake*, J. Geophys. Res, **116** (D01302), doi:10.1029/2010JD014599, 2011.

Bovy, P. H. L. and Salomon, I.: *Traffic congestion in Europe: Netherlands*, in: Report of the hundred and tenth round table on transport economics 1998, Paris, France, 1999.

Brand, W. A. and Coplen, T. B.: *Stable isotope deltas: tiny, yet robust signatures in nature*, Isotopes in Environmental and Health Studies, 1–17, doi:10.1080/10256016.2012.666977, 2012.

Brenninkmeijer, C. A. M., Crutzen, P., Boumard, F., Dauer, T., Dix, B., Ebinghaus, R., Filippi, D., Fischer, H., Franke, H., Frieß, U., Heintzenberg, J., Helleis, F., Hermann, M., Kock, H. H., Koeppel, C., Lelieveld, J., Leuenberger, M., Martinsson, B. G., Miemczyk, S., Moret, H. P., Nguyen, H. N., Nyfeler, P., Oram, D., O'Sullivan, D., Penkett, S., Platt, U., Pupek, M., Ramonet, M., Randa, B., Reichelt, M., Rhee, T. S., Rohwer, J., Rosenfeld, K., Scharffe, D., Schlager, H., Schumann, U., Slemr, F., Sprung, D., Stock, P., Thaler, R., Valentino, F., van Velthoven, P., Waibel, A., Wandel, A., Waschitschek, K., Wiedensohler, A., Xueref-Remy, I., Zahn, A., Zech, U., and Ziereis, H.: *Civil Aircraft for the regular investigation of the atmosphere based on an instrument container: The new CARIBIC system*, Atmos. Chem. Phys., **7**, 4953–4976, doi:10.5194/acp-7-4953-2007, 2007.

Cantrell, C. A.: *Technical Note: Review of methods for linear least-squares fitting of data and application to atmospheric chemistry problems*, Atmos. Chem. Phys., **8**, 5477–5487, doi:10.5194/acp-8-5477-2008, 2008.

Conrad, R. and Seiler, W.: *Field measurements of hydrogen evolution by nitrogen-fixing legumes*, Soil Biol. Biochem., **11**, 689–690, doi:10.1016/0038/0717(79)90041-5, 1979.

Conrad, R. and Seiler, W.: *Contribution of hydrogen production by biological nitrogen fixation to the global hydrogen budget*, J. Geophys. Res., **85** (C10), 5493–5498, doi:10.1029/JC085iC10p05493, 1980.

Conrad, R. and Seiler, W.: *Decomposition of atmospheric hydrogen by soil microorganisms and soil enzymes*, Soil Biol. Biochem, **13**, 43–49, doi:10.1016/0038-0717(81)90101-2, 1981.

Constant, P., Chowdhury, S. P., Pratscher, J., and Conrad, R.: *Streptomycetes contributing to atmospheric molecular hydrogen soil uptake are widespread and encode a putative high-affinity [NiFe]-hydrogenase*, Env. Microbiol., **12** (3), 821–829, doi:10.1111/j.1462-2920.2009.02130.x, 2010.

Duglokencky, E. J., Bruhwiler, L., White, J. W. C., Emmons, L. K., Novelli, P. C., Montzka, S. A., Masarie, K. A., Lang, P. M., Crotwell, A. M., Miller, J. B., and Gatti, L. V.: *Observational constraints on recent increases in the atmospheric CH_4 burden*, Geophys. Res. Lett., **36** (L18803), doi:10.1029/2009GL039780, 2009.

Ehhalt, D., Israel, G., Roether, W., and Stich, W.: *Tritium and deuterium content of atmospheric hydrogen*, J. Geophys. Res., **68** (13), 3747–3751, 1963.

Ehhalt, D., Roether, W., and Stich, W.: *Der Anstieg des Tritiumgehaltes im atmosphärischen Wasserstoff seit 1960*, Z. Naturforsch. A, **21**, 1703–1709, 1966.

Ehhalt, D. H. and Rohrer, F.: *The tropospheric cycle of H_2: a critical review*, Tellus B, **61** (3), 500–535, doi:10.1111/j.1600-0889.2009.00416.x, 2009.

Ehhalt, D. H. and Rohrer, F.: *The dependence of soil H_2 uptake on temperature and moisture: a reanalysis of laboratory data*, Tellus, **63B**, 1040–1051, doi:10.1111/j.1600-0889.2011.00581.x, 2011.

Ehhalt, D. H., Schmidt, U., and Heidt, L. E.: *Vertical profiles of molecular hydrogen in the troposphere and stratosphere*, J. Geophys. Res., **82** (37), 5907–5911, doi:10.1029/JC082i037p05907, 1977.

Ehhalt, D. H., Davidson, J. A., Cantrell, C. A., Friedman, I., and Tyler, S.: *The kinetic isotope effect in the reaction of H_2 with OH*, J. Geophys. Res., **94** (D7), 9831–9836, doi:10.1029/JD094iD07p09831, 1989.

Engel, A.: *EUROHYDROS, A European network for atmospheric hydrogen observations and studies, final report*, available upon request from A. Engel (an.engel@iau.uni-frankfurt.de), 2009.

Estupiñán, E. G., Nocovich, J. M., Li, J., Cunnold, D. M., and Wine, P. H.: *Investigation of N_2O Production from 266 and 532 nm Laser Flash Photolysis of $O_3/N_2/O_2$ Mixtures*, J. Phys. Chem., **106** (24), 5880–5890, doi:10.1021/jp014242c, 2002.

Feck, T., Grooß J.-U., and Riese, M.: *Sensitivity of Arctic ozone loss to stratospheric H_2O*, Geophys. Res. Lett., **35** (1), 1–20, doi:10.1029/2007GL031334, 2008.

Feilberg, K. L., Johnson, M. S., Bacak, A., Röckmann, T., and Nielsen, C.: *Relative photolysis rates of HCHO and HCDO measured at the European Photoreactor Facility*, J. Phys. Chem. A, **111** (37), 9034–9046, doi:10.1029/2007GL031334, 2007.

Fowler, M., Lowry, D., Fisher, R., Lanoisellé, M., and Nisbet, E.: *The long-term (1996-2010) London record of carbon monoxide and molecular hydrogen: evidence for improved air quality*, in: paper presented at European Geosciences Union General Assembly 2011, Vienna, Austria, 2011.

Friedman, I. and Scholz, T. G.: *Isotopic composition of atmospheric hydrogen, 1967-1969*, J. Geophys. Res., **79** (6), 6 785–788, doi:10.1029/JC079i006p00785, 1974.

Gerst, S. and Quay, P.: *The deuterium content of atmospheric molecular hydrogen: Method and initial measurements*, Journal of geophysical research, **105** (D21), 26 433–26 445, doi:10.1029/2000JD900387, 2000.

Gerst, S. and Quay, P.: *Deuterium component of the global molecular hydrogen cycle*, J. Geophys. Res., **106**, 5021–5031, doi:10.1029/2000JD900593, 2001.

Glueckauf, E. and Kitt, G. P.: *The hydrogen content of atmospheric air at ground level*, Q. J. Roy. Meteorol. Soc., **83** (358), 522–528, doi:10.1002/qj.49708335808, 1957.

Gonfiantini, R., Stichler, W., and Rozanski, K.: *Standards and intercomparison materials distributed by the International Atomic Energy Agency for stable isotope measurements*, in: Reference and intercomparison materials for stable isotopes of light elements: Proceedings of a consultants meeting held in Vienna, 1-3 December 1993, IAEA-TECDOC-825, International Atomic Energy Agency, 1993.

Gonsoir, B. and Friedman, I.: *Tritium und Deuterium im atmosphärischen Wassertoff*, Z. Naturforsch. A, **17**, 1088–1091, 1962.

Gonsoir, B., Friedman, I., and Ehhalt, E.: *Measurements of the tritium and deuterium concentration in atmospheric hydrogen*, J. Geophys. Res., **68** (13), 3753–3756, 1963.

Gonsoir, B., Friedman, I., and Lindenmayr, G.: *New tritium and deuterium measurements in atmospheric hydrogen*, Tellus, **18**, 256–261, 1966.

Grant, A., Stanley, K. F., Henshaw, S. J., Shallcross, D. E., and O'Doherty, S.: *High-frequency urban measurements of molecular hydrogen and carbon monoxide in the United Kingdom*, Atmos. Chem. Phys., **10**, 4715–4724, doi:10.5194/

acp-10-4715-2010, 2010a.

Grant, A., Witham, C. S., Simmonds, P. G., Manning, A. J., and O'Doherty, S.: *A 15 year record of high-frequency, in situ measurements of hydrogen at Mace Head, Ireland*, Atmos. Chem. Phys., **10**, 1203–1214, doi:10.5194/acp-10-1203-2010, 2010b.

Hammer, S. and Levin, I.: *Seasonal variation of the molecular hydrogen uptake by soils inferred from continuous atmospheric observations in Heidelberg, southwest Germany*, Tellus, **61B**, 556–565, doi:10.1111/j.1600-0889.2009.00417.x, 2009.

Hammer, S., Vogel, F., Kaul, M., and Levin, I.: *The H_2/CO ratio of emissions from combustion sources: comparison of top-down with bottom-up measurements in southwest Germany*, Tellus, **61B**, 547–555, doi:10.1111/j.1600-0889.2009.00418.x, 2009.

Hauglustaine, D. A. and Ehhalt, D. H.: *A three-imensional model of molecular hydrogen in the troposphere*, J. Geophys. Res., **107** (D17), 4330, doi:10.1029/2001JD001156, 2002.

Haumann, A., Batenburg, A. M., Pieterse, G., Gerbig, C., and Röckmann, T.: *Molecular hydrogen from biomass burning over the Amazonian tropical rainforest*, In preparation, 2012.

Heidt, L. E. and Ehhalt, D. H.: *Gas chromatographic measurement of hydrogen, methane, and neon in air*, Journal of Chromatography, **69**, 103–113, doi:10.1016/S0021-9673(00)83088-5, 1972.

Henne, S., Brunner, D., Folini, D., Solberg, S., Klausen, J., and Buchmann, B.: *Assessment of parameters describing representativeness of air quality in-situ measurement sites*, Atmos. Chem. Phys., **10**, 3561–3581, doi:10.5194/acp-10-3561-2010, 2010.

Holton, J. R., Haynes, P. H., McIntyre, M. E., Douglas, A. R., Rood, R. B., and Pfister, L.: *Stratosphere-troposphere exchange*, Rev. Geophys., **33** (4), 403–439, doi:10.1029/95RG02097, 1995.

Jacob, D. J.: *Introduction to atmospheric chemistry*, Princeton University Press, ISBN 0-691-00185-5, 1999.

Jacobsen, M. Z.: *Effects of wind-powered hydrogen fuel cell vehicles on stratospheric ozone and global climate*, Geophys. Res. Lett., **35** (L19803), doi:10.1029/2008GL035102, 2008.

Jacobsen, M. Z., Colella, W. G., and Golden, D. M.: *Cleaning the air and improving health with hydrogen fuel-cell vehicles*, Science, **308**, 1901–1905, doi:10.1126/science.1109157, 2005.

Jordan, A. and Steinberg, B.: *Calibration of atmospheric hydrogen measurements*, Atmos. Meas. Tech., **4**, 509–521, doi:10.5194/amt-4-509-2011, 2011.

Kammen, D. M., Lipman, T. E., Lovins, A. B., and Lehman, P. A.: *Assessing the future hydrogen economy: Letters to the editor in response to the paper "Potential environmental impact of a hydrogen economy on the stratosphere"*, Science, **32**, 226–228, 2003.

Kaye, J. A.: *Mechanisms and observations for isotope fractionation of molecular species in planetary atmospheres*, Reviews of Geophysics, **25** (8), 1606–1658, doi:10.1029/

RG025i008p01609, 1987.

Khalil, M. A. K. and Rasmussen, R. A.: *Global increase of atmospheric molecular hydrogen*, Nature, **347**, 743–745, doi:10.1038/347743a0, 1990.

Krystek, M. and Anton, M.: *A weighted total least-squares algorithm for fitting a straight line*, Mes. Sci. Technol., **18**, 3438–3442, doi:10.1088/0957-0233/18/11/025, 2007.

Lallo, M., Aalto, T., Laurila, T., and Hatakka, J.: *Seasonal variations in hydrogen deposition to boreal forest soil in southern Finland*, Geophys. Res. Lett., **35** (L04402), doi:10.1029/2007GL032357, 2008.

Mar, K. A., McCarthy, M. C., Connell, P., and Boering, K. A.: *Modeling the photochemical origins of the extreme deuterium enrichment in stratospheric H_2*, J. Geophys. Res., **112** (D19302), doi:10.1029/2006JD007403, 2007.

McCarthy, M. C., Boering, K. A., Rahn, T., Eiler, J., , Rice, A., Tyler, S. C., Atlas, E., and Johnson, D. G.: *The hydrogen isotopic composition of water vapor entering the stratosphere inferred from high precision measurements of δD-CH_4 and δD-H_2*, J. Geophys. Res., **109** (D07304), doi:10.1029/2003JD004003, 2004.

Miller, J. B. and Tans, P. P.: *Calculating isotopic fractionation from atmospheric measurements at various scales*, Tellus, **55B**, 207–214, doi:10.1034/j.1600-0889.2003.00020.x, 2003.

Nilsson, E. J. K., Johnson, M. S., Taketani, F., Matsumi, Y., Hurley, M. D., and Wallington, T. J.: *Atmospheric deuterium fractionation: HCHO and HCDO yields in the $CH_2DO + O_2$ reaction*, Atmos. Chem. Phys., **7**, 5873–5881, doi:10.5194/acp-7-5873-2007, 2007.

Nilsson, E. J. K., Andersen, V. F., Skov, H., and Johnson, M. S.: *Pressure dependence of the deuterium isotope effect in the photolysis of formaldehyde by ultraviolet light*, Atmos. Chem. Phys., **10**, 3455–3462, doi:10.5194/acp-10-3455-2010, 2010.

Novelli, P. C., Lang, P. M., Masarie, K. A., Hurst, D. F., Myers, R., and Elkins, J. W.: *Molecular Hydrogen in the troposphere: Global distribution and budget*, J. Geophys. Res., **104** (D23), 30 427–30 444, doi:10.1029/1999JD900788, 1999.

Paneth, F. A.: *The chemical composition of the atmosphere*, Q. J. R. Meteorol. Soc., **63**, 433–438, doi:10.1002/qj.49706327114, 1937.

Pieterse, G., Krol, M. C., and Röckmann, T.: *A consistent molecular hydrogen isotope chemistry scheme based on an independent bond approximation*, Atmos. Chem. Phys., **9**, 8503–8529, doi:10.5194/acp-9-8503-2009, 2009.

Pieterse, G., Krol, M. C., Batenburg, A. M., Steele, L. P., Kummel, P. B., Langenfelds, R. L., and Röckmann, T.: *Global modelling of H_2 mixing ratios and isotopic compositions with the TM5 model*, Atmos. Chem. Phys., **11**, 7001–7026, doi:10.5194/acp-11-7001-2011, 2011.

Pieterse, G., Krol, M. C., Batenburg, A. M., Brenninkmeijer, C. A. M., Popa, M. E., O'Doherty, S., Grant, A., Steele, L. P., Krummel, P. B., Langenfelds, R. L., Wang, H. J., Vermeulen, A. T., Schmidt, M., Jordan, A., Engel, A., Fisher, R. E., Lowry, D., Nisbet, E. G., Reimann, S., Vollmer, M. K., Steinbacher, M., Levin, I., Hammer, S., Sturges,

W. T., and Röckmann, T.: *Modelling the global and regional scale variability in atmospheric H_2 with the two-way nested TM5 model*, accepted by J. Geophys. Res., 2012.

Plumb, R.: *Tracer interrelationships in the stratosphere*, Rev. Geophys., **45** (RG4005), doi:10.1029/2005RG000179, 2007.

Popa, M. E., Vermeulen, A. T., van den Bulk, W. C. M., Jongejan, P. A. C., Batenburg, A. M., Zahorowski, W., and Röckmann, T.: *H_2 vertical profiles in the continental boundary layer: measurements at the Cabauw tall tower in the Netherlands*, Atmos. Chem. Phys., **11**, 6425–6443, doi:10.5194/acp-11-6425-2011, 2011.

Price, H., Jaeglé, L., Rice, A., Quay, P., and Novelli, P. C.: *Global budget of molecular hydrogen and its deuterium content: Constraints from ground station, cruise and aircraft observations*, J. Geophys. Res., **112** (D22108), doi:10.1029/2006JD008152, 2007.

Rahn, T., Eiler, J. M., Kitchen, N., Fessenden, J. E., and Randerson, J. T.: *Concentration and δD of molecular hydrogen in boreal forests: Ecosystem-scale systematics of atmospheric H_2*, Geophys. Res. Lett, **29** (18), 1888, doi:10.1029/2002GL015118, 2002a.

Rahn, T., Kitchen, N., and Eiler, J.: *D/H ratios of atmospheric H_2 in urban air: Results using new methods for analysis of nano-molar H_2 samples*, Geochim. Cosmochim. Ac., **66** (14), 2475–2481, doi:10.1016/S0016-7037(02)00858-X, 2002b.

Rahn, T., Eiler, J. M., Boering, K. A., Wennberg, P. O., McCarthy, M. C., Tyler, S., Schauffler, S., Donnelly, S., and Atlas, E.: *Extreme deuterium enrichment in stratospheric hydrogen and the global atmospheric budget of H_2*, Nature, **424**, 918–921, doi:10.1038/nature01917, 2003.

Rhee, T. S., Mak, J., Röckmann, T., and Brenninkmeijer, C. A. M.: *Continuous-flow isotope analysis of the deuterium/hydrogen ratio in atmospheric hydrogen*, Rapid Commun. Mass Spectrom., **18**, 299–306, doi:10.1002/rcm.1309, 2004.

Rhee, T. S., Brenninkmeijer, C. A. M., Braß M., and Brühl, C.: *Isotopic composition of H_2 from CH_4 oxidation in the stratosphere and the troposphere*, J. Geophys. Res., **111** (D23303), doi:10.1029/2005JD006760, 2006a.

Rhee, T. S., Brenninkmeijer, C. A. M., and Röckmann, T.: *The overwhelming role of soils in the global atmospheric hydrogen cycle*, Atmos. Chem. Phys., **6**, 1611–1625, doi:10.5194/acp-6-1611-2006, 2006b.

Rhee, T. S., Brenninkmeijer, C. A. M., and Röckmann, T.: *Hydrogen isotope fractionation in the photolysis of formaldehyde*, Atmos. Chem. Phys., **8**, 1353–1366, doi:10.5194/acp-8-1353-2008, 2008.

Rice, A., Quay, P., Stutsman, J., Gammon, R., Price, H., and Jaeglé, L.: *Meridional distribution of molecular hydrogen and its deuterium content in the atmosphere*, J. of Geophys. Res., **115** (D12), D12306, doi:10.1029/2009JD012529, 2010.

Rice, A., Dayalu, A., Quay, P., and Gammon, R.: *Isotopic fractionation during soil uptake of atmospheric hydrogen*, Biogeosciences, **8**, 763–769, doi:10.5194/acp3-2015-2003, 2011.

Röckmann, T., Rhee, T. S., and Engel, A.: *Heavy hydrogen in the stratosphere*, Atmos. Chem. Phys., **3**, 2015–2023, doi:10.5194/acpd-3-3745-2003, 2003.

Röckmann, T., Álvarez, C. X., Walter, S., van der Veen, C., , Wollny, A. G., Gunthe, S. S., Helas, G., Pöschl, U., Keppler, F., Greule, M., and Brand, W. A.: *Isotopic composition of H_2 from wood burning: Dependency on combustion efficiency, moisture content, and δD of local precipitation*, J. Geophys. Res., **115** (D17308), doi:10.1029/2009JD013188, 2010a.

Röckmann, T., Walter, S., Bohn, B., Wegener, R., Spahn, H., Brauers, T., Tillmann, R., Schlosser, E., Koppmann, R., and Rohrer, F.: *Isotope effect in the formation of H_2 from H_2CO studied at the atmospheric simulation chamber SAPHIR*, Atmos. Chem. Phys., **10**, 5343–5357, doi:10.5194/acp-10-5343-2010, 2010b.

Rothe, M., Jordan, A., and Brand, W. A.: *Trace gases, $\delta^{13}C$ and $\delta^{18}O$ of CO_2-in-air samples: Storage in glass flasks using PCTFE seals and other effects*, in: GAW report 161, 12^{th} WMO/IAEA meeting of experts on carbon dioxide concentration and related tracer measurement techniques, edited by Worthy, D. and Huang, L., WMO TD No. 1275, 2004.

van Ruijven, B., van Vuuren, D. P., and de Vries, B.: *The potential role of hydrogen in energy systems with and without climate policy*, Int. J. of Hydrogen Energy, **32**, 1655–1672, doi:10.1016/j.ijhydene.2006.08.036, 2007.

van Ruijven, B., Hari, L., van Vuuren, D. P., and de Vries, B.: *The potential role of hydrogen energy in India and Western Europe*, Energy Policy, **36**, 1649–1665, doi:10.1016/j.enpol.2008.01.020, 2008.

Sander, S. P., Finlayson-Pitts, B. J., Friedl, R. R., Golden, D. M., Huie, R. E., Keller-Rudek, H., Kolb, C. E., Kurylo, M. J., Molina, M. J., Moortgat, G. K., Orkin, V. L., and Wine, P. H.: *Chemical kinetics and photochemical data for use in atmospheric studies*, in: Evaluation number 15, Technical Report, Jet Propulsion Laboratory, Pasadena, USA, JPL Publication 06-2 1275, 2006.

Sanderson, M. G., Collins, W. J., Derwent, R. G., and Johnson, C. E.: *Simulation of global hydrogen levels using a Lagrangian three-dimensional model*, J. Atmos. Chem., **46**, 15–28, doi:10.1023/a:1024824223232, 2003.

Scharffe, D., Slemr, F., Brenninkmeijer, C. A. M., and Zahn, A.: *Carbon monoxide measurements onboard the CARIBIC passenger aircraft using UV resonance fluorescence*, Atmos. Meas. Tech., **5**, 1753–1760, doi:10.5194/amt-5-1753-2012, 2012.

Schmidt, M., Graul, R., Sartorius, H., and Levin, I.: *Carbon dioxide and methane in continental Europe: a climatology, and ^{222}Radon-based emission estimates*, Tellus, **48B**, 457–473, doi:10.1034/j.1600-0889.1994.t01-2-00002.x-i1, 1996.

Schmidt, U.: *Molecular hydrogen in the atmosphere*, Tellus, **26** (1–2), 78–90, doi:10.1111/j.2153-3490.1974.tb01954.x, 1974.

Schmidt, U.: *The latitudinal and vertical distribution of molecular hydrogen in the troposphere*, J. Geophys. Res., **83** (C2), 941–946, doi:10.1029/JC083iC02p00941, 1978.

Schmidt, U. and Seiler, W.: *A new method for recording molecular hydrogen in atmospheric air*, J. Geophys. Res., **75** (9), 1713–1716, doi:10.1029/JC075i009p01713, 1970.

Schmitt, S., Hanselmann, A., Wollschläger, U., Hammer, S., and Levin, I.: *Investigation*

of parameters controlling the soil sink of atmospheric molecular hydrogen, Tellus, **61B**, 416–423, doi:10.1111/j.1600-0889.2008.00402.x, 2009.

Schuck, T. J., Brenninkmeijer, C. A. M., Slemr, F., Xueref-Remy, I., and Zahn, A.: *Greenhouse gas analysis of air samples collected onboard the CARIBIC passenger aircraft*, Atmos. Meas. Tech., **2**, 449–464, doi:10.5194/amt-2-449-2009, 2009.

Schuck, T. J., Brenninkmeijer, C. A. M., Baker, A. K., Slemr, F., van Velthoven, P. F. J., and Zahn, A.: *Greenhouse gas relationships in the Indian summer monsoon plume measured by the CARIBIC passenger aircraft*, Atmos. Chem. Phys., **10**, 3965–3984, doi:10.5194/acp-10-3965-2010, 2010.

Schultz, M. G., Diehl, T., Brasseur, G. P., and Zittel, W.: *Air pollution and climate-forcing impacts of a global hydrogen economy*, Science, **302**, 624–627, doi:10.1126/science.1085169, 2003.

Simmonds, P. G., Derwent, R. G., O'Doherty, S., Ryall, D. B., Steele, L. P., Langenfelds, R. L., Salameh, P., Wang, H. J., Dimmer, C. H., and Hudson, L. E.: *Continuous high-frequency observations of hydrogen at the Mace Head baseline atmospheric station over the 1994-1998 period*, J. Geophys. Res., **105** (D10), 12 105–12 121, doi:10.1029/2000JD900007, 2000.

Smith-Downey, N. V., Randerson, J. T., and Eiler, J. M.: *Temperature and moisture dependence of soil H_2 uptake measured in the laboratory*, Geophys. Res. Lett., **33** (L14813), doi:10.1029/2006GL026749, 2006.

Smith-Downey, N. V., Randerson, J. T., and Eiler, J. M.: *Molecular hydrogen uptake by soils in forest, desert and marsh ecosystems in California*, J. Geophys. Res., **113** (G03037), doi:10.1029/2008JG00701, 2008.

Sprung, D. and Zahn, A.: *Acetone in the upper troposphere/lowermost stratosphere measured by the CARIBIC passenger aircraft: Distribution, seasonal cycle, and variability*, J. Geophys. Res., **115** (D16301), doi:10.1029/2009JD012099, 2010.

Steinbacher, M., Fischer, A., Vollmer, M. K., Buchmann, B., Reimann, S., and Hueglin, C.: *Perennial observations of molecular hydrogen (H_2) at a suburban site in Switzerland*, Atmos. Env., **41**, 2111–2124, doi:10.1016/j.atmosenv.2006.10.075, 2007.

Talukdar, R. K., Gierczak, T., Goldfarb, L., Rudich, Y., Rao, B. S. M., and Ravishankara, A. R.: *Kinetics of Hydroxyl Radical Reactions with Isotopically Labeled Hydrogen*, J. Phys. Chem., **100**, 3037–3047, doi:10.1021/jp9518724, 1996.

Tromp, T. K., Shia, R.-L., Allen, M., Eiler, J. M., and Yung, Y. L.: *Potential environmental impact of a hydrogen economy on the stratosphere*, Science, **300**, 1740–1742, doi:10.1126/science.1085169, 2003.

UNECE: *The UNECE transport statistics for Europe and North America*, Tech. rep., United Nations Economic Commission for Europe, Geneva, 2012.

van Velthoven, P. F. J.: *Meteorological analysis of CARIBIC by KNMI*, URL `http://www.knmi.nl/samenw/campaign_support/CARIBIC/#LH`, last access December 2nd, 2011, 2009.

Vermeulen, A. T., Hensen, A., Popa, M. E., van den Bulk, W. C. M., and Jongejan, P.

A. C.: *Greenhouse gas observations from Cabauw Tall Tower (1992-2010)*, Atmos. Meas. Tech., **4**, 617–644, doi:10.5194/amt-4-617-2011, 2011.

Vingarzan, R.: *A review of surface ozone background levels and trends*, Atmos. Env., **38**, 3431–3442, doi:10.1016/j.atmosenv.2004.03.030, 2004.

Vogel, B., Feck, T., Grooß, J.-U., and Riese, M.: *Impact of a possible future global hydrogen economy on Arctic stratospheric ozone loss*, Energy Environ. Sci., **5**, 6445–6452, doi:10.1039/c2ee03181g, 2012.

Vollmer, M. K., Walter, S., Bond, S. W., Soltic, P., and Röckmann, T.: *Molecular hydrogen (H_2) emissions and their isotopic signatures (H/D) from a motor vehicle: implications on atmospheric H_2*, Atmos. Chem. Phys., **10**, 5707–5718, doi:10.5194/acp-10-5707-2010, 2010.

Vollmer, M. K., Walter, S., Mohn, J., Steinbacher, M., Bond, S. W., Röckmann, T., and Reimann, S.: *Molecular hydrogen (H_2) combustion emissions and their isotope (D/H) signatures from domestic heaters, diesel vehicle engines, waste incinerator plants, and biomass burning*, Atmos. Chem. Phys., **12**, 6275–6289, doi:10.5194/acp-12-6275-2012, 2012.

Walter, S., Laukenmann, S., Stams, A. J. M., Vollmer, M. K., Gleixner, G., and Röckmann, T.: *The stable isotopic signature of biologically produced molecular hydrogen (H_2)*, Biogeosciences Discuss., **8**, 12 521–12 541, doi:10.5194/bgd-8-12521-2011, 2011.

Warneck, P.: *Chemistry of the natural atmosphere*, vol. 41, Academic Press, Inc., San Diego, California, 1988.

Warwick, N. J., Bekki, S., Nisbet, E. G., and Pyle, J. A.: *Impact of a hydrogen economy on the stratosphere and troposphere studied in a 2-D model*, Geophys. Res. Lett, **31** (5), 2–5, doi:10.1029/2003GL019224, 2004.

van der Werf, G. R., Randerson, J. T., Collatz, G. J., and Giglio, L.: *Carbon emissions from fires in tropical and subtropical ecosytems*, Global Change Biology, **9**, 547–562, doi:10.1046/j.1365-2486.2003.00604.x, 2003.

de Wit, J. C., van der Straten, C. M., and Mook, W. G.: *Determination of the absolute hydrogen isotopic ratio of V-SMOW and SLAP*, Geostandards Newsletter, **4** (1), 33–36, doi:10.1111/j.1751-908X.1980.tb00270.x, 1980.

WMO: *WMO greenhouse gas bulletin: the state of greenhouse gases in the atmosphere based on global observations through 2010*, http://www.wmo.int/pages/prog/arep/gaw/ghg/GHGbulletin.html, 2011.

Xiao, X., Prinn, R. G., Simmonds, P. G., Steele, L. P., Novelli, P. C., Huang, J., Langenfelds, R. L., O'Doherty, S., Krummel, P. B., Fraser, P. J., Porter, L. W., Weiss, R. F., Salameh, P., and Wange, R. H. J.: *Optimal estimation of the soil uptake rate of molecular hydrogen from the Advanced Global Atmospheric Gases Experiment and other measurements*, J. Geophys. Res., **112** (D07303), doi:10.1029/2006JD007241, 2007.

Yashiro, H., Sudo, K., Yonemura, S., and Takigawa, M.: *The impact of soil uptake on the global distribution of molecular hydrogen: chemical transport model simulation*, Atmos. Chem. Phys., **11**, 6701–6719, doi:10.5194/acp-11-6701-2011, 2011.

Yver, C.: *Estimation des sources et puits du dihydrogène troposphérique: développements instrumentaux, mesures atmosphériques et assimilation variationnelle*, Ph.D. thesis, University of Versailles, Saint Quentin, France, `http://www.sudoc.abes.fr/xslt/DB=2.1/SET=1/TTL=1/SHW?FRST=2`, 2010.

Yver, C., Schmidt, M., Bousquet, P., Zahorowski, W., and Ramonet, M.: *Estimation of the molecular hydrogen soil uptake and traffic emissions at a suburban site near Paris through hydrogen, carbon monoxide, and radon-222 semicontinuous measurements*, J. Geophys. Res., **114** (D18304), doi:10.1029/2009JD012122, 2009.

Yver, C., Pison, I., Fortems-Cheiney, A., Schmidt, M., Bousquet, P., Ramonet, M., Jordan, A., Søvde, A., Engel, A., Fisher, R., et al.: *A new estimation of the recent tropospheric molecular hydrogen budget using atmospheric observations and variational inversion*, Atmos. Chem. Phys, **11**, 3375–3392, doi:10.5194/acp/11-3375-2011, 2011a.

Yver, C., Schmidt, M., Bousquet, P., and Ramonet, M.: *Measurements of molecular hydrogen and carbon monoxide on the Trainou tall tower*, Tellus, **63B**, 52–63, doi:10.1111/j.1600-0889.2010.00520.x, 2011b.

Ziereis, H., Schlager, H., Schulte, P., van Velthoven, P., and Slemr, F.: *Distributions of NO, NO_x , and NO_y in the upper troposphere and lower stratosphere between 28° and 61° N during POLINAT 2*, J. Geophys. Res., **105** (D3), 3653–3664, doi:10.1029/1999JD900870, 2000.

Samenvatting (in Dutch)

De scheikundige samenstelling van de aardse dampkring beïnvloedt het klimaat en de gezondheid van mensen, dieren en planten. Om deze redenen wordt de samenstelling van de dampkring en de processen die die bepalen bestudeerd binnen het vakgebied van de atmosferische chemie. Opmerkelijk genoeg concentreert het grootste deel van dit onderzoek zich op een zeer klein deel van de dampkring, namelijk de sporegassen. De sporegassen omvatten alle gassen die geen stikstof (N_2), zuurstof (O_2), argon (Ar) of waterdamp (H_2O) zijn. Omdat N_2, O_2 en Ar chemisch relatief inert zijn en weinig langgolvige straling absorberen, bepalen de sporegassen het grootste deel van de atmosferische chemie en een groot deel van het klimaat.

Het onderwerp van dit proefschrift is het sporegas (moleculaire) waterstof (H_2). H_2 is geen broeikasgas en ook niet direct schadelijk voor de gezondheid. Maar door de reacties waaruit H_2 wordt geproduceerd of die H_2 zelf aangaat, is het verbonden met gassen die wèl dat soort eigenschappen hebben. Het is daarom nuttig om de processen waarbij atmosferische H_2 ontstaat en weer wordt afgebroken (tezamen de H_2-kringloop) te leren begrijpen. Daarbij is er tegenwoordig nog een andere reden om de H_2-kringloop te bestuderen. Met de overduidelijke nadelen die er aan het verbranden van fossiele brandstoffen kleven is H_2 een aantrekkelijke alternatieve energiedrager, aangezien het schoon is te verbranden tot water. H_2 is echter zeer vluchtig, en het is onvermijdelijk dat er altijd een deel weglekt bij opslag, transport of verbruik ervan. Bij een massale omschakeling zou hierdoor de H_2-concentratie in de dampkring (genoteerd als mengverhouding, $\chi(H_2)$) sterk kunnen stijgen, wat nadelige gevolgen zou kunnen hebben die een deel van de milieuvoordelen teniet zouden kunnen doen. In de eerste plaats is dat omdat H_2 reageert met fotochemisch geproduceerde hydroxylradicalen (OH), die normaliter een grote rol spelen bij het afbreken van vervuiling en broeikasgassen in de atmosfeer. Bij een hoge H_2-concentratie zou de OH-concentratie dus kunnen dalen met als gevolg dat broeikasgassen en ongezonde stoffen langer in de atmosfeer blijven. In de tweede plaats zou een deel van de extra H_2 in de stratosfeer terecht kunnen komen, waar het geoxideerd wordt tot water. Dit vochtiger worden van de stratosfeer zou het ontstaan kunnen bevorderen van de polaire stratosferische wolken waarin ozon (O_3) wordt afgebroken, met als gevolg dat het herstel van de ozonlaag wordt vertraagd. Er is dus genoeg reden om de atmosferische kringloop van H_2 beter te willen begrijpen.

In dit proefschrift wordt daarvoor gebruik gemaakt van concentratiemetingen en isotoopmetingen. Een “isotoop” is eigenlijk een subklasse van een chemisch “element”. Een element omvat alle atomen die een bepaald aantal protonen in hun kern hebben; een isotoop omvat alle atomen van een bepaald element die, naast hetzelfde aantal protonen, ook nog hetzelfde aantal neutronen bevatten. Door het verschillende aantal neutronen

hebben de afzonderlijke isotopen van een element elk een andere massa. Sommige isotopen zijn instabiel en vervallen onder het uitzenden van radioactieve straling; andere zijn stabiel. Dit proefschrift behandelt verder alleen stabiele isotopen. De verschillende isotopen van een element zijn scheikundig vrijwel identiek, wat wil zeggen dat ze (meestal) dezelfde chemische verbindingen kunnen vormen die (meestal) dezelfde reacties kunnen aangaan. Er kunnen echter verschillen optreden in de snelheden en de evenwichtsverhoudingen van deze reacties voor de verschillende isotopologen (moleculen met een een verschillende isotoopsamenstelling). Verschillende reservoirs van een bepaald element of van een bepaalde stof kunnen daardoor een verschillende isotoopsamenstelling hebben. Verschillende productie- en afbraakprocessen kunnen de isotoopsamenstelling van een reservoir van een stof ook nog eens op verschillende manieren veranderen. Het zijn deze verschillen die het analyseren van het isotoopgehalte van verschillende gassen nuttig maken voor de studie van de atmosfeer.

Het element waterstof (H) heeft twee stabiele isotopen, namelijk protium of "gewoon"waterstof (H of ^{1}H) en deuterium (D of ^{2}H). H_2 bestaat zodoende uit twee isotopologen, HH en HD, met een groot relatief massaverschil ($\approx 50\%$). DD is zo schaars dat het hier niet wordt beschouwd. Het deuteriumgehalte in de H_2 van een monster wordt over het algemeen uitgedrukt als δD(H_2), of hier voor het gemak, δD. Dit duidt de relatieve afwijking van de D:H-verhouding in het monster van de D:H-verhouding in een internationaal standaardmateriaal (VSMOW, ofwel "Vienna Standard Mean Ocean Water") aan, en wordt meestal gegeven in ‰. Bij een positieve δD-waarde zit er dus relatief meer deuterium in de H_2 van het monster dan in VSMOW, en bij een negatieve minder.

De grootste bron van atmosferische H_2 is de fotochemische oxidatie van methaan (CH_4) en andere koolwaterstoffen (zie ook Figuur 1.8 in de Introduction). Hieruit ontstaat H_2 die "verrijkt" is in D, en dus een positieve δD-waarde heeft. Een iets kleiner deel van de atmosferische H_2 wordt geproduceerd door incomplete verbranding, van fossiele brandstoffen of van biomassa. Dit levert "verarmde" H_2 op, dus met een negatieve δD. De kleinste bron van atmosferische H_2 is het vrijkomen van H_2 bij het vastleggen van stikstof door micro-organismen, in zee of op land. Deze produceren H_2 die nog verarmder is dan die van verbrandingsprocessen. Ongeveer driekwart van de door deze processen geproduceerde H_2 wordt opgenomen en afgebroken in de bodem, en het resterende deel wordt geoxideerd door OH. Beide afbraakprocessen verlopen sneller voor HH dan voor HD, maar deze "fractionering" is sterker voor de afbraak door OH dan voor de bodemopname. Deze opsomming maakt duidelijk dat het deuteriumgehalte van H_2 in een bepaalde luchtmassa de sporen draagt van de processen die op de H_2 in die luchtmassa hebben ingewerkt. Door dit deuteriumgehalte te bestuderen, kunnen we dus informatie krijgen over de bronnen en afbraakprocessen van H_2. Bovendien is het mogelijk om het deuteriumgehalte als extra variabele toe te voegen aan modellen van de H_2-kringloop, waardoor de onzekerheden (de "speelruimte") in de omvang van de verschillende processen kunnen worden teruggebracht. Om dit soort modellen te toetsen en de onzekerheden terug te brengen zijn er wel veel waarnemingen van δD nodig. Tot voor kort waren deze data er amper, omdat deze metingen lastig uit te voeren waren. Met het Gas Chromatografie - IsotoopRatio MassaSpectrometrie (GC-IRMS) systeem in het laboratorium van het IMAU kan δD routinematig worden gemeten. Hiermee hebben we een aantal aspecten van de H_2-kringloop en de isotoopeffecten daarin kunnen onderzoeken.

In Hoofdstuk 2 van dit proefschrift bestuderen we de seizoensvariatie en de variatie met de breedtegraad in δD. Hiervoor zijn metingen van $\chi(H_2)$ en δD gedaan in monsters die jarenlang verzameld zijn op zes meteorologische stations, die deel uitmaken

van het "EUROHYDROS"-netwerk van stations voor H_2-observaties. Deze zes zijn uitgekozen om een goede spreiding over de breedtegraden te krijgen, met het zwaartepunt in Europa. Het zijn overwegend "achtergrond"-stations, wat wil zeggen dat ze ver weg liggen van vervuilingsbronnen. Drie van deze stations liggen aan zee en op het noordelijk halfrond (NH), namelijk Alert (Arctisch Canada), Mace Head (Ierland) en Kaapverdië (Atlantische Oceaan). In de tijdsseries van deze drie stations zien we duidelijke seizoenscycli in zowel $\chi(H_2)$ als δD. $\chi(H_2)$ en δD lopen vijf tot zes maanden uit fase: $\chi(H_2)$ piekt in de lente/zomer terwijl δD laag is, en $\chi(H_2)$ is op zijn laagst in de herfst/winter terwijl δD dan het hoogst is. Dit is een resultaat van de ophoping van verarmd H_2 uit verbrandingsbronnen gedurende de winter, wanneer de bodemopname zwak is, en een sterke bodemopname gedurende de zomer, wat tot een stijging van δD leidt. In Schauinsland (Zuid-Duitsland), Amsterdam Eiland (Indische Oceaan) en Neumayer (Antarctische kust) is er geen seizoenscyclus in δD waar te nemen, hoewel er soms een cyclus in $\chi(H_2)$ is. Aan de hand van de seizoensgemiddelden kan de breedtegraad-gradiënt in $\chi(H_2)$ en δD worden bestudeerd. Zowel $\chi(H_2)$ als δD zijn hoger op het zuidelijk halfrond (ZH) dan op het noordelijk, wat vanuit de literatuur ook werd verwacht. De gradiënt in δD lijkt wel iets groter dan voorheen gedacht, en het minimum blijkt niet in het hoge noorden, maar op de gematigde breedtegraden van het NH te liggen. Dit minimum wordt waarschijnlijk veroorzaakt door antropogene (door mensen veroorzaakte) verbranding van fossiele brandstoffen. Met deze data kunnen we ook een simpele analyse maken van de relatieve grootte van de twee afbraakprocessen rond Alert, Mace Head en Kaapverdië. Deze uitkomst van deze analyse geeft aan dat de relatieve grootte van de bodemopname (t.o.v. afbraak door OH) toeneemt met de breedtegraad, in lijn met de verwachting. We hebben met deze data kortom de variatie van δD met seizoen en breedtegraad gekarakteriseerd, en dit bevat informatie over de bronnen en afbraakprocessen die de achtergrondniveaus van H_2 bepalen. Daarbij kunnen de data gebruikt worden om de uitkomsten van modellen te beoordelen.

In het daarop volgende hoofdstuk (Hoofdstuk 3) proberen we te te komen tot een goede beschrijving van de δD-waarde van H_2 dat vanuit de stratosfeer in de troposfeer terecht komt. In de stratosfeer raakt de H_2 namelijk enorm verrijkt in D doordat er alleen fotochemische productie en afbraak plaatsvinden, die allebei een D-verrijkend effect hebben. Doordat de productie en afbraak ongeveer even snel gaan, verandert er weinig aan $\chi(H_2)$. Bij de uitwisseling van lucht tussen stratosfeer en troposfeer treden er daardoor weinig $\chi(H_2)$-veranderingen op, maar δD neemt er wel door toe in de troposfeer. In modellen van de isotoopkringloop blijkt dit een aanzienlijk verrijkend effect op de troposferische H_2 te hebben, en een correcte beschrijving ervan is dus belangrijk voor het goed modelleren van het isotoopbudget van H_2. Met dit doel hebben we $\chi(H_2)$ en δD gemeten in monsters die door het "CARIBIC"- vliegtuig verzameld zijn in de "UTLS"("upper troposphere - lower stratosphere"), het grensgebied tussen troposfeer en stratosfeer (rond de tropopauze). Het CARIBIC-project gebruikt een commercieel lijnvliegtuig dat is uitgerust met een luchtinlaatsysteem en een container met geautomatiseerde apparatuur om op kruishoogte metingen te doen en luchtmonsters te verzamelen. Doordat de kruishoogte meestal tussen de 9 en 12 km is, doorkruist het vliegtuig regelmatig de tropopauze en is ongeveer 40% van de monsters stratosferisch. We vinden inderdaad de verwachte D-verrijking in de stratosferische monsters, en weinig variatie in $\chi(H_2)$. δD blijkt, zoals uit eerder onderzoek verwacht, sterk gecorreleerd met CH_4 en lachgas (N_2O). Met deze vernieuwde, preciezere correlaties kan de δD-waarde van de H_2 die vanuit de stratosfeer de troposfeer inkomt beter geparametriseerd worden in modellen.

In de CARIBIC data hebben we ook onverwachte effecten aangetroffen. Een deel van de monsters bleek een hoge $\chi(H_2)$ en een lage δD te hebben. Omdat dit vaak in de monsters plaatsvond die het dichtst bij de start en de landing van het vliegtuig werden genomen, heeft dit mogelijk te maken met het doorkruisen van de uitlaatsporen van andere vliegtuigen, maar we hebben dat niet definitief kunnen vaststellen. Onverwacht bleken ook de δD-waarden in de troposferische monsters die genomen zijn boven India tijdens de zomermoesson van 2008 verlaagd. Bij gebrek aan metingen op de grond is ook hier de oorzaak niet met volledige zekerheid vast te stellen, maar het is goed mogelijk dat er in de natte bodems tijdens de moesson meer productie van H_2 door micro-organismen plaatsvindt die bijdraagt aan deze δD-verlaging. Dit was voorheen onbekend, en is niet meegenomen in de gangbare schattingen van de grootte van de H_2-productie door micro-organismen.

Daarna richten we ons in Hoofdstuk 4 op de vraag hoe de H_2-kringloop in dichtbevolkte gebieden afwijkt van die op meer afgelegen plekken (zoals de stations die besproken zijn in Hoofdstuk 2), en proberen we ook uit te vinden of we tot een karakterisering van de isotoop-effecten door de bodemopname in Noordwest Europa kunnen komen. Met dit doel verrichtten we drie jaar metingen van de $\chi(H_2)$ en δD in monsters die genomen zijn op 200 meter hoogte vanaf de meettoren in Cabauw. De toren van Cabauw bevindt zich in het Groene Hart, omringd door de Randstad, en staat daardoor onder sterke invloed van door mensen uitgestoten vervuiling. In de tijdsserie zien we de hoge $\chi(H_2)$-pieken die ook in eerder gepubliceerde continue metingen van $\chi(H_2)$ zijn waargenomen, en we zien bovendien dat deze gepaard gaan met lage δD-waarden. Deze uitschieters komen extra duidelijk naar voren als de data vergeleken worden met die van achtergrondstation Mace Head. De lage δD-waarden zijn een aanwijzing dat de $\chi(H_2)$-pieken worden veroorzaakt door verbranding van fossiele brandstoffen (wat verarmde H_2 produceert). In de literatuur wordt geschat dat verkeer verantwoordelijk is voor ongeveer 60% van de H_2-uitstoot door verbranding van fossiele brandstoffen. Dat het verkeer een grote rol speelt in Cabauw blijkt ook uit het feit dat er in de continue $\chi(H_2)$-metingen een duidelijke toename te zien is tijdens de spitsuren. Een analyse van de bronsignatuur (δD) levert een waarde op die lager is dan waarden die rond het jaar 2000 zijn gepubliceerd. Dit kan te maken hebben met verschillen in voertuigtechniek en de gemiddelde verkeerscondities ten opzichte van die vroege studies; een recente laboratoriumstudie met een moderne automotor lijkt dat te ondersteunen. We vergelijken dit met twee dagcycli die bemonsterd zijn in Royal Holloway, een voorstad van Londen, en komen daar op een soortgelijke bronsignatuur.

De toren biedt als bijkomend voordeel dat er monsters genomen kunnen worden van verschillende hoogten (20, 60, 120 en 200 meter). Door profielen te meten van deze monsters zouden we een sterke bodemopname moeten kunnen zien als een verlaging van $\chi(H_2)$ en een verhoging van δD op de laagste niveaus. We hebben verschillende profielen gemeten, maar vinden geen significant verschil in $\chi(H_2)$ tussen de verschillende hoogten, en δD blijkt op 20 en 60 m zelfs significant lager dan op 120 en 200 m. Hieruit moeten we wel concluderen dat de bodemopname in Cabauw zeer zwak is, wat ook uit de continue $\chi(H_2)$ metingen is gebleken, en we kunnen dan ook de fractionering van de bodemopname hier niet karakteriseren. Het verschil in δD tussen de niveaus komt waarschijnlijk door een verschil in de samenstelling van de bronnen in de verschillende invloedsgebieden van de niveaus (de hogere niveaus ontvangen vervuiling van verder weg). Mogelijk zijn er verschillen in de samenstelling van het wagenpark of in de gemiddelde verkeerscondities tussen de verschillende Noordwest-Europese landen. De metin-

gen van Cabauw zijn waarschijnlijk ook bruikbaar in het beoordelen van modellen die de effecten van H_2-uitstoot op regionale luchtkwaliteit beschrijven.

Tot slot worden in het laatste hoofdstuk de conclusies samengevat, en wordt er een overzicht gegeven van de deelgebieden die, ons inziens, de meeste aandacht verdienen bij het bestuderen van de H_2-kringloop in de nabije toekomst.

Dankwoord

Niemand doet een promotie-onderzoek werkelijk alleen. En dat is maar goed ook, want juist het feit dat je vier jaar lang mag werken temidden van bevlogen collega's en ideeën mag uitwisselen met razend intelligente mensen in binnen- en buitenland, dát is een groot deel van de lol van het promovendus-zijn. Er is dan ook een groot aantal mensen dat ik hier wil bedanken.

Allereerst is daar natuurlijk mijn promotor, Thomas Röckmann. Thomas is verantwoordelijk voor steeds meer personen en projecten, maar is toch verbazingwekkend betrokken bij elk van zijn promovendi (of wekt in ieder geval de indruk dat te zijn). Hij maakte als maar enigszins mogelijk tijd voor mij vrij als ik wat met hem te bespreken had, of dat nu direct ging over het onderzoek dat in dit proefschrift wordt besproken, of over wat meer "softe" zaken, zoals wat een loopbaan in de wetenschap echt inhoudt, wat je daar dan wel voor vaardigheden en ervaringen voor zou moeten opdoen, en waar het met het vakgebied heengaat. Thomas, ik waardeer dat je geprobeerd hebt me dat soort dingen bij te brengen, en ik probeer ervan te leren. Ik hoop ook dat je de traditie van de "Feuerzangenbohle" bij je thuis blijft voortzetten.

Dan is daar de rest van de atmosfeerchemie-groep. Ik vind het opvallend hoe goed de sfeer is in deze groep, en hoe groot de bereidheid om elkaar te helpen. Of je nu wilt weten hoe je de instellingen van de meetsoftware verandert, hoe je een verbinding maakt tussen een pijp en een kraan, hoe je je data met Python omtovert tot professioneel ogende plaatjes, of wat je nog moet veranderen aan een presentatie die je gaat geven op een congres, in deze groep word je ermee geholpen. Bedankt daarvoor!

Bijzonder veel hulp was natuurlijk afkomstig van de technici, Carina, Michel, Henk en Marcel. Zij verdienen niet alleen lof voor de hulp die ze hebben geboden bij de alledaagse gang van zaken in het lab, maar ook voor de fantastische manier waarop ze het GC-IRMS systeem hebben geautomatiseerd. Deze automatisering betekent een enorme vooruitgang in de efficiëntie waarmee we $\delta D(H_2)$ kunnen meten, en ik hoop dat daar veel gebruik van gemaakt gaat worden. Sylvia wil ik bedanken voor de inwijding in de (toen nog half handmatige) bediening van het GC-IRMS systeem die ze me aan het begin van mijn promotietraject heeft gegeven, en ook omdat ze me heeft laten zien hoe stimulerend het is om samen te werken met mensen uit andere disciplines. Ik ben blij met haar werk en ook met het werk dat gedaan is door Gerben en Elena; volgens mij heeft er vruchtbare kruisbestuiving plaatsgevonden tussen onze projecten waarmee ons begrip van de H_2-kringloop werkelijk vooruit is gegaan. Ik heb de afgelopen jaren ook een heel stel studenten voorbij zien komen die voor langere of kortere tijd in het lab aan H_2 hebben gewerkt. Zonder ze allemaal op te willen noemen (want dan vergeet ik er geheid een paar), wil ik die graag bedanken voor hun aanstekelijke enthousiasme.

Ook de rest van het IMAU mag niet onvermeld blijven. Er hangt dan wel een gemoedelijke sfeer op dit instituut (mede door het voortreffelijke secretariaat), maar door alle colloquia, lunchpraatjes, gesprekken tijdens de koffiepauzes en het assisteren bij vakken heb ik sluipenderwijs dan toch nog het één en ander geleerd over oceanen en ijs. Verder is hulp bij LaTeX-problemen hier nooit ver weg, wat de *looks* van dit proefschrift zeker ten goede is gekomen. Een bedankje aan mijn kamergenoten mag niet ontbreken; met sommigen heb ik jarenlang een kantoor gedeeld, met sommigen maar een paar weken, maar in ieder geval was ik altijd in goed gezelschap. Een bijzondere vermelding verdienen Marion en Markella. Het is voor promovendi bijzonder heilzaam om regelmatig de stress en de frustratie van zich af te sporten, maar zonder een stok achter de deur schiet dat er vaak bij in. Gelukkig wisten dit stel meestal genoeg sociale druk uit te oefenen om me toch naar de sportschool te krijgen. Markella is daarbij nog bereid om mijn paranimf te zijn, samen met de immer goedgehumeurde Supun. Bedankt, dames.

Now, I would like to change the focus to our collaborators outside the IMAU. We would not have come far with the research in this thesis without our external partners in different projects. First, I would like to thank everyone who was involved in the EURO-HYDROS project. Through this project, we had the invaluable opportunity to measure samples that were collected around the world, which has resulted in Chapter 2. I found the cooperation very pleasant and I have learned a lot at the different meetings and workshops. Secondly, I would like to thank all those involved in CARIBIC. The CARIBIC people have been very helpful to me, and I am much impressed by their achievements. Their project's technical challenges alone must be huge, and yet it works. Ik wil ook de mensen van ECN bedanken die met ons hebben samengewerkt aan het hoofdstuk over Cabauw. Er zijn daarnaast verschillende mensen geweest die met de bemonstering hebben geholpen of de flessen een lift hebben gegeven van Utrecht naar Cabauw of andersom; ook bedankt daarvoor. Misschien is dit dan ook het moment om de portiers van het BBL te noemen die zoveel zendingen voor ons hebben moeten aannemen. Finally, I would like to thank the people of the Earth Sciences department of the University of London for taking the Royal Holloway diurnal samples.

Mijn ouders hebben vanaf het begin bijgedragen aan mijn wetenschappelijke carrière door me op te voeden met een waardering voor kennis en voor de natuur, en door me altijd financieel en moreel te steunen in het volgen van mijn interesses. Ik voel me hierdoor een bevoorrecht mens. Het was ook een voorrecht om mijn ervaringen te kunnen delen met mijn zus Sietske, die met een promotietraject in de aardwetenschappen bezig is. Het was bijzonder om samen congressen te bezoeken. Dan zijn er nog alle (schoon)familieleden en vrienden, die voor de broodnodige ontspanning en gezelligheid na het werk zorgden, maar vooral: mijn stoere zeebonk Karel. Karel, bedankt voor je geduld wanneer het weer eens uitliep op het lab. Hopelijk hebben we de komende jaren wat meer tijd om met elkaar door te brengen.

Curriculum Vitae

Anneke Batenburg werd op 31 januari 1983 geboren in Haren (Groningen). Drie jaar later verhuisde het gezin naar het westen, waar het via De Lier terechtkwam in Maassluis. Na het behalen van haar gymnasium-diploma op het Stedelijk Gymnasium Schiedam in 2001 begon Anneke aan de TWIN-opleiding Scheikunde en Natuur- en sterrenkunde aan de Universiteit Utrecht. Met twee propedeuses op zak schakelde ze na een jaar over op Natuur- en sterrenkunde, wat ze in het collegejaar 2003–2004 een jaar onderbrak om plaats te nemen in het bestuur van studievereniging A–Eskwadraat. Ze koos voor de masteropleiding "Chemistry and Physics" en deed in 2006–2007 haar masteronderzoek op het gebied van de niet-lineaire spectroscopie in de groep "Spectroscopy at bio-interfaces" van het Max-Planck-Institut für Metallforschung in Stuttgart. In 2008 zag ze een vacature voor een promovendus bij de atmosfeerchemie-groep van het IMAU. In de beschrijving van het project herkende ze een combinatie van verschillende wetenschapsgebieden die haar interesseerden, en ze besloot daarop te solliciteren; een beslissing die tot dit proefschrift heeft geleid. Tijdens haar promotietraject bezocht Anneke twee zomerscholen en verschillende workshops en congressen.

Anneke Batenburg was born on 31 January 1983 in Haren (Groningen, the Netherlands). Three years later, the family moved "west": first to De Lier and finally to Maassluis. After obtaining her grammar school diploma from the "Stedelijk Gymnasium Schiedam" in 2001, she embarked upon a double major program in Chemistry and Physics & Astronomy at Utrecht University. After successfully finishing the first year program of both majors, she switched to Physics & Astronomy. In the school year 2003–2004 she interrupted her studies for a year to become a member of the board of study association "A–Eskwadraat". She chose the "Chemistry and Physics" MSc program, and in 2006–2007, she performed her MSc research project in nonlinear spectroscopy in the Spectroscopy at bio-interfaces Group of the Max Planck Institute for Metals Research in Stuttgart. In 2008, she saw a vacancy for a PhD student in the Atmospheric Physics and Chemistry Group of the IMAU. She recognized a combination of interesting research areas in the description of the project and decided to apply; that decision resulted in this thesis. During her PhD project, Anneke attended two summer schools and various workshops and conferences.

Publications

First author publications (incorporated in this thesis)

- Batenburg, A. M., Walter, S., Pieterse, G., Levin, I., Schmidt, M., Jordan, A., Hammer, S., Yver, C., and Röckmann, T.: *Temporal and spatial variability of the stable isotopic composition of atmospheric molecular hydrogen: observations at six EUROHYDROS stations*, Atmos. Chem. Phys., **11**, 6985–6999, doi:10.5194/acp-11-6985-2011, 2011. URL: `www.atmos-chem-phys.net/11/6985/2011/acp-11-6985-2011.html`
- Batenburg, A. M., Schuck, T. J., Baker, A. K., Zahn, A., Brenninkmeijer, C. A. M., and Röckmann, T.: *The stable isotopic composition of molecular hydrogen in the tropopause region probed by the CARIBIC aircraft*, Atmos. Chem. Phys., **12**, 4633–4646, doi:10.5194/acp-12-4633-2012, 2012. URL: `www.atmos-chem-phys.net/12/4633/2012/acp-12-4633-2012.html`
- Batenburg, A. M., Popa, M. E., Vermeulen, A. T., van den Bulk, W. C. M., Jongejan, P. A. C., Fisher, R. E., Nisbet, E. G., Röckmann, T.: *Hydrogen mixing ratio and stable isotopic composition observations at the Cabauw tall tower*, to be submitted, 2012

Co-authored publications (not incorporated in this thesis)

- Popa, M. E., Vermeulen, A. T., van den Bulk, W. C. M., Jongejan, P. A. C., Batenburg, A. M., Zahorowski, W., and Röckmann, T.: *H_2 vertical profiles in the continental boundary layer: measurements at the Cabauw tall tower in the Netherlands*, Atmos. Chem. Phys., **11**, 6425–6443, 10.5194/acp-11-6425-2011, 2011. URL: `www.atmos-chem-phys.net/11/6425/2011/acp-11-6425-2011.html`
- Pieterse, G., Krol, M. C., Batenburg, A. M., Steele, L. P., Kummel, P. B., Langenfelds, R. L., and Röckmann, T.: *Global modelling of H_2 mixing ratios and isotopic compositions with the TM5 model*, Atmos. Chem. Phys., **11**, 7001–7026, doi: 10.5194/acp-11-7001-2011, 2011. URL: `www.atmos-chem-phys.net/11/7001/2011/acp-11-7001-2011.html`
- Pieterse, G., Krol, M. C., Batenburg, A. M., Brenninkmeijer, C. A. M., Popa, M. E., O'Doherty, S., Grant, A., Steele, L. P., Krummel, P. B., Langenfelds, R. L., Wang, H. J., Vermeulen, A. T., Schmidt, M., Jordan, A., Engel, A., Fisher, R. E., Lowry, D., Nisbet, E. G., Reimann, S., Vollmer, M. K., Steinbacher, M., Levin, I., Hammer, S., Sturges, W. T., and Röckmann, T.: *Modelling the global and regional scale variability in atmospheric H_2 with the two-way nested TM5 model*, accepted by J. Geophys. Res., 2012.